Mixed glass former effect of 0.5 Na_2S + 0.5[xSiS_2 + (1-x) $PS_{5/2}$] and **0.67 Na_2S + 0.33[xSiS_2 + (1-x) $PS_{5/2}$] glass systems**

by

Deborah Elizabeth Watson

A dissertation submitted to the graduate faculty

in partial fulfillment of the requirements for the degree of

DOCTOR OF PHILOSOPHY

Major: Materials Science and Engineering

Program of Study Committee:
Steve W Martin, Major Professor
Nicola Bowler
Xiaoli Tan
Jing Xu
Theresa Windus

The student author, whose presentation of the scholarship herein was approved by the program of study committee, is solely responsible for the content of this dissertation. The Graduate College will ensure this dissertation is globally accessible and will not permit alterations after a degree is conferred.

Iowa State University

Ames, Iowa

2017

DEDICATION

To my father, George, my mother, Sonia and dear sister Diannah.

TABLE OF CONTENTS

LIST OF FIGURES vii

LIST OF TABLES x

ABSTRACT xi

CHAPTER 1. INTRODUCTION 1
1.1 Thesis Introduction 1
1.2 Thesis Organization 2
1.3 Background 5
1.3.1 The Mixed Glass Former Effect 5
1.3.2 Goals of Research 8
1.4 Proposed Research 9
1.4.1 Mixed Glass Former System under Investigation 9
1.4.2 Experimental Methods and Characterization 10
1.4.2.1 Sample Preparation 10
1.4.2.2 Glass Batching 11
1.4.2.3 Differential Scanning Calorimetry (DSC) – Glass Transition Temperature (T_g) 12
1.4.2.4 Archimedes Principle – Density 13
1.4.2.5 Impedance Spectroscopy – Ionic Conductivity 13
1.4.2.6 Raman Spectroscopy 13
1.4.2.7 Infrared Spectroscopy (Mid and Far IR) 14
1.4.2.8 Magic Angle Spinning Nuclear Magnetic Resonance (MAS-NMR) 14
1.4.3 Glass Notation 15
1.4.4 Composition Dependence of Physical Properties Figures 15
1.5 References 18

CHAPTER 2. SHORT RANGE ORDER CHARACTERIZATION OF THE NA_2S+ SIS_2 GLASS SYSTEM USING RAMAN, INFRARED AND ^{29}SI MAGIC ANGLE SPINNING NUCLEAR MAGNETIC RESONANCE SPECTROSCOPIES 20
2.1 Abstract 20
2.2 Introduction 21
2.2.1 Background 21
2.3 Experimental Methods 25
2.3.1 Sample Preparation 25
2.3.2 IR and Raman Spectra of the Glasses and Polycrystals 27
2.3.3 ^{29}Si MAS NMR Spectra of the Glasses and Polycrystals 27
2.4 Results 28
2.4.1 $yNa_2S + (1-y)\ SiS_2$ glass samples 28
2.4.2 $yNa_2S + (1-y)SiS_2$ polycrystal samples 29

2.4.3 Raman and IR Spectroscopy 29
2.4.3.1 Raman Spectra of $yNa_2S + (1-y)SiS_2$ glass and polycrystal samples 29
2.4.3.2 IR of $yNa_2S + (1-y)SiS_2$ glass and polycrystal samples 31
2.4.3.3 Deconvolution of Raman Spectra for $yNa_2S + (1-y)SiS_2$ glass samples .. 32
2.4.4 ^{29}Si MAS NMR Spectroscopy 33
2.4.4.1 $yNa_2S + (1-y)SiS_2$ glass samples 33
2.4.4.2 $yNa_2S + (1-y)SiS_2$ polycrystal samples 35
2.4.4.3 Deconvolution of ^{29}Si MAS NMR Spectra for $yNa_2S + (1-y)SiS_2$ glass samples 37
2.5 Discussion 37
2.5.1 Low Modified sodium thiosilicate glasses ($y < 0.5$) 37
2.5.2 High Modified sodium thiosilicate glasses ($y \geq 0.50$) 42
2.6 Conclusions 48
2.7 Acknowledgments 49
2.8 References 58

CHAPTER 3. STRUCTURAL CHARACTERIZATION OF THE SHORT RANGE ORDER IN HIGH ALKALI CONTENT SODIUM THIO-SILICOPHOSPHATE GLASSES 61
3.1 Abstract 61
3.2 Introduction 62
3.2.1 Structures of MGF Glasses 63
3.3 Experimental Methods and Materials 67
3.3.1 Sample preparation of glasses in the series $0.5Na_2S + 0.5[xSiS_2 + (1-x)PS_{5/2}]$ 67
3.3.2 Sample preparation of glasses in the series $0.67Na_2S + 0.33[xSiS_2 + (1-x)PS_{5/2}]$ 68
3.3.3 Raman and IR Spectroscopy 69
3.3.4 MAS-NMR Spectroscopy 70
3.4 Results and Discussion 70
3.4.1 IR Spectra 70
3.4.1.1 $0.5Na_2S + 0.5[xSiS_2 + (1-x)PS_{5/2}]$ Glasses 70
3.4.1.2 $0.67Na_2S + 0.33[xSiS_2 + (1-x)PS_{5/2}]$ Glasses 73
3.4.2 Raman Spectra 74
3.4.2.1 $0.5Na_2S + 0.5[xSiS_2 + (1-x)PS_{5/2}]$ Glasses 74
3.4.2.2 $0.67Na_2S + 0.33[xSiS_2 + (1-x)PS_{5/2}]$ glasses 76
3.4.3 ^{31}P MAS NMR Spectroscopy 77
3.4.3.1 $0.5Na_2S + 0.5[xSiS_2 + (1-x)PS_{5/2}]$ Glasses 77
3.4.3.2 $0.67Na_2S + 0.33[xSiS_2 + (1-x)PS_{5/2}]$ Glasses 78
3.4.4 ^{29}Si MAS-NMR Spectroscopy 79
3.4.4.1 $0.5Na_2S + 0.5[xSiS_2 + (1-x)PS_{5/2}]$ Glasses 79
3.4.4.2 Deconvolution of ^{29}Si MAS-NMR Spectra 80
3.4.4.3 $0.67Na_2S + 0.33[xSiS_2 + (1-x)PS_{5/2}]$ glasses 81
3.4.4.4 Deconvolution of ^{29}Si MAS NMR Spectra 82

3.4.5 Composition Dependence of the various SRO units in the $0.5Na_2S + 0.5[xSiS_2 + (1-x)PS_{5/2}]$ Glasses....82
3.4.6 Composition Dependence of the Various SRO Units in the $0.67Na_2S + 0.33[xSiS_2 + (1-x)PS_{5/2}]$ Glasses....84
3.5 Conclusions....85
3.6 Acknowledgements....97
3.7 References....98

CHAPTER 4. THE COMPOSITION DEPENDENCE OF THE GLASS TRANSITION TEMPERATURE AND DENSITY IN MGF SODIUM THIOSILICOPHOSPHATE GLASSES: A STRUCTURAL PERSPECTIVE....101
4.1 Abstract....101
4.2 Introduction....102
4.3 Experimental Methods....104
4.3.1 Sample preparation....104
4.3.1.1 $0.5Na_2S + 0.5[xSiS_2 + (1-x) PS_{5/2}]$ glass system....104
4.3.1.2 $0.67Na_2S + 0.33[xSiS_2 + (1-x)PS_{5/2}]$ glass system....105
4.3.2 Glass Transition Temperature – Differential Scanning Calorimetry....105
4.3.3 Density – Archimedes Principle....105
4.4 Results....106
4.4.1 Glass Transition Temperatures of the $0.5Na_2S + 0.5[xSiS_2 + (1-x)PS_{5/2}]$ glasses....106
4.4.2 Glass Transition Temperatures of the $0.67Na_2S + 0.33[xSiS_2 + (1-x)PS_{5/2}]$ glasses....106
4.4.3 Densities of the $0.5Na_2S + 0.5[xSiS_2 + (1-x) PS_{5/2}]$ glasses....106
4.4.4 Densities of the $0.67Na_2S + 0.33[xSiS_2 + (1-x)PS_{5/2}]$ glasses....107
4.5 Discussion....107
4.5.1 Glass Transition Temperature....107
4.5.2 Density and Molar Volume....109
4.6 Conclusions....111
4.7 Acknowledgements....112
4.8 References....125

CHAPTER 5. THE MIXED GLASS FORMER EFFECT IN THE IONIC CONDUCTIVITY OF $0.67NA_2S + 0.33[XSIS_2 + (1-X)PS_{5/2}]$ GLASSY ELECTROLYTES....126
5.1 Abstract....126
5.2 Introduction....127
5.2.1 Background....127
5.2.2 Glassy Solid State Electrolytes....128
5.2.3 The Mixed Glass Former Effect....128
5.3 Materials and Methods....129
5.3.1 Sample Preparation....129
5.3.2 Impedance Spectroscopy....130
5.4 Results....130
5.5 Discussion....131

5.5.1 The Composition Dependence of the Ionic Conductivity....131
5.5.2 Ionic Conduction in Glass and the Anderson Stuart Model....132
5.5.3 Evaluation of the MGFE....136
5.6 Conclusion....137
5.7 Acknowledgements....138
5.8 References....153

CHAPTER 6. CONCLUSIONS....155
6.1 General Conclusions....155
6.2 Proposed Future work....156
6.3 Acknowledgements....157

LIST OF FIGURES

Figure 1.1 Ternary Composition Diagram of $yNa_2S + (1-y)[xSiS_2 + (1-x)PS_{5/2}]$ where y = 0.5 and 0.67 16

Figure 1.2 Example of the positive and negative MGFE as glass formers are varied....17

Figure 2.1 Short Range Order Structure in the $y\ Na_2S + (1-y)\ SiS_2$ system (a) Si^4 SRO structure in pure SiS_2 (b) Si^3 SRO structures at theoretical composition (c) Si^2 SRO structures (d) Si^1 SRO structures (e) Si^0 SRO structures 51

Figure 2.2 Raman Spectra of (a) $yNa_2S + (1-y)SiS_2$ glasses and (b) polycrystals 52

Figure 2.3 Infrared Spectra of $yNa_2S + (1-y)SiS_2$ (a) glasses and (b) polycrystals....53

Figure 2.4 ^{29}Si MAS NMR Spectra of $yNa_2S + (1-y)SiS_2$ (a) glasses and (b) polycrystals 54

Figure 2.5 Deconvolution of Raman Spectra for $yNa_2S + (1-y)SiS_2$ glasses 55

Figure 2.6 Deconvolution of ^{29}Si MAS NMR Spectra for $yNa_2S + (1-y)SiS_2$ glasses....56

Figure 2.7 Composition Dependence of the SRO of $yNa_2S+(1-y)SiS_2$. Determined from ^{29}Si MAS NMR and Raman Spectroscopy analysis 57

Figure 3.1 Phosphorus SRO structures in the sodium thiophosphate system....87

Figure 3.2 Silicon SRO Structures in the sodium thiosilicate system 88

Figure 3.3 IR spectra of $yNa_2S + (1-y)\ [xSiS_2 + (1-x)\ PS_{5/2}]$ (a) y = 0.5 and (b) y = 0.67 glass series 89

Figure 3.4 Raman spectra of $yNa_2S + (1-y)\ [xSiS_2 + (1-x)\ PS_{5/2}]$ (a) y = 0.5 and (b) y = 0.67 glass series 90

Figure 3.5 $0.5Na_2S + 0.5[xSiS_2 + (1-x)\ PS_{5/2}]$ (a) ^{31}P MAS NMR spectra x = 0.0 – 0.9 and (b) ^{29}Si MAS NMR spectra x = 0.1 to 1.0....91

Figure 3.6 $0.67Na_2S + 0.33[xSiS_2 + (1-x)\ PS_{5/2}]$ (a) ^{31}P MAS NMR spectra x = 0.0 – 0.9 and (b) ^{29}Si MAS NMR spectra x = 0.1 to 1.0 92

Figure 3.7 Deconvolution of ^{29}Si MAS NMR spectrum of $0.5Na_2S + 0.5[xSiS_2 + (1-x)PS_{5/2}]$ x=1.0 93

Figure 3.8. Composition Dependence of SRO structures in the $0.5Na_2S + 0.5[xSiS_2 + (1-x)\ PS_{5/2}]$ glass system 94

Figure 3.9. Composition Dependence of SRO structures in the $0.67Na_2S + 0.33[xSiS_2 + (1-x) PS_{5/2}]$ glass system 95

Figure 3.10. Composition (x) dependence of the excess Na_2S added to the glass from $0.67Na_2S + 0.33 PS_{5/2}$, from the formation of ESi^2 from Si^0 groups, and the total added Na_2S as a fraction of the total Na_2S in the glass, 0.67. The former two amounts are absolute mole numbers. 96

Figure 4.1: Composition Dependence of the glass transition temperature in the $0.5Na_2S + 0.5[xSiS_2 + (1-x) PS_{5/2}]$ system. 115

Figure 4.2: Composition Dependence of the glass transition temperature in the $0.67Na_2S + 0.33[xSiS_2 + (1-x) PS_{5/2}]$ system. 116

Figure 4.3: Composition Dependence of the densities in the $0.5Na_2S + 0.5[xSiS_2 + (1-x) PS_{5/2}]$ system. 117

Figure 4.4: Composition Dependence of the densities in the $0.67Na_2S + 0.33[xSiS_2 + (1-x) PS_{5/2}]$ system. 118

Figure 4.5: Composition Dependence of the T_g in the $0.5Na_2S + 0.5[xSiS_2 + (1-x) PS_{5/2}]$ system and the fraction of bridging sulfurs across the system 119

Figure 4.6: Composition Dependence of the T_g in the $0.67Na_2S + 0.33[xSiS_2 + (1-x) PS_{5/2}]$ system and the fraction of bridging sulfurs across the system 120

Figure 4.7: Composition Dependence of the Molar Volume in the $0.5Na_2S + 0.5 [xSiS_2 + (1-x) PS_{5/2}]$ system 121

Figure 4.8: Composition Dependence of the Molar Volume and the fraction of bridging sulfurs in the $0.5Na_2S + 0.5[xSiS_2 + (1-x) PS_{5/2}]$ system 122

Figure 4.9: Total fraction of bS in the $0.5Na_2S + 0.5[xSiS_2 + (1-x) PS_{5/2}]$ system compared with the fraction of nbS from P^0 structures 123

Figure 4.10: Composition Dependence of the Molar Volume in the $0.67Na_2S + 0.33[xSiS_2 + (1-x) PS_{5/2}]$ system 124

Figure 5.1 Complex Impedance Plot of x = 0.1 $0.67Na_2S + 0.33[xSiS_2 + (1-x)PS_{5/2}]$ 142

Figure 5.2 Composition Dependence of the Ionic Conductivities in the $0.67Na_2S + 0.33[xSiS_2 + (1-x)PS_{5/2}]$ 143

Figure 5.3 Arrhenius Plots of the $0.67Na_2S + 0.33[xSiS_2 + (1-x)PS_{5/2}]$ glasses 144

Figure 5.4 Experimental Activation Energies of the $0.67Na_2S + 0.33[xSiS_2 + (1-x) PS_{5/2}]$ system 145

Figure 5.5 Measurement of the high frequency permittivity of x = 0.0 $0.67Na_2S + 0.33[xSiS_2 + (1-x)PS_{5/2}]$ 146

Figure 5.6 Composition Dependence of the High Frequency Permittivity in the $0.67Na_2S + 0.33[xSiS_2 + (1-x)PS_{5/2}]$ system 147

Figure 5.7 Composition Dependence of the calculated Coulombic binding energy 148

Figure 5.8 Composition Dependence of the calculated volumetric strain Energy 149

Figure 5.9 Experimental activation energies with the Anderson Stuart model calculated activation energies 150

Figure 5.10 Composition Dependence of SRO Structures in the $0.67Na_2S + 0.33[xSiS_2 + (1-x)PS_{5/2}]$ 151

Figure 5.11 Fraction of Free Na_2S in the $0.67Na_2S + 0.33[xSiS_2 + (1-x)PS_{5/2}]$ 152

LIST OF TABLES

Table 2.1 Number of BS, NBS_j, and NBS, N_{NBSj}, associated with each Q^n structural unit. 50

Table 4.1 Number of bridging and non-bridging sulfurs per SRO structure in the $0.50Na_2S + 0.50[xSiS_2 + (1-x)PS_{5/2}]$ 113

Table 4.2 Number of bridging and non-bridging sulfurs per SRO structure in the $0.67Na_2S + 0.33[xSiS_2 + (1-x)PS_{5/2}]$ 114

Table 5.1 Parameters for the calculation of the Coulombic binding energy 139

Table 5.2 Parameters for the calculation of the volumetric strain energy 140

Table 5.3 Calculated Anderson Stuart Model Activation Energies and experimental activation energies 141

ABSTRACT

With the growing interest in using renewable energy resources such as wind and solar to generate and harvest electricity, there is a demand to develop new electrical energy storage systems to accommodate the growth. All solid state sodium batteries may be one potential solution for this demand as sodium has a high natural abundance and low cost compared to lithium, making it a great candidate for solid state batteries in large grid scale applications. In order for this goal to be realized, research into electrolyte materials to allow the use of high energy dense sodium metal is imperative.

This research studies two mixed glass former $yNa_2S + (1-y)[xSiS_2 + (1-x)PS_{5/2}]$ systems ($y= 0.50$ & 0.67) as potential models for glassy electrolytes. The mixed glass former effect is a nonlinear, non-additive change in the physical properties of the glass that may lead to an increase or decrease in the properties. The $y = 0.50$ system exhibits a negative MGFE in the glass transition temperature (T_g). The structural analysis via Raman, Infrared and ^{29}Si and ^{31}P magic angle spinning nuclear magnetic resonance showed the non-equal sharing of Na^+ between the P and Si glass formers in the $y = 0.50$ where the Na^+ preferentially associates with P short range order (SRO) structures over Si SRO structures. The immediate depolymerization is what leads to a minimum in $T_g(s)$. In the $y = 0.67$ system a weak negative MGFE is observed in the T_g, density while exhibiting a positive MGFE in the ionic conductivity. The SRO of these glasses contain fully depolymerized, non-networking structures and an excess of Na_2S which lead to a negative MGFE in these properties.

CHAPTER 1. INTRODUCTION

1.1 Thesis Introduction

The US Energy Information Administration estimated that 10% of the U.S. energy consumption came from renewable energy resources including wind, solar, geothermal, biomass and hydroelectric in 2016[1]. With this there has been advances in energy storage systems (ESS) to accommodate this growth. It acknowledges the reality that fossil energy converters simply cannot keep up with the amount of electrical energy generated by these renewable resources and therefore finding a way to store the energy for later use is of the upmost importance. Of the many technologies employed in this effort, advance solid state batteries have been incorporated into future plans for ESS. The lithium ion battery (LIB) technology has already recruited in this endeavor as they have high energy storage and power capabilities useful in large scale applications. Building on this foundation, sodium batteries are sought after as an analogous electrochemical system that comes at a lower cost.

The growing cost of lithium due to its limited availability is an issue this field is experiencing. Because of the increased demand for LIBs, the cost of lithium carbonate, a main starting material for lithium battery components, has reached $5000/ton in 2010[2]. While the natural abundance of lithium in the Earth's crust is on the order of 20 ppm[3], sodium is the fourth most abundant element in the Earth's crust[2] alone. Some drawbacks to the sodium are that Na metal, as a potential anode material, is much heavier that Li metal and is also significantly less energy dense with a gravimetric capacity of 1165 mAh g^{-1} compared to Li metal's at 3829 mAh g^{-1} [2]. Sodium batteries also differed enough

from LIBs in the way of "operating voltage, electrochemical reactivity, phase transition mechanisms and kinetics[3]," to make it less attractive for high energy applications. Nevertheless, sodium batteries may better suited for large scale power sources that need high energy storage but not the high operating power [2, 3].

This research focuses on the study and engineering of an electrolyte material that would move sodium solid state batteries forward in terms of energy density, lifetimes, long term availability and costs. A number of different materials and substances have been explored since the idea of solid state batteries were introduced. Other promising materials include polymers, ionic liquids (ILs), glass and glass-ceramics electrolytes [4-8]. Glassy electrolytes are another alternative to solid state electrolytes and have a variety of ways in which they can be synthesized. Glassy bulk electrolytes, in particular, are an attractive opportunity to compete with the high conductivities of current organic polymer electrolytes, while satisfying the goals outlined earlier[9]. By virtue of resistance to unfavorable chemical reactions and lack of grain boundaries, these materials may effectively increase voltages and energy capacities of batteries by allowing the utilization of lithium and sodium metal. The study of the mixed glass former systems aims to support electrolyte research.

1.2 Thesis Organization

This thesis is comprised of six chapters. Chapter 1 includes background information on the proposed work of investigating the Mixed Glass Former Effect, the glass systems used in this investigation, and theory behind sodium ion conduction in glass electrolytes materials.

Chapter 2 is a paper on the structure of the sodium thiosilicate glass system $yNa_2S + (1-y) SiS_2$, where $0.33 \leq y \leq 0.70$, one of the binary end member glasses used to construct the ternary systems investigated in this dissertation. The aim of this paper was to better elucidate the short range order structures of the sodium thiosilicates in order to inform our grander study of future ternary systems involving silicon sulfide as a glass former. Glasses and their crystalline analogues where synthesized and characterized by Raman and Infrared spectroscopy, and ^{29}Si MAS NMR spectroscopy. Through this, the following units were identified: edge shared Si^4 and Si^2 structures and corner shared Si^3, Si^2, Si^1 and Si^0 structures. Significant results from this study include the characterization of the Si^3 structure in the form of $Na_4Si_4S_{10}$, in the y=0.33 glass and crystal as well as the y=0.40 – 0.45 glasses and y = 0.40 crystal and the stability of the ESi^2 structure as it was present in all glasses studied here. This observation is important as it changes the population of SRO structures that are expected to occur.

Chapter 3 is examines and compares the structure of two mixed glass former systems $0.5Na_2S + 0.5[x\ SiS_2 + (1-x)\ PS_{5/2}]$ and $0.67Na_2S + 0.33[x\ SiS_2 + (1-x)\ PS_{5/2}]$. Using ^{29}Si and ^{31}P MAS NMR spectroscopy alongside Raman and infrared spectroscopies, the formation of various short range order structures were observed as the composition went from one glass former to another. In the y = 0.5 system, the unequal sharing of Na^+ by P is seen as P^1 goes to P^0 and Si^2 become more polymerized as Si^3. In the highly modified y=0.67 system, P^0 and Si^0 structures exchange one for another in a nearly linear fashion. ^{29}Si and ^{31}P MAS NMR revealed $P^{:0}$ and ESi^2 in the network as a result of disproportionation reactions occurring at even this high modifier concentration where all units should be depolymerized. Another important find was the presence of

polysulfide structures in these glasses and were found to be arising from two sources: (1) the excess Na_2S introduced by the sodium thiophosphate glass, where the composition contains P^0 and ½ mol of Na_2S, and (2) presence of ESi^2 in the sodium thiosilicate glass, where the composition should contain solely Si^0 structures. These polysulfide structures are readily observed in the Raman and were corroborated with the excess Na2S concentrations calculated from the NMR results.

Chapter 4 reports on the composition dependence of the glass transition temperature (T_g) and density in mixed glass former systems $0.5Na_2S + 0.5[x\ SiS_2 + (1\text{-}x)\ PS_{5/2}]$ and $0.67Na_2S + 0.33[x\ SiS_2 + (1\text{-}x)\ PS_{5/2}]$ and the presence of the MGFE in these properties. At y =0.5, a negative MGFE of the T_g was identified while the densities have a slight positive deviation in the $PS_{5/2}$ rich glasses and a slight negative deviation in the SiS_2 rich glasses. In the y = 0.67 system, the glass transition temperatures decreased from that of the y = 0.5 series, conferring the connection between the T_g and the amount of bridging and non-bridging sulfur in the glass network. The less polymerized the network is, the lower the T_g. The T_g of the y = 0.67 exhibited a negative MGFE like the y = 0.5 glasses. The densities also exhibited a negative MGFE experiencing minima in two compositions, x =0.2 and 0.6. The concentration of polysulfides in the y = 0.67 was observed to coincide with the behavior of the density and molar volume across the glass system.

Chapter 5 presents the ionic conductivity for the high modifier $0.67Na_2S + 0.33[x\ SiS_2 + (1\text{-}x)\ PS_{5/2}]$ glass system. The conductivities experience a positive MGFE having a DC conductivity at 30 C of 2.08×10^{-5} S/cm at x = 0.6. The activation energies of the glasses were modeled using the Anderson Stuart model by finding the Coulombic binding

energy (E_b) and volumetric strain energy (E_s). The E_b appeared to be effected by the defect structures present in the network such as $P^{:0}$ and ESi^2. When ESi^2 increases significantly in the series, it introduces an amount of Na_2S that rapidly increases the E_b; when the ESi^2 concentration plateaus, the E_b continues to decrease along the trend before the Na_2S increase. The E_s appears to correlate with the concentration of Na_2S (Na_2S_x) structures produced by these defect structures mentioned earlier. This demonstrates the caveat of having a highly modified glass like this presented here. The Na_2S concentration can begin to have a negative effect on the overall activation energy of the glass.

Chapter 6, the final chapter, will conclude the dissertation with final thoughts and suggestions for future work toward this project.

1.3 Background

1.3.1 The Mixed Glass Former Effect

The glasses made in this project are ternary glasses comprising of two glass formers, a glass forming oxide or sulfide[10], and one modifier species, the component added to give rise to certain properties in the glass[10], such as ionic conduction. When the modifier concentration is held constant, the composition (x) is varied by the amount of one glass former to the other glass former i.e. x = 0 to 1 as shown in Figure 1.1. The Mixed Glass Former Effect (MGFE) is a phenomena observed when there is a non-linear, non-additive increase or decrease in the physical properties observed across the glass system[11]. A positive MGFE can be observed where the physical property reaches a maximum as shown in Figure 1.2 in a composition between the two binary end members[12]. Therefore a negative MGFE would manifest as a minimum in the observed physical[11]. There are many mixed glass former (MGF) glasses, some in commercial use already such as

container and window glasses. However, it is unknown how many glass systems actually exhibit the MGFE. Investigation of these systems not only extends the breadth of glass science knowledge, but also enables the optimization of a key property necessary for electrolyte materials: the ionic conductivity.

Christensen et al. [13] studied the sodium borophosphate $0.35Na_2O + 0.65[xB_2O_3 + (1-x)P_2O_5]$ (Na B P O), where $0.0 \leq x \leq 1.0$, and sodium borosilicate $0.2Na_2O + 0.8[xB_2O_3 + (1-x)SiO_2]$ (Na B Si O), where $0.0 \leq x \leq 1.0$, oxide systems, each exhibiting a positive and negative MGFE respectively and found to have an ionic conductivity of 10^{-8} S/cm. In the Na B P O system, a strong MGFE in the ionic conductivity was attributed to the changes in the composition dependent Coulombic (or electrostatic) binding energy which lead to a negative MGFE in the activation energy of the glass system[12]. The Anderson Stuart model proposes two components that make up the total activation energy for ion conduction to occur: the Coulombic binding energy, the attractive potential between the conducting ion and the non-bridging oxygen (or sulfur) site it occupies, and the volumetric strain energy, the energy from nearby sites that the ion experiences as it moves through the network[11]. The E_b controls the amount of ions available for conduction while E_s controls the ion mobility through the network. The effect of the Coulombic binding energy was shown to have a stronger influence on the ionic conductivity than the volumetric strain energy that would be dependent on the free volume in the glass network. In the investigation of the densities and molar volumes of this glass system, while a strong positive MGFE was seen in the densities, a weak negative MGFE was observed in the molar volumes and free volume[14]. This suggest that the amount space of available in the glass network has little influence on the Na ion's

mobility. To support these conclusions, ^{11}B and ^{31}P MAS NMR studies along with Raman spectroscopy, were used to determine what the structural units of the glasses were to give insight into the MGFE manifested in the physical properties. Through this, Christensen et al. [15] not only found the different species occurring over the composition changes in the glass series, but discovered that the delocalization of charge on certain structural units changed how strongly they could hold on to Na^+. The B species changed from predominantly trigonal planar units to an increase presence of tetrahedral B units. This structure ends up having a partial negative charge on B itself, drawing back on the non-bridging oxygens (NBOs) and decreasing how tightly NBO holds on to the Na ion.

In the sodium thio-germanophosphate $0.5Na_2S + 0.5[xGeS_2 + (1-x)PS_{5/2}]$ (Na Ge P S) glass system, Bischoff discovered a negative MGFE in the ionic conductivity, seeing a minimum of 5×10^{-7} S/cm at $x = 0.5$[11]. Through structural analysis using IR, Raman and ^{31}P MAS-NMR spectroscopies, and observations made in the densities and glass transition temperatures of the system, it was determined that the SRO of the glasses and unequal sharing of the Na ion between these glass formers led to this unique negative MGFE[16]. The spectroscopic analyses revealed the unequal sharing of the Na^+ meaning that although the concentration of Na_2S GeS_2 is far greater than the concentration of Na_2S $PS_{5/2}$, the number of depolymerized P units increased, suggesting that the P units hold the majority of the Na ions. In order to get more information on the Ge units in the glass, since the shift from Ge^2 to G^3 is not immediately apparent from these results, and Ge NMR is unavailable due to low abundance and a complex quadrupolar nuclei (spin 9/2), Bischoff analyzed the negative MGFE of the glass transition temperature and the slightly positive MGFE in the densities and created models based on the structural results

measurements mentioned before but also proposed new structures[17]. In his work, Bischoff et al. proposed the existence of molecular anion $Na_4Ge_4S_{10}$, formed by Ge^3 units. This structure helped explained the slight densification of the glass seen the density results because these units were able to pack more efficiently in the network. The negative deviation of the glass transition temperatures can also be understood by this model in that the presence of these molecular anions means that there is less polymerization in the network which in turn would lower the glass transition temperature. These results led to new and powerful understanding of the mechanism of the MGFE. Analysis of this sulfide based glass system also help confirmed that sulfide based ternary glasses have higher conductivities than oxide glasses and therefore will continued to be studied in this work. Pursuit of sulfide based glasses would also match the efforts of using sulfur based batteries that have high theoretical capacities and are also a richly abundant resource.

1.3.2 Goals of Research

The goal of this project is to understand the structure and chemistry of these mixed glass former glasses under investigation to enable insightful and intentional engineering of electrolyte materials. It is necessary to understand how much the MGFE impacts properties like the ionic conductivity. As described above, there is a need for electrolyte materials that are chemically durable and have high ionic conductivity. Using these glasses may create a solid state electrolyte that may be less susceptible to the adverse chemical reactions experienced with liquid electrolytes. Understanding the origins of these properties could also lead to optimizing them for specific applications. There is also a call for materials that are not only cheaper but also safer for use. By thoroughly and

carefully planning the composition of these materials, suitable components can be chosen to give rise to more improved properties but also materials that cater to performance requirements. For example, this project investigates sodium as the ion conductor in the material, therefore exploring the possibility of sodium batteries rather than LIBs. While lithium batteries work well for the devices that depend on them today, there are other devices that could benefit from an ion conducting battery, but perhaps do not require the power rate or lightweight that a cellphone or a laptop would demand. Such applications would be large scale batteries that would power a building, wind turbines or maybe even a grid.

The study of the MGFE may give new insights on how to tailor composition to affect the structure and properties of a glass, thus optimizing desirable attributes of electrolyte material. While this research does not work toward producing batteries based on its findings, it will serve to increase the breadth and depth of information available to the battery industry.

1.4 Proposed Research

1.4.1 Mixed Glass Former System under Investigation

The glass systems under investigation include the $0.5Na_2S + 0.5[xSiS_2 + (1-x)PS_{5/2}]$ system and the highly modified $0.67Na_2S + 0.33[xSiS_2 + (1-x)PS_{5/2}]$ invert glass system. The sodium thiosilicates and sodium thiophosphates have demonstrated good glass forming character and therefore make good candidates for this study. The structure of the $yNa_2S + (1-y)PS_{5/2}$ has been extensively studied and followed by the $0.5Na_2S + 0.5[xGeS_2 + (1-x)PS_{5/2}]$ in which a negative MGFE was exhibited in the ionic conductivities and T_g(s). The $yNa_2S + (1-y)[xSiS_2 + (1-x)PS_{5/2}]$ system is expected to

exhibit a negative MGFE, as it is a system that is analogous to the $0.5Na_2S + 0.5[xGeS_2 + (1-x)PS_{5/2}]$ system. The ionic conductivities and infrared of the $yNa_2S + (1-y)SiS_2$ were reported by Cho et al.[18] and Pradel et al report on the ^{29}Si MAS NMR of this system. The y = 0.5 in the sodium thiosilicate system, the ionic conductivity was 10^{-5} S/cm at 25 °C.. For the sodium thiophosphate at composition y = 0.5, the ionic conductivity at room temperature was 10^{-6} S/cm[11]. One advantage this study will have is the ability to obtain both the ^{29}Si and ^{31}P MAS NMR information. This provides a framework of what may be expected for these glasses in this study.

1.4.2 Experimental Methods and Characterization

1.4.2.1 Sample Preparation

Sodium sulfide was prepared via the thermal decomposition of sodium sulfide nonahydrate ($Na_2S{\cdot}9H_2O$). Sodium sulfide nonahydrate crystals are placed in a vitreous carbon crucible and held under vacuum. While under vacuum, the crystals undergo a 30 hour vacuum heating schedule. When completed, the sample is brought into a nitrogen glove box to undergo mechanical milling. The substance is mechanically milled in a with a stainless steel ball in a stainless steel pot for an additional 5 minutes. Finally, the powder is heat treated inside a tube furnace at 260 °C for a period of 5 – 10 minutes. This final powder is sodium sulfide. X ray diffraction (XRD), Infrared (IR) and Raman spectroscopies are used to determine the phase purity of the material.

Silicon sulfide was prepared by combining stoichiometric amounts of silicon (Puratonics) and sulfur (Sigma Aldrich) that are mechanically milled to ensure thorough mixing. The mixture undergoes a 50 hour heating schedule in vacuum sealed Si coated silica glass ampoules and then is allowed to cool down to room temperature over a period

of 24 hours. The ampoule is opened inside a N_2 glove box and the product is mechanically milled to create a powder for ease of use in later glass batching. Raman spectroscopy, IR and XRD was used to confirm the phase purity of silicon sulfide.

Phosphorus pentasulfide (Sigma Aldrich) was purchased by a commercial vendor. The phosphorus sulfide is nevertheless, pre-reacted through mechanical milling. Phosphorus sulfide is fairly volatile and can lose significant amounts of both phosphorus and sulfur upon heating. Therefore, the mechanical milling pre-reaction step is used to decrease the amount lost due to this.

Manganese sulfide (Alfa Aesar) was used as a paramagnetic dopant that helps decrease the spin lattice relaxation time, T_1, of the silicon nuclei for ^{29}Si MAS NMR experiments.

1.4.2.2 Glass Batching

The binary end member glasses, $0.5Na_2S + 0.5SiS_2$ and $0.5Na_2S + 0.5PS_{5/2}$, of this ternary system were first synthesized by combining the stoichiometric amounts of each component of the composition in a vitreous carbon crucible. The mixture is melted for 3 minutes at a temperature of 670 °C for $0.5Na_2S + 0.5PS_{5/2}$ and 733 °C for $0.5Na_2S + 0.5SiS_2$. After a weight loss is collected for the first melt, the samples are melted again for an additional 3 minutes and then splat quenched between polished brass plates. Next, stoichiometric amounts of these binary glasses were combined to synthesize the ternary glass $0.5Na_2S + 0.5[xSiS_2 + (1-x)PS_{5/2}]$. Samples were splat quenched between brass plates for initial characterization.

The $0.67Na_2S + 0.33[xSiS_2 + (1-x)PS_{5/2}]$ glasses were made by milling stoichiometric amounts of Na_2S, SiS_2 and $PS_{5/2}$ and then melting the compositions in vitreous carbon crucibles inside the tube furnace hermetically sealed to the N_2 glove box. After this 1st melt, a weight loss is measured to check if the composition was still consistent with the target composition, accepting no more than 2% weigh loss. The sample was melted a second to obtain a melt that was casted and either splat quenched between brass plates or into a mold to make bulk disc samples.

1.4.2.3 Differential Scanning Calorimetry (DSC) – Glass Transition Temperature (T_g)

DSC measurements were taken using a Perkin Elmer Diamond calorimeter. Two sets of samples were placed in aluminum pans and hermetically sealed in a nitrogen glove box. The first sample pan was heated over a range of 50 to 400 °C at a rate of 20 °C per minute to determine both the T_g and crystallization temperature (T_x) of the glasses. Once this information was obtained, a second pan was heated pass the expected T_g, but before the T_x. This second experiment involved first a heating and cooling profile which was cycled through three times to ensure that the sample had a strong and consistent thermal history as well as provide multiple onset values to get the average T_g. Within the Pyris software, the glass transition temperature was collected by taking the onset value of the thermogram generated during a differential scanning calorimetry experiment. Three onset values were collected and averaged to give an average T_g of the glass sample. The T_g of the glass was also useful in predicting the maximum temperature for ionic conductivity measurements as well as providing annealing temperatures for bulk conductivity discs. The annealing of the glasses is of particular importance to the ionic conductivity

measurements in that the rate of annealing needs to match the heating rate for the frequency experiments in conductivity to prevent crystallization of samples.

1.4.2.4 Archimedes Principle – Density

Density measurements were made inside a nitrogen glove box on splat quench samples previously described above or when possible on cast bulk disc samples that were consistent in dimensions. Mineral oil was used as the immersion fluid since measurements were performed in a argon environment on hygroscopic samples. Three measurements were collected per sample and averaged to get the average density value of each sample.

1.4.2.5 Impedance Spectroscopy – Ionic Conductivity

Ionic conductivity measurements were carried out using the Novocontrol Technologies Concept 80 Impedance Spectrometer, using frequency scans from 0.1Hz to 10MHz over a temperature range -50 °C to 150 °C. These experiments were made on bulk glass discs on silver electrodes were painted on the samples to make electrical contact with the electrodes of the equipment. Because the samples are hygroscopic and measurements cannot be performed in a nitrogen environment, a special conductivity cell is built to protect the samples when they are removed from the glove box, but still enable accurate impedance measurements to be made. A schematic of this cell is shown in Fig 3.

1.4.2.6 Raman Spectroscopy

Raman spectra were collected using a 488 nm Argon laser on a Reinshaw inVia Spectrometer scanning from 100 to 700 cm^{-1} with a 5x objective lens. 10 accumulations are taken per sample lasting 20 seconds each in length. Because the samples are

susceptible to hygroscopic attack, they are contained in an acrylic sample holder which was sealed off by glass slide and vacuum grease.

1.4.2.7 Infrared Spectroscopy (Mid and Far IR)

Infrared spectra are collected using a Bruker IFS 66v/s Spectrometer. Samples measured in the mid and far infrared range (IR) were prepared by grinding and pressing it in dried cesium iodide (CsI) pellets. The mid IR was measured over the range of 400 cm^{-1} to 4000 cm^{-1} using a KBr beam splitter performing 32 scans at a 4 cm^{-1} resolution For the far IR 32 scan at a resolution of 4 cm^{-1} were collected over a scanning range of 100 – 700 cm^{-1} using a germanium coated Mylar beam splitter.

1.4.2.8 Magic Angle Spinning Nuclear Magnetic Resonance (MAS-NMR):

^{29}Si MAS NMR and ^{31}P MAS NMR experiments were done on a Bruker Avance II 600 Spectrometer. Phosphorus-31 is a dipolar nucleus with a Larmor frequency at 242 Hz. It is 100% abundant making it a great candidate for NMR spectroscopy. Silicon-29 is a dipolar nucleus but it only 4% abundant making it difficult but not impossible to probe. The Larmor frequency of silicon-29 is 119 MHz. Experiments using 4 mm zirconia rotors are spun at 12 kHz which also proved helpful in increasing the sample size and therefore signal of the low NMR active Si samples. Hydroxyapatite and siloxane were used for standards for phosphorus and silicon respectively. To observe the ratio of structural units, the NMR spectra are deconvoluted using Mestre Nova. Peak and side band areas of the spectra are fitted using Lorentzian-Gaussian curves.

1.4.3 Glass Notation

The structural units of the glasses will be noted with their periodic table symbol and a superscript denoting the amount of bridging sulfurs (BS), the amount of sulfurs networking, for that unit. For example Si^2 refer to the silicon tetrahedron that would have 2 BS and 2 non-bridging sulfurs (NBS).

1.4.4 Composition Dependence of Physical Properties Figures

Figures displaying the composition dependence of the physical properties of a glass system will include a linear interpolation between the binary end member glass values to help display the presence of a positive of negative MGFE as demonstrated in Figure 1.2.

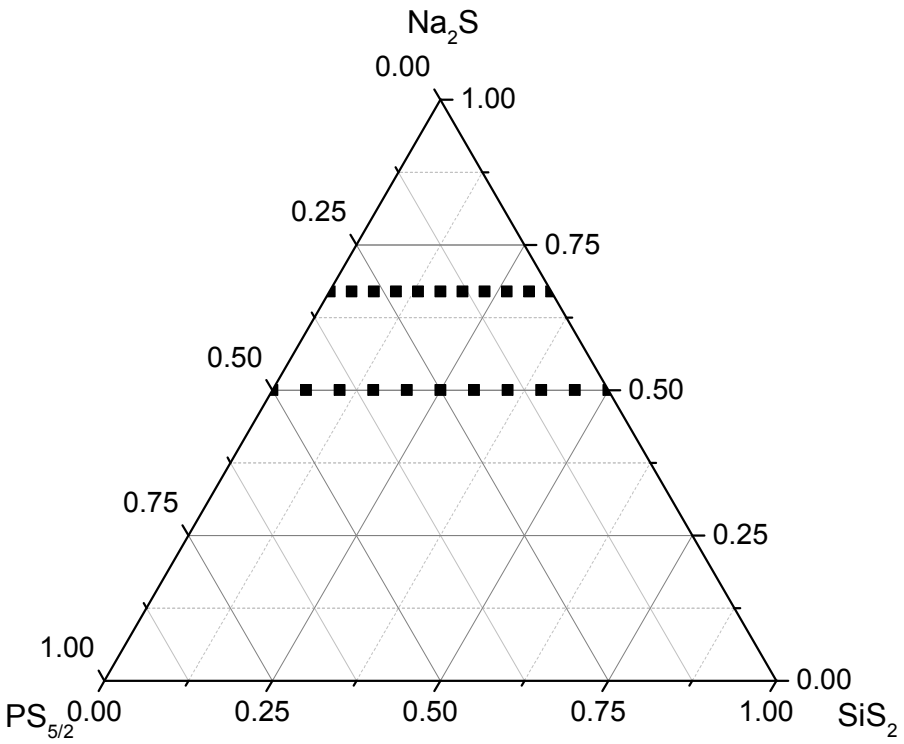

Figure 1.1 Ternary Composition Diagram of $yNa_2S + (1-y)[xSiS_2 + (1-x)PS_{5/2}]$ where y = 0.5 and 0.67

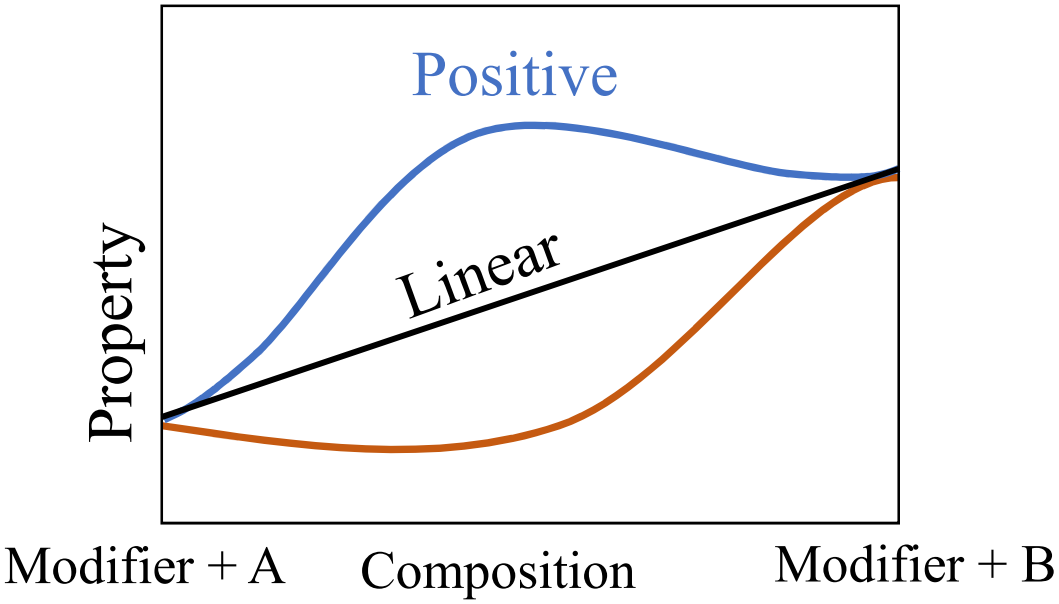

Figure 1.2 Example of the positive and negative MGFE as glass formers are varied

1.5 References

1. Administration, U.S.E.I., *Monthly Energy Review*, U.S.E.I. Administration, Editor. 2017.
2. Slater, M.D., et al., *Sodium-Ion Batteries.* Advanced Functional Materials, 2013. **23**(8): p. 947-958.
3. Kubota, K., et al., *Layered oxides as positive electrode materials for Na-ion batteries.* MRS Bulletin, 2014. **39**(5): p. 416-422.
4. Agrawal, R.C. and G.P. Pandey, *Solid polymer electrolytes: materials designing and all-solid-state battery applications: an overview.* Journal of Physics D-Applied Physics, 2008. **41**(22).
5. Navarra, M.A., *Ionic liquids as safe electrolyte components for Li-metal and Li-ion batteries.* MRS Bulletin, 2013. **38**(7): p. 548-553.
6. Kobayashi, T., et al., *All solid-state battery with sulfur electrode and thio-LISICON electrolyte.* Journal of Power Sources, 2008. **182**(2): p. 621-625.
7. Machida, N., et al., *Electrochemical properties of sulfur as cathode materials in a solid-state lithium battery with inorganic solid electrolytes.* Solid State Ionics, 2004. **175**(1–4): p. 247-250.
8. Nagao, M., et al., *In situ SEM study of a lithium deposition and dissolution mechanism in a bulk-type solid-state cell with a Li_2S-P_2S_5 solid electrolyte.* Physical Chemistry Chemical Physics, 2013. **15**(42): p. 18600-18606.
9. Linda F. Nazar , M.C., and Quan Pang, *Lithium-sulfur batteries.* MRS Bulletin, 2014. **39**(May): p. 436-42.
10. Shelby, J.E., *Introduction to Glass Science and Technology*. 2 ed. 2005, Cambridge UK: The Royal Society of Chemistry. 291.
11. Bischoff, C., *The Mixed Glass Former Effect in $0.5Na_2S + 0.5[xGeS_2 + (1-x)PS_{5/2}]$ glasses*, in *Materials Science and Engineering*. 2013, Iowa State University. p. 193.
12. Christensen, R., G. Olson, and S.W. Martin, *Ionic conductivity of Mixed Glass Former $0.35\ Na_2O + 0.65\ [xB_2O_3 + (1-x)\ P_2O_5]$ Glasses.* Journal of Physical Chemistry B, 2013. **117**: p. 16577-16586.
13. Christensen, R., *The mixed glass former effect in $0.35Na_2O + 0.65[xB_2O_3 + (1-x)P_2O_5]$ glasses*, in *Materials Science and Engineering*. 2012, Iowa State University. p. 172.
14. Christensen, R., et al., *The densities of mixed glass former $0.35\ Na_2O + 0.65\ [xB_2O_3 + (1-x)\ P_2O_5]$ glasses related to the atomic fractions and volumes of short range structures.* Journal of Non-Crystalline Solids, 2012. **358**: p. 253-589.
15. Christensen, R., G. Olson, and S.W. Martin, *Structural studies of mixed glass former $0.35\ Na_2O + 0.65\ [xB_2O_3 + (1-x)\ P_2O_5]$ glasses by Raman and ^{11}B and ^{31}P Magic Angle Spinning Nuclear Magnetic Resonance Spectroscopies.* Journal of Physical Chemistry B, 2013. **117**: p. 2169-2179.
16. Bischoff, C., et al., *IR, Raman and NMR Studies of the Short-Range Structures of $0.5Na_2S + 0.5[xGeS_2 + (1-x)PS_{5/2}]$ Mixed Glass Former Glasses.* Journal of Physical Chemistry B, 2014. **118**: p. 1943-1953.
17. Bischoff, C., K. Schuller, and S.W. Martin, *Short Range Structural Models of the Glass Transition Temperatures and Densities of $0.5Na_2S+0.5[xGeS_2 + (1-x)PS_{5/2}]$*

Mixed Glass Former Glasses. Journal of Physical Chemistry B, 2014. **118**: p. 3710-3719.

18. Cho, J. and S.W. Martin, *Structures and Ionic Conduction of $xNa_2S+ (1-x)SiS_2$ Glasses.* Role of Ceramics in Advanced Electrochemical Systems: p. 85-99.

CHAPTER 2. SHORT RANGE ORDER CHARACTERIZATION OF THE NA_2S+SIS_2 GLASS SYSTEM USING RAMAN, INFRARED AND ^{29}SI MAGIC ANGLE SPINNING NUCLEAR MAGNETIC RESONANCE SPECTROSCOPIES

A paper published in the Journal of Non-Crystalline Solids[1]

Deborah E. Watson[1], Steve. W Martin[2]

Department of Materials Science and Engineering, Iowa State University
Ames, Iowa 50010-2300

KEYWORDS : Sulfide Glasses, Thiosilicates, Fast Ion Conducting Glasses, Solid State Electrolyte, Sodium ion, Raman Spectroscopy, Infrared Spectroscopy, ^{29}Si MAS NMR Spectroscopy

2.1 Abstract

Sodium thiosilicate glasses are of interest in electrochemical applications as fast ion conducting solid state electrolyte materials. While some structural studies have been performed on this glass series, their short range order (SRO) structure has not been fully realized. Specifically the SiS_4 tetrahedra corner sharing behavior in these glasses appears to be less understood, particularly the existence and nature of the Si^3, where the superscript describes the number of bridge bonds of the form ≡Si-S-Si≡, structure in this glass system has not been fully examined. In this paper, glasses and polycrystals in the sodium thiosilicate system have been explored and characterized using a combination ^{29}Si Magic Angle Spinning Nuclear Magnetic Resonance (MAS NMR) spectroscopy,

---

[1] Primary researcher and author

[2] Corresponding author and principle investigator

infrared (IR) spectroscopy and for the first time Raman spectroscopy. Raman and IR spectroscopy have been used to determine the composition dependence of the structural units in this system. Specifically, the Raman spectra was used to differentiate corner shared Si^3, Si^2, and Si^1 units and edge shared Si^2 structure units.^{29}Si MAS NMR spectra were then deconvoluted to determine the composition dependence of the populations of these different structural units.

2.2 Introduction

2.2.1 Background

Electrochemical storage of grid level electrical energy has become important to the full implementation of renewable energy harvesters such as wind turbines and solar thermal and solar photovoltaic systems. In regions where adaptations of the existing fossil energy converters can no longer be adjusted either fast enough in real time to effectively manage the temporal nature of renewable energy, or enough in magnitude to effectively manage the large quantity of renewably sourced electrical energy, saturation levels of these renewable energy harvesters have been reached[2-6]. For these reasons, there is a renewed worldwide interest in developing effective means to "shave" and "shift" the electrical energy being harvested renewably[3]. One of the most efficient and cost effective means is to employ electrochemical battery-based systems. All-solid-state batteries based in part on glassy solid electrolytes, while in their early stages of development, none-the-less, have significant potential advantages over traditional liquid electrolyte based battery systems. Low cost, scalable, high conductivity and safe solid glassy electrolytes are gaining renewed research interest, even though such ion conducting glasses have been known and studied for more than a century [7-13].

Perhaps the most widely known and studied of all alkali ion conducting glasses are the simple binary alkali silicate glasses, of general composition $M_2O + SiO_2$ [8, 14-16]. These glasses are relatively poor conductors of alkali ions, exhibiting room temperature conductivities of typically no more than ~10^{-9} $(\Omega cm)^{-1}$ [17]. However, these glasses are nonetheless exceptionally low cost, strong glass formers, easy to prepare, and chemically durable. For these reasons, binary alkali silicate glasses are often model glass systems used to study the many orders of magnitude decoupling of the mobile alkali ion motion from the viscous-structural relaxation motions of the host glassy silicate network structure [18-20].

More recent work on sulfide analogues of alkali oxide glasses have reported many orders of magnitude higher room temperature conductivities, in some cases reaching ~10^{-2} $(\Omega cm)^{-1}$ [21] which has spurred renewed interest in exploring them as solid electrolytes in a new class of all solid state alkali-based batteries. For example, binary $Li_2S + P_2S_5$ glasses (and glass ceramics) have received significant research interest by Tatsumisago et al. [22-25]. Martin et al. have explored nearly all of the binary alkali thioborate glasses, $M_2S + B_2S_3$ [26-29], and have reported on them extensively. Quite surprisingly, the binary alkali thiosilicate glasses, $M_2S + SiS_2$, have received far less attention, although a few early reports on these glasses are available [30-32]. The binary lithium thiosilicate, $yLi_2S + (1-y)SiS_2$, glasses have been more extensively investigated, likely due to the greater interest in lithium-based batteries and the known higher ionic conductivities of lithium-based solid electrolytes. However, glass formation in the binary lithium thiosilicate system is very limited and appears to lie only in a narrow composition range around the y = 0.60 composition for normal splat quenching methods. Presumably, a

wider glass formation region could be achieved at more extreme quenching rates. For this reason, studies of the lithium thiosilicate system have focused more heavily on crystalline and partially crystalline glass ceramic materials and oxy-sulfide glass-ceramics [33-35].

In contrast, the sodium thiosilicates, $yNa_2S + (1-y) SiS_2$, while being much less studied, interestingly appear to be much better glass formers. For example, using roller quenching techniques, Pradel et al., were able to prepare glasses in the low modifier range of y = 0.1 to y = 0.33[32]. Martin et al. used splat quenching to prepare glasses from y = 0.4 to y = 0.75, a significantly wider glass forming range than that for the binary lithium thiosilicates[36]. The infrared (IR) spectra for all of these glasses were reported along with conductivities[36]. Eckert et al. has examined the ^{29}Si Magic Angle Spinning Nuclear Magnetic Resonance (MAS NMR) of these sodium thiosilicate glasses up to y = 0.6[32]. So far, it seems that no Raman spectra have been reported for the binary $Na_2S + SiS_2$ glasses. Therefore, a unique opportunity exists to use a combination of vibrational and NMR spectroscopies to explore the atomic level structures of this glass family.

In this new report, the $Na_2S + SiS_2$ glass forming system has been revisited because it serves as the foundation of a larger study of ternary mixed glass former solid electrolytes that are based upon the mixing of two different glass formers, such as $Na_2S + SiS_2 + PS_{5/2}$. In the study of this latter ternary system, it has been found that there are significant gaps in the precise details of the atomic level structures of the binary sodium thiosilicate glasses and which has proven to be a significant barrier to the full understanding of ternary glasses.

For these reasons, the short-range order (SRO) structure for all of the silicon Si^i structures has been investigated, where i is the number of bridging sulfur (BS) atoms, ≡Si-S-Si≡, to other Si atoms, see Figure 2.1. The coordination sphere around the Si atom in the binary $yNa_2S + (1-y)\ SiS_2$ glass forming system using IR, Raman, and NMR spectroscopies have all been examined. In particular, the full composition (y) dependence of the various SRO Si^i structures have been determined that exist in these glasses from the low alkali range, $yNa_2S < 0.5$, to the high alkali range, $yNa_2S > 0.5$. The number of non-bridging sulfur ions per Si, (NBSs), is 4-i, and these are charge compensated by the mobile Na^+ ions, see Figure 2.1 for the structure of these units. Glasses with high concentrations of Na_2S have received much more attention because it is these glasses that have the significantly higher Na^+ ion conductivities and are of more electrochemical interest. Hence, more is known of the structure of those glasses where the structure is based upon more depolymerized "salt-like" ions such as Si^1 and Si^0 groups, where $yNa_2S > 0.5$ and the number of NBS are relatively high, 3 and 4, and are the so-called molecular ions. In this study and for this reason, we have purposefully also examined the glass formation into the lower Na_2S content range (where it is possible to still prepare glasses) to explore the more network forming SRO groups, Si^4, Si^3, and Si^2 groups, that have received significantly less research attention.

It has been found that pure SiS_2 is a very high vapor pressure liquid and is a very poor glass former due to the strong preference of the Si^4 group to form edge-sharing groups, E^2Si^4, Figure 2.1, which form into long chain structures. Similarly, it has been reported that the Si^2 group, Figure 2.1, also forms these edge-shared structures, E^1Si^2, which in this case form molecular dimer anion $(NaS)_2Si(S_2)Si(NaS)_2$ units due to the fact

that this unit must also carry two NBSs [31]. Unknown so far is whether the Si^3 SRO group forms these-edge shared units, E^1Si^3, and if so, what is its structure.

Given the lack of detailed knowledge of the structures of these binary alkali thio-silicate glasses, we have begun a detailed study of the structure of these binary glasses and we report here on the use of IR, Raman, and NMR spectroscopies to probe the atomic level structures of the binary $Na_2S + SiS_2$ glass system. The SRO structures of some of the crystalline phases that exist in this system have been explored and used to help interpret the SRO structure of the glasses. As seen in other studies of these glasses and unlike their analogous alkali oxide silicate glasses, it is found that the edge-sharing structural SRO plays an important role in the structures of these sodium thiosilicate glasses for $yNa_2S \leq 0.5$. This study combines IR, Raman, and ^{29}Si MAS NMR spectroscopies to determine both the concentration (Na_2S) dependence of the various Si^i SRO structural groups that exist in these glasses and the connectivity of different SRO groups.

2.3 Experimental Methods

2.3.1 Sample Preparation

Sodium sulfide (Na_2S) and silicon sulfide (SiS_2) were synthesized to obtain highest purity. Sodium sulfide was synthesized via thermal dehydration of sodium sulfide nonahydrate ($Na_2S{\cdot}9H_2O$) (Sigma Aldrich) under vacuum over a temperature range of 25° to 200°C for 35 hours. The dehydrated crystals were then mechanically milled for 5 minutes in a stainless steel pot inside a N_2 glove box, and then heat treated at 200°C for 10 minutes. The x-ray diffraction pattern (XRD) of the resulting sodium sulfide was obtained to determine phase purity. Silicon sulfide was synthesized by combining

stoichiometric amounts of Si (Alfa Aesar 99.999% metals basis) and S (Alfa Aesar Puratronics 99.999% metals basis). To ensure thorough mixing, the Si and S were mechanically milled together before being placed in the silica ampoule. The ampoule was evacuated, placed in a tilted furnace and rotated at a 45° angle for a 48 hours during which reactants were heated from 50 to 970°C at 1 ºC/min, followed by cooling to room temperature. The final product was then removed from the ampoule in a N_2 glove box and mechanically milled to obtain a fine powder for glass batching purposes. XRD was used to evaluate the phase purity of each batch.

Samples were prepared by mixing stoichiometric amounts of Na_2S and SiS_2, melting these in vitreous carbon crucibles at temperatures between 770 and 800 °C for 6 to 7 minutes each in a tube furnace hermetically sealed to a nitrogen glove box. After the first melt, a weight of the melted charge was taken to ensure the composition was maintained. All batches exhibited a weight loss of less than 2%. Samples were then melted a second time and splat quenched (SQ) between brass plates.

In some compositions, where glasses could not be prepared by splat quenching, mechanochemical milled (PM)glasses were prepared by mixing stoichiometric amounts of sodium sulfide and silicon sulfide in a zirconia mill pot with 20 10mm diameter zirconia balls for 20 hours at 450 revolutions per minute (RPM). Amorphous character was verified by Raman spectroscopy and x-ray powder diffraction.

Polycrystal samples were prepared using the same initial procedure as the glass samples. After the first melt and determination of the weight loss, samples were poured into 2 mm thick discs and held at their respective crystallization temperatures for

approximately 45 minutes using an electrically heated mold. The crystallization temperatures were determined through differential scanning calorimetry by heating the glass sample at 20^{o}C/min and determining the onset temperature of the exothermic crystallization event. After an isothermal hold at the crystallization temperature for 45 minutes, samples were slow cooled at a rate of 1 °C/min from the crystallization temperature to room temperature.

2.3.2 IR and Raman Spectra of the Glasses and Polycrystals

The IR spectra were collected on the Bruker 66v/s spectrometer in the mid-IR (MIR) region using a KBr beam splitter and in the far-IR (FIR) region using a Ge coated Mylar beam splitter. Samples were diluted into dried CsI, ~ 2 to 5% concentration depending upon the composition, and pressed into pellets for analysis. 32 scans over the 110 to 4000 cm^{-1} range at a resolution of 4 cm^{-1} were collected for each sample. The Raman spectra were collected on a Renishaw inVia confocal micro-Raman spectrometer using a 488 nm Argon laser. A survey scan from 100 to 3000 cm^{-1} using 10 accumulations for 10 seconds per accumulation was collected to observe spectral regions of interest to the glass structure. The co-added spectra at a focused region were collected.

2.3.3 ^{29}Si MAS NMR Spectra of the Glasses and Polycrystals

^{29}Si MAS NMR experiments for these samples were performed on a 600 MHz Avance II Bruker spectrometer in 4 mm zirconia rotors spun at 12 kHz. A primary reference of TMS was used with siloxane as a secondary reference. Due to the long relaxation times of the silicon nuclei, the samples were doped with 0.5% manganese (II) sulfide (99.9% Alfa Aesar), a paramagnetic dopant, during melting. A recycle delay time of 45 seconds was found adequate to avoid saturation of the signal. To obtain good signal

to noise (S/N) ratios, however, in most cases, it was required to scan for multiple hours, up to 48 hours. The pulse width for these samples were 4.5 μsec.

2.4 Results

2.4.1 $yNa_2S + (1-y) SiS_2$ glass samples

Glass samples were prepared as described over the composition range of $0.4 \leq y \leq 0.60$, in 0.05 increments, and at $y = 0.67$ and 0.70 using the splat quenching method. The theoretical compositions corresponding to expected structural units are shown in Figure 2.1.Glasses beyond $y = 0.67$ have been studied previously[36] and are known to be comprised of stoichiometric amounts of the excess Na_2S and Na_4SiS_4 (Si^0) groups and are, for this reason, not as structurally important for this study. The $y = 0.70$ glass was prepared and studied to investigate the presence of polysulfides coming from Na_2S, see below, and to observe the structural characteristics of these glasses at the highest modifier content. It is, nonetheless, a significant observation that glasses can easily be prepared in this ultra-high Na_2S composition region where there are no network forming BS units; all of the sulfurs present are NBS. Such behavior is unique for the sulfide systems where highly modified glasses are found to be much better glass formers than their simple oxide analogues. For example, the binary $Na_2O + SiO_2$ is glass forming only out to ~ 40 mole % Na_2O, whereas described above glass formation in the $Na_2S + SiS_2$ system ***begins*** at 40 mole% Na_2S. Hence, we observe that the $0.33Na_2S + 0.67SiS_2$ composition is not readily glass forming with splat quenching methods but can be achieved using the roller quenching method [32] . In this study, it is shown that this composition can also be accessed through planetary milling. In this way, the $y = 0.33$ glass was prepared and will be further examine in the discussion section. The polycrystal analog of this composition

could be prepared and was used to examine the Si^3 SRO in this glass system. Intermediate compositions between the different theoretical compositions were synthesized to evaluate the compositional trends throughout the series.

2.4.2 $yNa_2S + (1-y)SiS_2$ polycrystal samples

Polycrystal samples were successfully synthesized according to the theoretical compositions described above as well as the y = 0.4 composition which has a composition intermediate between the Si^2 and Si^3 SRO structures and was examined to help better understand the character of the Si^3 unit. Crystallographic information on the y = 0.00 (SiS_2), 0.33 ($Na_4Si_4S_{10}$) and 0.67 (Na_4SiS_4) compositions are well known and have been reported elsewhere [37-39].

2.4.3 Raman and IR Spectroscopy

2.4.3.1 Raman Spectra of $yNa_2S + (1-y)SiS_2$ glass and polycrystal samples

The Raman spectra of the glasses and polycrystals in this series are shown in Figure 2.2. Pure SiS_2 is included as a reference (Figure 2.2b) with 5 spectral peaks which are well known: A_1 symmetric stretch (432 cm^{-1}), A_1^B companion mode (353 cm^{-1}), 2 T_2 modes (177 and 184 cm^{-1}), another T_2 mode (627 cm^{-1}) and E mode (140 cm^{-1}). The A_1, E and T_2 modes are associated with vibrations of the silicon tetrahedron, and the A_1^B companion mode is associated vibrations of the outer sulfurs of the edge sharing unit [38, 40]. The region between 320 and 450 cm^{-1} is where the most prominent peaks are observed for each composition. The polycrystal corresponding to the Si^3 SRO at y = 0.33 has one strong mode at 372 cm^{-1} and this peak is also present in the Raman spectra of the y = 0.40 polycrystal composition and as weak peak in the Raman spectra of the y = 0.50 composition. In contrast, the PM y = 0.33 glass shows two main peaks at 369 cm^{-1} and

410 cm^{-1}. It may be argued that the broadness of the peak due to the amorphous nature of the material causes it to be slightly shifted, approximately 3 cm^{-1}. In the Raman spectrum of the y = 0.33 polycrystal, a small peak at 391 cm^{-1} is observed and persists as a shoulder in the Raman spectra of the y = 0.40 composition polycrystal though it has not been defined previously. This peak is too far to be related to the peak at 410 cm^{-1} in the glass. It is nonetheless important to note that the PM glass spectrum is consistent with the spectra of the SQ glasses. For the y = 0.4 glass composition, these two main peaks are at 367 cm^{-1} and 407 cm^{-1} and are observed and persist out to the y = 0.50 composition. In the Raman spectra of the y = 0.40 and y = 0.50 polycrystals, there is a peak at 405 cm^{-1}. Notice that in contrast to the spectrum of the y = 0.50 glass, there is only one prominent peak in the polycrystal as opposed to the two found in the glass. It appears as if one conformation is preferred. Two structural units that could exist having the edge-sharing character of the alkali thiosilicates are a corner sharing Si^2 unit or an edge sharing E^1Si^2 unit, where one edge is shared by the two BS, Figure 2.1, see below.

As the Na_2S content increases, the peak at 367 cm^{-1} shifts to 374 cm^{-1}, growing in both width and magnitude, in comparison to the 407 cm^{-1} peak that appears little changed even up to the y = 0.55 composition. While the peak at 374 cm^{-1} remains in this position for the y = 0.60 composition, the peak at 407 cm^{-1} for the low y glasses, $y < 0.5$, shifts downward to 395 cm^{-1}. In the Raman spectra of the y = 0.60 polycrystal, the Si^1 SRO composition, a new peak is present at 376 cm^{-1} and is assigned to the symmetric stretch of the Si^1 unit. At the y = 0.67 composition, these two peaks merge to a single main peak at 397 cm^{-1}. A small broad peak is also observed at 468 cm^{-1}, which is associated with polysulfides in the form of Na_2S_n[41]. The Raman spectrum of the 0.67 polycrystal shows

one main peak at 400 cm^{-1}, which is assigned to the Si^0 SRO structure. The y = 0.70 composition retains the peak at 397 cm^{-1} but another peak is seen at 469 cm^{-1} which at this time is assigned to polysulfides.

2.4.3.2 IR of $yNa_2S + (1-y)SiS_2$ glass and polycrystal samples

The IR spectra of the glasses and polycrystal samples are shown in Figure 2.3. The IR of the glasses appear to exhibit similar trends and behaviors that were evident in the Raman spectra. In the FIR region, modes occurring at 300 cm^{-1} and lower, are attributed to Na^+ S^- vibrations, where the FIR spectrum of pure sodium sulfide, Na_2S, exhibits two modes at 203 cm^{-1} and 260 cm^{-1}. The main vibrational modes in these sodium thiosilicate glasses are in the MIR from 400 to 700 cm^{-1}. Above 900 cm^{-1}, the IR peaks are attributed to minor oxide contamination in the glasses that is estimated to be no more than 5 wt. %. The IR spectrum of the y = 0.33 PM glass again resembles spectra of the SQ glassed samples. The spectrum shows three modes at 460 cm^{-1}, 530 cm^{-1} and 612 cm^{-1}. The IR spectrum of the y = 0.40 glass shows three main modes at 450 cm^{-1}, 515 cm^{-1} and 606 cm^{-1}, with a weak shoulder at 546 cm^{-1}. In the IR spectra of the rest of the glasses in this series, the three modes first seen in the y = 0.40 glass composition decrease in intensity up to the y = 0.60 and 0.67 glass compositions. The consistency between the IR spectra of the y = 0.55 and 0.60 glasses, having modes at 561 cm^{-1} and 560 cm^{-1} respectively, indicate a shared structure between this intermediate and theoretical compositions. Finally, these modes are replaced in the y = 0.67 (Si^0) glass composition with one main mode at 500 cm^{-1}.

The IR spectra of the polycrystal $yNa_2S + (1-y)SiS_2$ series are shown in Figure 2.3b. In the MIR spectrum of the y = 0.33 polycrystal, a pair of doublets can be observed

at 522 cm^{-1} and 540 cm^{-1}, and also at 584 cm^{-1} and 608 cm^{-1}. A similar, less resolved set of doublets are seen in the spectrum of the y = 0.40 composition as well, the first at 525 cm^{-1} and 540 cm^{-1} and the second at 588 cm^{-1} and 605 cm^{-1}. At higher Na_2S concentrations, these doublet pairs each gradually converge into one main mode, at 525 cm^{-1} and 600 cm^{-1}, respectively. The mode at ~520 cm^{-1} has been assigned[35] to the vibration of the Si-S^- Na^+ NBS bond, whereas the mode at ~600 cm^{-1} has been assigned to the Si-S-Si BS vibration. In the y = 0.60 composition, these two modes are present, as in the IR spectra of the lower concentration polycrystals. The mode at ~ 600 cm^{-1}, the BS mode, becomes a shoulder in the y = 0.60 composition, Si^1, which as 1 BS and 3 NBS, while the 525 cm^{-1} NBS mode remains strong. The modes at 469 cm^{-1} and 550 cm^{-1} – characteristic of the $Na_6Si_2S_7$ structure – and 567 cm^{-1} continue to become more defined (Figure 2 3b). In the IR spectra of the y = 0.67 polycrystal phase, Na_4SiS_4, these peaks merge together and a prominent mode at 522 cm^{-1} is observed with a shoulder at ~602 cm^{-1}. At this composition, the network should be completely depolymerizes due to the Na_2S concentration, which would support this assignment of NBS at ~520 cm^{-1}.

2.4.3.3 Deconvolution of Raman Spectra for $yNa_2S + (1-y)SiS_2$ glass samples

To further understand which SRO structural units may be giving rise to the different features in the spectra, Raman spectra of each composition was deconvoluted using Gaussian curves to fit the spectra. The spectra were deconvoluted over the entire range from 100 – 700 cm^{-1}, an example of which is given in Figure 2.5 for the y=0.33 glass, but special focus was given to the main spectral region of interest, 320 to 460 cm^{-1}. Successful fits were achieved using four to five Gaussian curves underneath the two main peaks that exist throughout the compositions in this series. These Gaussians consistently

were found at 335 ± 1 cm^{-1}, 342 ± 3 cm^{-1}, 365 ± 4 cm^{-1}, 372 ± 1 cm^{-1}, 385 ± 4 cm^{-1} and 400 ± 4 cm^{-1}, and 408 ±5 cm^{-1}. The peaks beyond this region can be attributed to polysulfide vibrations[41]. The fits of these spectra are given in the Figure 2.5 and the analysis in Table 2. The Raman spectra of the polycrystal samples were used to determine to further identify the modes at these particular positions and will be discussed later in the discussion section.

2.4.4 ^{29}Si MAS NMR Spectroscopy

2.4.4.1 $yNa_2S + (1-y)SiS_2$ glass samples

The ^{29}Si MAS NMR spectra of the $yNa_2S + (1-y)SiS_2$ glass series are shown in Figure 2.4a. The spectra are defined by two main resonances that evolve over the compositional range. In past studies of these thiosilicate glasses, the resonances occurred in the region between -5 ppm and -15 ppm and have been assigned to edge-sharing structures, e.g., E^1Si^2, see Figure 2.1, while resonances above 0 ppm were assigned to corner sharing structures, e.g., Si^2. The ^{29}Si MAS NMR spectrum of the y = 0.33 PM glass has two resonances at 1.45 ppm and – 10.68 ppm. In the spectrum of the y = 0.40 glass, the two resonances appeared at 2.02 ppm and -11.01 ppm. Eckert et al. have attributed the resonance at 2 ppm to either the corner sharing Si^3, or Si^2 groups and the resonance at -11 ppm to the E^1Si^2 unit [32]. The up field peaks change little until the y = 0.60 composition while the peaks downfield seem to systematically shift further downfield, by ~1 ppm. The fully depolymerized glass, y = 0.67, where all SRO is NBS, Si^0, appears to change little from the y = 0.60 composition. Interestingly, in the ^{29}Si MAS NMR spectrum of the y = 0.67 glass, the resonance located at -7.87 ppm is in the region expected for edge-sharing units. This composition is expected to be comprised solely of

the Si^0 SRO structural group, see Figure 2.1, and therefore no networking, i.e. no BS units, is expected among the silicon sites. Even so, some edge sharing (Si^2) structural group character remains in the glass. Perhaps this ESi^2 dimer is very stable and able to persist even at high modifier contents.

Significantly, the ^{29}Si MAS NMR of the y = 0.70 glass is little changed from that of the y = 0.67 glass in that there still is relatively large absorption intensity in the range where the edge-sharing Si^2 units have been assigned. At this composition, based upon the expected phase diagram and the lever rule of the appropriate compounds, one would expect that this glass would be comprised of approximately 91% Na_4SiS_4 (the Si^0 SRO) and 9% free Na_2S. Returning to the Raman spectra, Figure 2.2a shows that the y = 0.67 and 0.70 glasses show scattering intensity only arising from the Si^0 SRO group and none from the edge sharing Si^2 group. A possible explanation for this difference could arise from a disproportionation reaction where the Si^0 SRO groups splits into free polysulfides moieties such as Na_2S_n, where n is a small number like 2 or 3, and the Si^2 group. The veracity of this hypothesis will be explored further below using the ^{29}Si MAS NMR and Raman spectra deconvolution results to determine the Si SRO unit populations and map them as a function of composition. The ^{29}Si MAS NMR spectra are fitted with Gaussians representing specific SRO units. The areas are then collected and used to calculate the percentage each unit contributes to the spectrum. The population of each SRO unit can be determined from this. The deconvolution results from the Raman, while not as quantitative as the NMR, can still be used to inform what SRO units should be observed in the NMR spectrum. This SRO map as a function of composition is shown in Figure 2.7.

2.4.4.2 $yNa_2S + (1-y)SiS_2$ polycrystal samples

The ^{29}Si MAS NMR spectra of the polycrystal samples prepared in this study are shown in Fig. 7. The ^{29}Si MAS NMR spectrum, as seen in the previous literature[31, 32, 42], of the y = 0 polycrystal, c-SiS_2, shows a single sharp resonance at -21.7 ppm and arises from the single Si site in the dual edge-sharing E^2Si^4 group known to exist in the $SiS_{4/2}$ edge sharing chains in this structure, see Figure 2.1. The NMR spectrum of the y = 0.33 polycrystal, nominally the composition $Na_2Si_2S_5$, shows an intense doublet centered at 0 ppm and a very weak intensity doublet centered at -20 ppm. Eckert et al. have assigned the doublet resonances at 2.7 and 0.6 ppm to arise from the adamantane-like molecular structure $Na_4Si_4S_{10}$, see Figure 2.1[31, 32]. The adamantane structure is known for this composition and its formation is accompanied with the formation of the chain structure for SiS_2 are likely reasons that the low Na_2S content glasses are poor glass formers. In the case of SiS_2, the network bonding dimensionality is 1 and for the $Na_4Si_4S_{10}$ adamantane structure, its network dimensionality is zero, both leading presumably to low viscosity and hence facile crystallization of the melt. The two resonances for the y = 0.33 polycrystal demonstrate that there are two unique Si^3 units contained in the adamantane structure. The two very weak ^{29}Si MAS NMR resonances, that are barely visible above the background noise at -19.1 and -17.1 ppm have not been described in the literature but are in the region where edge sharing Si^4 units are found (~ -21 ppm), see the ^{29}Si NMR spectrum for the y = 0.00, pure c-SiS_2 phase. It is possible that a small concentration, < 2 %, of these edge sharing species remains in the structure.

The y = 0.40 polycrystal is expected to consist of a lever rule mixture of 59% of the y = 0.33 (Si^3) and 41% of the y = 0.50 (Si^2) crystalline phases, whereas a peak area

analysis of these resonances gives slightly different values of 49% and 51% for Si^3 and Si^2 groups, respectively. The spectrum consists of two sets of resonances, a doublet centered at ~ 2 ppm arising from the Si^3 adamantane SRO group and a single sharp resonance at ~-10 ppm arising from the edge sharing E^1Si^2 group, see Figure 2.1. This assignment agrees well with the spectrum collected for the y = 0.50 composition, which shows only the expected single resonance at -9.9 ppm arising from the expected ESi^2 SRO structure. These results match the spectra reported by Eckert et al. where they reported the ^{29}Si MAS NMR spectrum for the high temperature (HT) phase β-Na_2SiS_3 polycrystal, which is proposed to be solely E^1Si^2 molecular anion units[31]. The extended chain structure is the low temperature (LT) α-Na_2SiS_3 phase of the Si^2 composition, see Figure 2.1, and Eckert et al. were able to prepare this phase and observed a single sharp resonance at 3 ppm[31]. Surprisingly, while the slow cool preparation method was able to access the β-Na_2SiS_3 phase, it was unable to prepare this LT phase, despite lengthening the slow cool period. The y = 0.60 polycrystal is expected to consist of the $Na_3SiS_{2/2}S_3$ Si^1 SRO and the ^{29}Si MAS NMR of this phase is consistent with this structure in that it shows a single sharp resonance at 6.9 ppm due to the Si^1 unit and a weak resonance where the ESi^2 peak was seen in the y = 0.50 composition spectrum. Finally, the y = 0.67 polycrystal is expected to be comprised of the Si^0 SRO, Na_4SiS_4, and in agreement with this the spectrum has a single resonance at 8.4 ppm which is assigned to this Si^0 unit.

2.4.4.3 Deconvolution of ^{29}Si MAS NMR Spectra for $yNa_2S + (1-y)SiS_2$ glass samples

The deconvolution of the ^{29}Si MAS NMR spectra was carried out, like the Raman spectra, to give more insight into the SRO of the glasses. Using the analysis and peak assignments from the ^{29}Si MAS NMR spectra of the glasses and polycrystals, Gaussian, or Gaussian-Lorentzian mixed curves were used to fit the line shapes of each glass composition from y=0.33 to 0.70. Successful fits were achieved using three to four Gaussians to fit the line shape spanning from approximately 20 to -20 ppm. The Gaussians, relating to a specific SRO unit, were centered at approximately -11 ppm ± 3 (ESi^2), -1 ppm (Si^3-Site 1), 1 ppm (Si^3-Site 2), 4 ppm (Si^2), 6 ppm (Si^1), 7 ppm (Si^0), and 13 ppm (Si^{1Si}). The fits of these spectra are given in the S.I. Fig. 2 and the analysis in S.I. Table 2. These finding will be discussed below in the discussion.

2.5 Discussion

2.5.1 Low Modified sodium thiosilicate glasses (y <0.5)

The y = 0 glass, g-SiS_2, has been well studied [31, 38-40, 43] and is proposed to have both edge, E^2Si^4, and corner sharing Si^4 units, while the crystalline analog, c-SiS_2 consist only of chains of edge sharing units, E^2Si^4. The PM technique was able to synthesize the theoretical Si^3 structure glass at y = 0.33 which was inaccessible through splat quenching techniques. The Raman spectra for this y=0.33 glass shows five prominent peaks: 369 cm^{-1} associated with the Si-S-Si BS stretch, 410 cm^{-1} associated with NBS, 484 cm^{-1} associated with polysulfide compounds, and 520 cm^{-1} and 627 cm^{-1} which may be related to the T_2 mode associated with the silicon tetrahedron, also identified in pure SiS_2 [40]. The 520 cm^{-1} sharp peak is uncharacteristic in relation the character of this planetary milled glass and is also not seen in the remaining spectra of this glass series. However

this peak at 520 cm^{-1} is characteristic of elemental Si. Perhaps during the mechanical milling process Si is being ejected from the mixture. The peak at 627 cm^{-1} becomes less and less prominent as the composition shifts to higher and higher Na_2S concentrations, which supports the hypothesis that this mode has its origins from the T_2 mode of the silicon tetrahedron. In the spectrum of the corresponding y = 0.33 polycrystal, strong spectral peaks are observed at 210, 268 and 372 cm^{-1}.

These peaks are also observed in the y = 0.40 polycrystal, which is the intermediate composition, but not in the y = 0.50 Si^2 composition. These three peaks are therefore proposed to be the three A_1 symmetric stretching modes resulting from the $Na_4Si_4S_{10}$ adamantane structure [37, 44-46] and therefore characteristic of the Si^3 structure unit. The peaks at 372 and 391 cm^{-1} of the polycrystal fall between the two main spectral peaks at 369 and 410 cm^{-1} seen in the Raman spectrum of the glass. When deconvoluting the glass spectrum in the region between 340 and 420 cm^{-1}, a third Gaussian, in addition to the two Gaussian for the two visible peaks, can be placed in between them at 385 to 392 cm^{-1}. This peak is not reported in literature, but it could be associated with another structure type in the glass. The spectral peak at 410 cm^{-1} has been associated with NBS on the Si tetrahedra [47, 48], analogous to the lithium thiosilicates. This peak makes up approximately half of the area of the peak found at 369 cm^{-1}, which has been assigned with BS [47, 48]. Using the areas from the deconvolution of the spectra, the ratio of BS to NBS in this composition is found to be 2:1. The theoretical BS to NBS ratio is 3:1 and does not match up with this experimental result. A possible reason is that these peaks do not represent BS and NBS only, but could be further associated with populations of corner-sharing and edge-sharing structures.

In their ^{29}Si MAS NMR study of the sodium thiosilicate glasses ranging from y = 0.00 to 0.60, Eckert et al. observed the presence of the ESi^2 SRO structure unit in the y = 0.33 glass[32]. In our study here, the y = 0.33 and 0.40 polycrystals and glasses were synthesized in order to isolate the previously unreported Si^3 SRO. The Raman and ^{29}Si MAS NMR spectra both point to the presence of the $Na_4Si_4S_{10}$ structure. As described above, the Raman spectra of both the y = 0.33 and 0.40 polycrystals have Raman spectral modes at 372 and 374 cm^{-1}, respectively, and ^{29}Si MAS NMR resonances at 2.7 and 0.6 ppm which are consistent with the presence of Si^3 SROs in the adamantane structure. In comparison, the Raman and NMR spectra of the 0.33 and 0.40 glasses are too convoluted to show any distinct features relating to these adamantane Si^3 structures at 372 cm^{-1}. However, deconvolution of the Raman spectrum of the y = 0.40 glass shows that one weak Gaussian peak can be observed at 371 cm^{-1}. Perhaps it may be possible to assign this 372 cm^{-1} spectral peak to the Si^3 unit. Whether the Si^3 in the glass is a part of an adamantane structure, like in the polycrystal analogs, or in "free" corner-shared unit is unclear.

The ^{29}Si MAS NMR spectrum of the mechanically milled y = 0.33 composition agrees with the spectra of the SQ samples. The y = 0.33 spectrum shows two resonances at 1.45 ppm and - 10.68 ppm. The NMR spectrum of the y = 0.4 glass has an intense peak at 2.02 ppm, slightly shifted from y = 0.33, which could be assigned to the Si^3 SRO seen at 2.7 ppm in the NMR spectrum of the y = 0.40 polycrystal. In the glass, the doublet for the two Si^3 SRO sites in the adamantane structure, merge to a single broad resonance in the glass presumably due to the disorder of the glassy state structure. The width of this peak is sufficiently broad to encompass both Si sites of the adamantane structure, or it

could simply arise from one Si^{3B} structural SRO group. If this latter hypothesis were indeed the case that only one resonance existed in this glass for the Si^3 unit, this would suggest that the glass structure has broken up the adamantane cage in such a way that now leads to one type of Si^3 unit, the "normal" Si^{3B} unit. The IR and Raman spectra of the polycrystals at the y = 0.33 and y = 0.40 compositions are entirely conclusive on this point. The Raman spectra of the y = 0.33 and 0.40 polycrystals as discussed above have only a single peak for the two Si^3 sites in the adamantane structure. However, as discussed above, the deconvolution of the broad Raman spectral feature centered at 370 cm^{-1} can be deconvoluted into two components, one for each of the two Si sites in the adamantane structure. The IR spectra of the y = 0.33 and 0.40 polycrystals clearly show two distinct resonances for the Si^3 structure. However, the IR spectra of the y = 0.33 and 0.40 glasses are so broad that the spectral features in the 550 cm^{-1} to 400 cm^{-1} region could be deconvoluted to nearly any number of separate peaks and it is therefore inconclusive of the presence of two separate Si^3 species in the adamantane structure in the glass.

Deconvolution of the ^{29}Si MAS NMR spectrum of the y = 0.33 PM glass with two Gaussians, one centered at 1.06 ppm and another at -11.61 ppm gives a distribution of 61:39 Si^3 structures to Si^2 structures. The presence of the Si^2 structures comes from the edge sharing dimers (ESi^2) that are maintained throughout the series. This supports the preference of the edge-sharing behavior in the thiosilicate systems despite containing enough sodium sulfide to create corner-sharing structures. A deconvolution modeling the two unique Si sites of adamantane structure yields a similar ratio of SRO units, having 60:40 Si^3:Si^2. The deconvolution of the broad NMR resonance at 2 ppm for the y = 0.40

glass results in two Gaussians, one at 1.64 and -1.27 ppm and therefore may be associated with the two Si^3 sites in the adamantane structure. The other resonance at -11 ppm for the y = 0.40 glass is assigned to Si centers in the E^1Si^2 SRO group. Finally, a Gaussian for corner shared Si^2 SRO group is included at 5.51 ppm. When the y = 0.40 spectrum is fit with four Gaussians, one to account for ESi^2 and another for CSi^2, and two peaks for each unique Si^3 in the $Na_4Si_4S_{10}$ structure, a ratio of 61:39 is found for Si^3:Si^2 and a ratio of 61:35:4 is found for Si^3:ESi^2:Si^2. For charge balance between the Si^3 and Si^2 SRO units to match the Na^+ charge for the y = 0.40 composition ($0.8Na^+/0.6Si = 1.33\ Na^+/1\ Si$), the expected ratio for Si^3 to Si^2 is 2:1. While the experimental values do not exactly match the theoretical values, a possible explanation could come from considering if this glass is not exactly y = 0.40. For example, in the composition y = 0.41, the theoretical populations turn out to be 61:39 Si^3 to Si^2 which matches the populations derived in this analysis. Perhaps it is reasonable to have a majority of edge sharing Si^2 instead of the corner sharing Si^2 since edge sharing is more favored in silicon sulfide than corner sharing.

In the y = 0.45 glass, the theoretical ratios of Si^2 to $Si^3$are 64:36. Using four Gaussians to deconvolute ^{29}Si MAS NMR spectrum of the 0.45 glass, the ratio of Si^2 to Si^3 is found to be 59:41, which is consistent with an increase in the fraction of Si^2 units as the composition approaches the pure Si^2 glass composition at y = 0.50. Both the edge-sharing and corner-sharing Si^2 population increases in the y = 0.45 glass as the Si^3 population decreases. If these fits are accurate, this again would point to two unique types of Si^3 units, much like its polycrystal counterpart which arose from the $Na_4Si_4S_{10}$ structure. The deconvolution of the Raman spectrum can be fit with four Gaussians

comprising the main peak region as found in the 0.40 spectrum; two Gaussians corresponding to the two unique Si^3 types, one for corner sharing Si^2 and another for ESi^2. This result complements the ^{29}Si MAS NMR deconvolution result of having two unique sites for Si^3. The y = 0.50 glass would have the theoretical Si^2 structure. The NMR spectra of the composition shows two distinct resonances at 4 ppm and -10 ppm, corresponding to corner sharing and edge sharing Si^2 structures, respectively.

2.5.2 High Modified sodium thiosilicate glasses (y ≥ 0.50)

As discussed above, the Raman spectra, much like the NMR spectra, shows two distinct peaks that are assigned to BS and NBS modes associated with the Si tetrahedra in the network rather than each spectral peak being associated with a specific structural unit. However, perhaps this BS and NBS assignment could be extended, through the results found here, to specific spectral peaks to unique structural units found in the glass network. As described above, the Raman spectrum of y = 0.50 polycrystal shows only one peak located at 405 cm^{-1}. From Eckert et al, NMR evidence shows that a high temperature (HT) and low temperature (LT) phase of the Na_2SiS_3 compound can exist[31]. The ^{29}Si MAS NMR spectrum of the y = 0.50 polycrystal shown in Figure 2.4b agrees with the spectrum Eckert provides for the HT-Na_2SiS_3 structure which consists of ESi^2 structural units. Perhaps then, this Raman peak at 405 cm^{-1} could be assigned to the ESi^2 unit. In this work, an unsuccessful attempt was made to prepare the LT- Na_2SiS_3 phase that is proposed to correspond to the corner shared Si^2 unit. However, if the ESi^2 peak does reside at ~405 cm^{-1}, then an explanation must be given to explain why there no longer is a peak visible for the ESi^2 unit in the Raman spectra of glasses at higher Na_2S contents, where the ^{29}Si MAS NMR spectrum suggest ESi^2 SRO group is still present.

Reflecting back on the deconvolution data for the Raman spectra of these glasses, the Si^2 peak is still present at 414 cm^{-1}, but it is hidden in the broadness of the Raman spectrum. The IR spectra demonstrate much of the same behavior that is exhibited in the Raman spectra. The Si-S-Si stretch at 600 cm^{-1}, which is analogous to the BS peak in the Raman at 360 cm^{-1}, diminishes as the composition goes to higher modifier concentrations. It is not difficult to see that the remnant of that mode may lie underneath the broadness of the spectrum of the y = 0.67 glass.

The y = 0.55 glass composition is expected to contain the Si^2 (y = 0.50) structure and Si^1 (y = 0.60) structure. The Raman spectrum of this glass shows two peaks that merge into a single peak at higher Na_2S contents. The peak at 360 cm^{-1} shifts to 374 cm^{-1} and broadens having a full-width at half-maximum (FWHM) value that increases from 18 to 28.5. The deconvolution of the spectrum shows that two Gaussians can be fitted under this peak, one at 361 and 376 cm^{-1}. This suggests the assignment of the 360 cm^{-1} peak to the CSi^2 structure and the 376 cm^{-1} peak to the Si^1 structure. The Raman spectrum of the polycrystal of y = 0.60 shows a single peak at 376 cm^{-1} which is consistent with this assignment. The ^{29}Si MAS NMR spectrum of the y = 0.55 glass has two main resonances at 4.7 ppm and -11.3 ppm, with a shoulder at 14.4 ppm. When deconvoluted, three Gaussians peaks can be used to fit the spectrum. The peak at 4.7 ppm corresponds to Si^1 SRO units, while the peak at -11.3 is known to correspond to ESi^2 units. There may be some corner shared Si^2 units within the 4.7 ppm peak as well. The peak at 14.4 ppm, however, has not been characterized in literature[32]. This feature has a stronger presence is the y = 0.60 glass.

The IR spectrum of y = 0.60 glass agrees with literature values indicating the presence of the Si^1 dimer in the $Na_6Si_2S_7$ structure[36]. This agrees well with the Raman spectra where the NBS and BS peaks shift closer together and have near equal area (44:56), perhaps implying these sulfurs are found on the same structural unit. The Raman spectrum of the polycrystal characterizes the BS peak from the glass as the Si^1 structural unit. Interestingly, no peak at 407 cm^{-1} is seen in the Raman spectra of the y = 0.60 polycrystal. This fact may suggest that it would be more suitable to assign the BS peak to corner -sharing structures. This merging of the corner-sharing and edge-sharing peaks may also indicate a conversion of the ESi^2 units to Si^1 units, perhaps even Si^0 units. In fact, the deconvolution and fitting of the Raman spectrum does show a Gaussian at 396 cm-^{1}, consistent with the presence of Si^0. The deconvolution of the ^{29}Si MAS NMR spectra shows a decrease in the population of ESi^2 structures from 27% to 23%, as well as evidence for Si^0 with a Gaussian at 8 ppm which would corroborate the Raman peak at 396 cm^{-1} assigned to Si^0. The 4% difference between the ESi^2 population of the 0.55 and 0.60, however, does not all directly transfer into the Si^1 resonance peak, but rather a portion manifests as a shoulder on the Si^1 peak at ~14 ppm. This behavior is also seen in the y = 0.55 spectrum. The intensity of this shoulder increases slightly from the 0.55 glass to the 0.60 glass, but drops to zero for the y = 0.67 and 0.70 glasses. No assignments of this resonance have been made in the literature for these sodium thiosilicate glasses. The higher chemical shift indicates this silicon site is much more deshielded than the other silicon sites in the glass. Perhaps this 14.4 ppm resonance in the y = 0.55 glass and 13.8 ppm in the 0.60 glass may belong to another type of Si^1 unit coming from the ESi^2 dimer.

In the y = 0.50 glass, there were two resonances, one for corner sharing Si^2 units and the other for the ESi^2 dimers. The corner sharing Si^2 unit may be a part of an "infinite" chain of Si^2 units. Perhaps when this chain structure reacts with Na_2S, a Si^1 unit is formed and resides at the end of the chain, a terminating unit. In the case of the ESi^2 dimers, reaction with Na_2S could create a Si^1 dimer. However, this structure may not produce a shift that is as deshielded as the structure at 14 ppm. One explanation for this highly deshielded structure is that perhaps this dimer contains a Si-Si bond rather than a Si-S-Si BS, much like the P^{1P} structure found in thiophosphate glasses[49]. In a study of the analogous sodium thiophosphate glass series, the P^1 structure had a resonance of 93 ppm while the P^{1P} structure, ≡P-P≡, had a resonance of 101 ppm, 8 ppm shift apart. Here, the Si^1 has a shift of 6.5 ppm while the other resonance (Si^{1Si}) is at 13.8, ~7.3 ppm apart. In the ^{29}Si MAS NMR spectra of the y = 0.55 glass, the shifts at 4.7 and 14.4 ppm are 9.7 ppm apart. In order to further confirm this, the ^{29}Si MAS NMR of analogous compounds to this structure such as Si_2S_6 as proposed by Tenhover in Si rich thiosilicate glasses should be studied[40]. The Raman spectra may give an indication that this could be correct due to the presence of polysulfides[41] with a spectral peak at ~460 to 470 cm^{-1}. This might be in the form of Na^+ ^-S-S^- Na^+ chains.

The y = 0.67 glass should consist solely of Si^0 SRO units. The IR and Raman spectra of these glass show modes at 500 cm^{-1} and 397 cm^{-1}, respectively, both due to Si^0. The vibrational spectra of this polycrystal also shows the existence of Si^0 structure. The ^{29}Si MAS NMR of the y = 0.67 glass, however, shows two resonances much like the rest of the glasses in this series. One resonance at 7 ppm and another at -7 ppm. The latter resonance lies in the region where edge-sharing structures exists. This implies that a

small population of ESi^2 groups (25%) exists at this composition despite the fact that the modifier concentration is enough to depolymerize all the tetrahedra. This peak is shifted higher than where it is expected to occur for ESi^2 (-10 ppm), but perhaps this is just due to changes or evolution of the Si^3 nuclei that is causing deshielding. Evidence to support this claim may be seen in the IR spectra of the glasses and polycrystals in the composition. As described above, in the IR spectra there is a weak mode at 432 cm^{-1} which may correspond with an edge sharing structure. This peak is seen throughout the series matching what we see in NMR.

The y = 0.70 glass is expected to contain Si^0 units with a slight excess of Na_2S. This is clearly displayed in the rise of polysulfide structures as shown in the Raman spectrum having an intense peak Raman peak at 460 cm^{-1} or higher and nearly matching the intensity of the peak coming from the Si^1units. The MIR spectra shows little to no changes between the y = 0.67 and 0.70 glasses, confirming the presence of Si^0 SRO unit. The ^{29}Si MAS NMR spectra strongly resembles the y = 0.67 spectrum as well, with resonances at 6.3 ppm and -7.1 ppm. There also seems to be broad resonance at -34 ppm which may be due to a Si-O contamination coming for the Na_2S starting material. One interesting note is the decrease in the population of units from the y = 0.67 composition to the 0.70. In the 0.67 glass, the ratio of Si^0 units to the remaining ESi^2 units was 3:1, while in the y = 0.70 glass, the ratio is almost 2:1. The population under the ESi^2 peak increased. Perhaps this is an indication that there are new species being formed that are not being accounted for. These structures could be Si tetrahedra motifs that lose sulfurs contributing to the increase in polysulfide concentration and the formation of new unique structural units.

Based on these trends shown in the composition mapping diagram from ^{29}Si MAS NMR and Raman spectra presented in Figure 2.7, the Si SRO structures at each composition can be further elucidated. In order to fit all of the spectral envelopes for all of the glass compositions in this series, it was necessary for each spectra to shift the centroids of the fitted bands slightly. For all bands, this peak shifting was at most 3 cm^{-1}. The peak positions shown in Table 1 therefore are the average positions of the individual peaks used in the fitting of all of the spectral envelopes for all of the glasses studied. While the area of the Raman spectral intensity cannot be taken to indicate exact populations, the area of the NMR spectral absorptions can. Further, as discussed at length above, the intensity and presence of the Raman peaks at certain frequencies can be used to identify which SRO structures are present at each composition. For example, the Si^3 SRO structure was believed to exist in the low modified glasses ($0.33 \geq y \geq 0.50$), and a spectral peak at 364 cm^{-1} is observed and the position of which appears to change only slightly across each of these four compositions. On the other hand, this peak was also thought to be characteristic of corner shared Si^2 units. Though it does not perfectly match the trend of the NMR map, the full compositional trend of the corner shared Si^2 SRO in both these techniques, however, suggests that this mode at 364 cm^{-1} is associated with the corner shared Si^2 SRO.

Further, in the NMR spectra of these glasses, a consistent resonance absorption which has been associated with the ESi^2 structure has been observed. These findings support the assignment of the 409 cm^{-1} spectral peak in the Raman to the ESi^2 structure. The continuous presence across the glass forming range of this system with a decrease in area at higher modifier contents suggest a behavior of the ESi^2 that is generally consistent

with the NMR results. In the higher modified glasses ($0.55 \geq y \geq 0.70$), a new set of spectral peaks begin to dominate the spectra. In the y = 0.55 and 0.60 compositions, a spectral peak at 373 cm^{-1} is observed, but not seen in the lower Na_2S content glasses. Both of these high alkali content glasses have been suggested to contain a high population of Si^1 units, so perhaps it is appropriate to assign this peak to the Si^1 structure. The polycrystal of the 0.60 composition, the Si^1 phase, has its most prominent peak residing at 377 cm^{-1}, and supports this assignment. Finally, the Si^0 structure may be tied to the spectral peak at 396 cm^{-1} which begins its rise in area at y = 0.60, reaches a maximum at y = 0.67 and decreases in the y = 0.70. The 0.67 polycrystal has a strong peak at 397 cm^{-1} which closely matches this result. This may further demonstrate the ability of Raman deconvolution to inform structure when used in conjunction with MAS NMR and data from polycrystal analogs at theoretical structure compositions.

2.6 Conclusions

In this study, the structures of glasses in the sodium thiosilicate system were examined and identified through the synthesis of new glasses and polycrystals of line compounds by combining information gained from IR, Raman, and ^{29}Si MAS NMR spectroscopy. The very first characterization of the Si^3 structural unit in an amorphous network was achieved by SQ synthesizing the glass forming y = 0.40 glass and the PM y = 0.33 glass and the y = 0.33 polycrystal. Through a combination of IR, Raman, and ^{29}Si MAS NMR spectral deconvolution, assignments were made to the Si^3 structural unit. Though it still remains unclear whether the glassy Si^3 units are “free” corner sharing units versus Si^3 within an adamantane cage, deconvolution results suggest that it may very well be possible that the cages do exist in the glassy network. These large molecular anions

would then contribute to the difficulty of synthesizing a SQ version of the y = 0.33 composition, and the presence of Si^2 units in the y = 0.40 glass may be in part the reason why this composition is a much better glass former.

This study was able to provide further information of the character and behavior of edge-sharing structures in the sodium thiosilicate system. Across the compositions covered in this study, a continued presence of ESi^2 units were observed in the ^{29}Si MAS NMR spectra, even in the highly modified y = 0.70 glass which is expected to have more than enough Na_2S to create the Si^0 SRO group. The ESi^2 structure also dominated the overall Si^2 population as seen by the deconvolution results. This suggests that the ESi^2 structure is favored in the glasses over the corner shared Si^2. As seen in the y = 0.50 compositions, the melt when quenched appears to only form the HT-Na_2SiS_3 structure, which is associated with the ESi^2 structure. So far in our work on this system, preparation of the LT-Na_2SiS_3 structure corresponding to the corner sharing Si^2 units, has been unsuccessful. Only at the y = 0.50 glass is a near 50:50 split between corner sharing and edge sharing Si^2 units are observed.

2.7 Acknowledgments

This research was supported by the National Science Foundation under grants number 1304977 and 0710564. The authors would like to thank the other members of the Glass and Optical Materials Research Group at ISU for their careful proof reading of the manuscript. The authors would also like to take Sarah Cady and Aaron Rossini of the Chemistry department at Iowa State University for providing instrument time on the NMR spectrometers and Karen Haman of the department of Chemical and Biological Engineering for reading and editing this manuscript.

Table 2.1 Number of BS, NBS_j, and NBS, N_{NBSj}, associated with each Q^n structural unit.

Si^n	Net Bridging Sulfur/Si^n	Net Non-Bridging Sulfur/Si^n
Si^4	2	0
Si^3	1.5	1
Si^2	1	2
Si^1	0.5	3
Si^0	0	4

Na:Si ratio	Si SROs	Connectivity	Composition
0:1	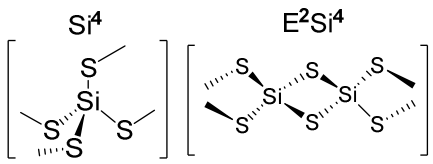	Branching Network -or- Chains	SiS_2
1:1	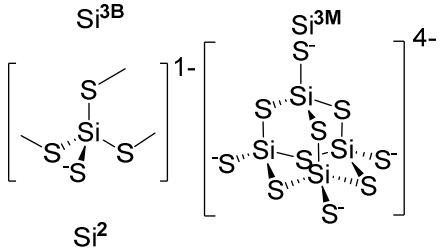	Branching Network -or- Anionic Moleculular Cages	0.33 Na_2S + 0.67 SiS_2
2:1	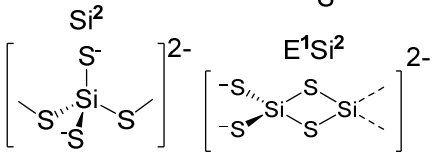	Chains -or- Dimeric Groups	0.50 Na_2S + 0.50 SiS_2
3:1	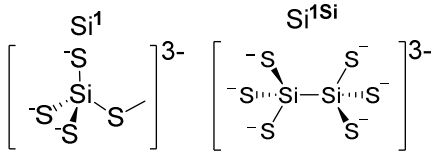	Dimeric Groups	0.60 Na_2S + 0.40 SiS_2
4:1	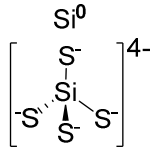	Isolated Tetrahedra	0.67 Na_2S + 0.33 SiS_2

Figure 2.1 Short Range Order Structure in the y Na_2S + (1-y) SiS_2 system (a) Si^4 SRO structure in pure SiS_2 (b) Si^3 SRO structures at theoretical composition (c) Si^2 SRO structures (d) Si^1 SRO structures (e) Si^0 SRO structures

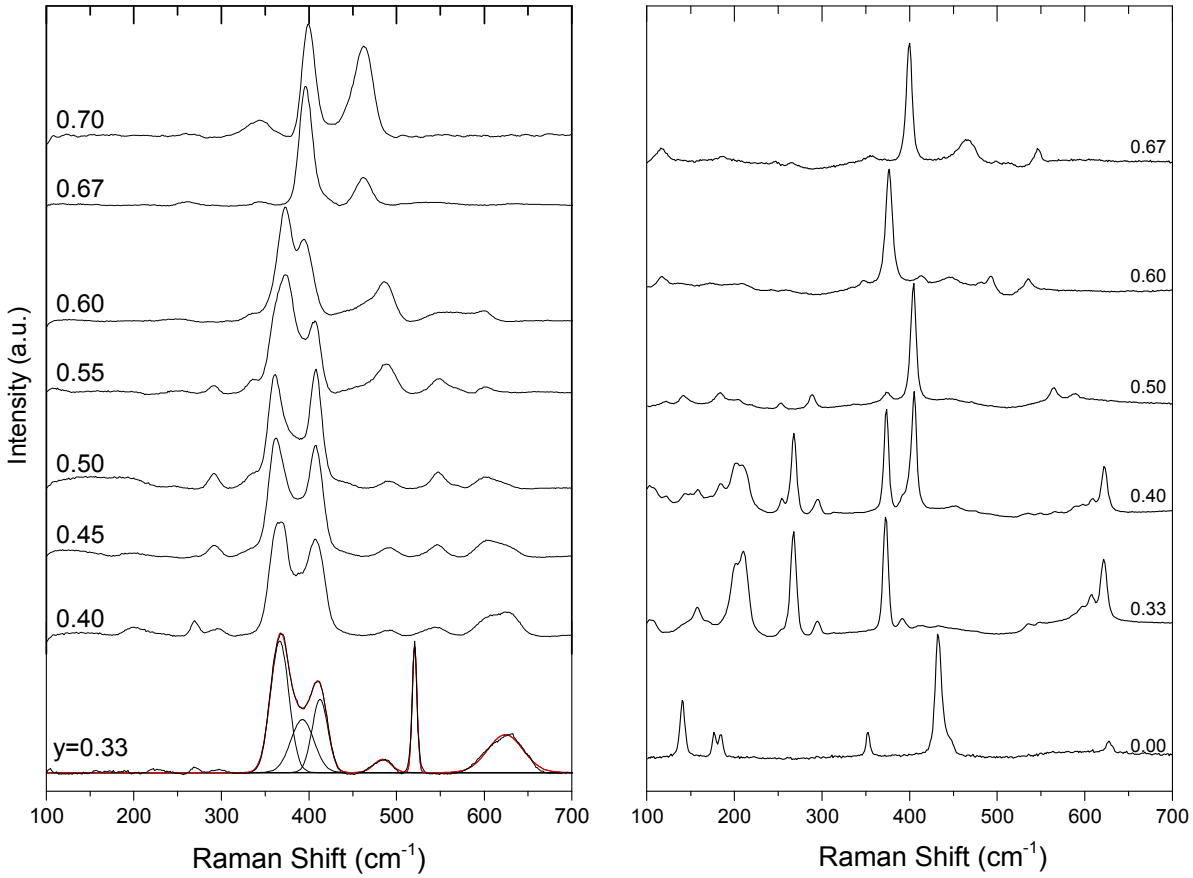

Figure 2.2 Raman Spectra of (a) $yNa_2S + (1-y)SiS_2$ glasses and (b) polycrystals

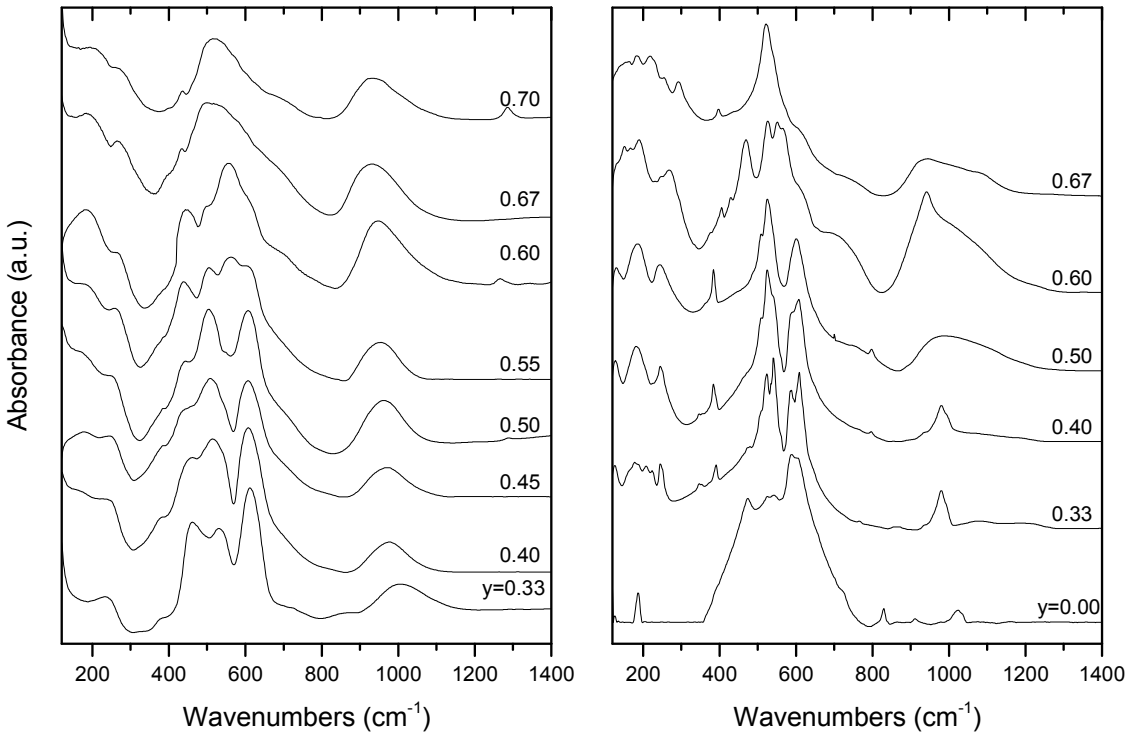

Figure 2.3 Infrared Spectra of $yNa_2S + (1-y)SiS_2$ (a) glasses and (b) polycrystals

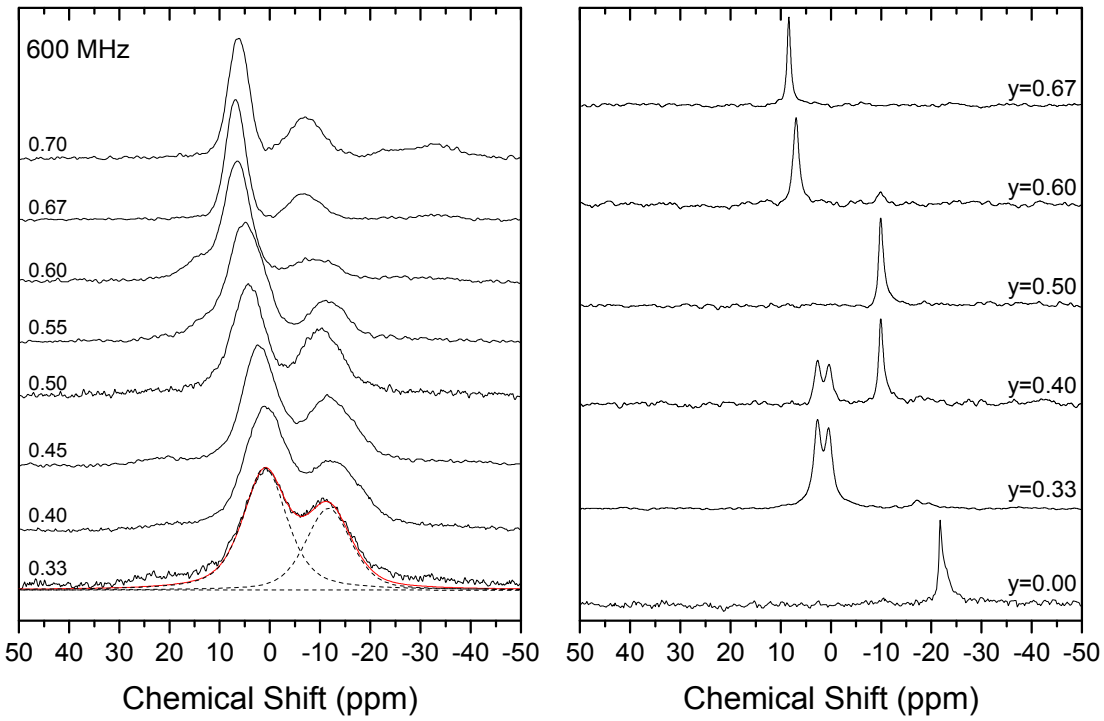

Figure 2.4 ^{29}Si MAS NMR Spectra of $yNa_2S + (1-y)SiS_2$ (a) glasses and (b) polycrystals

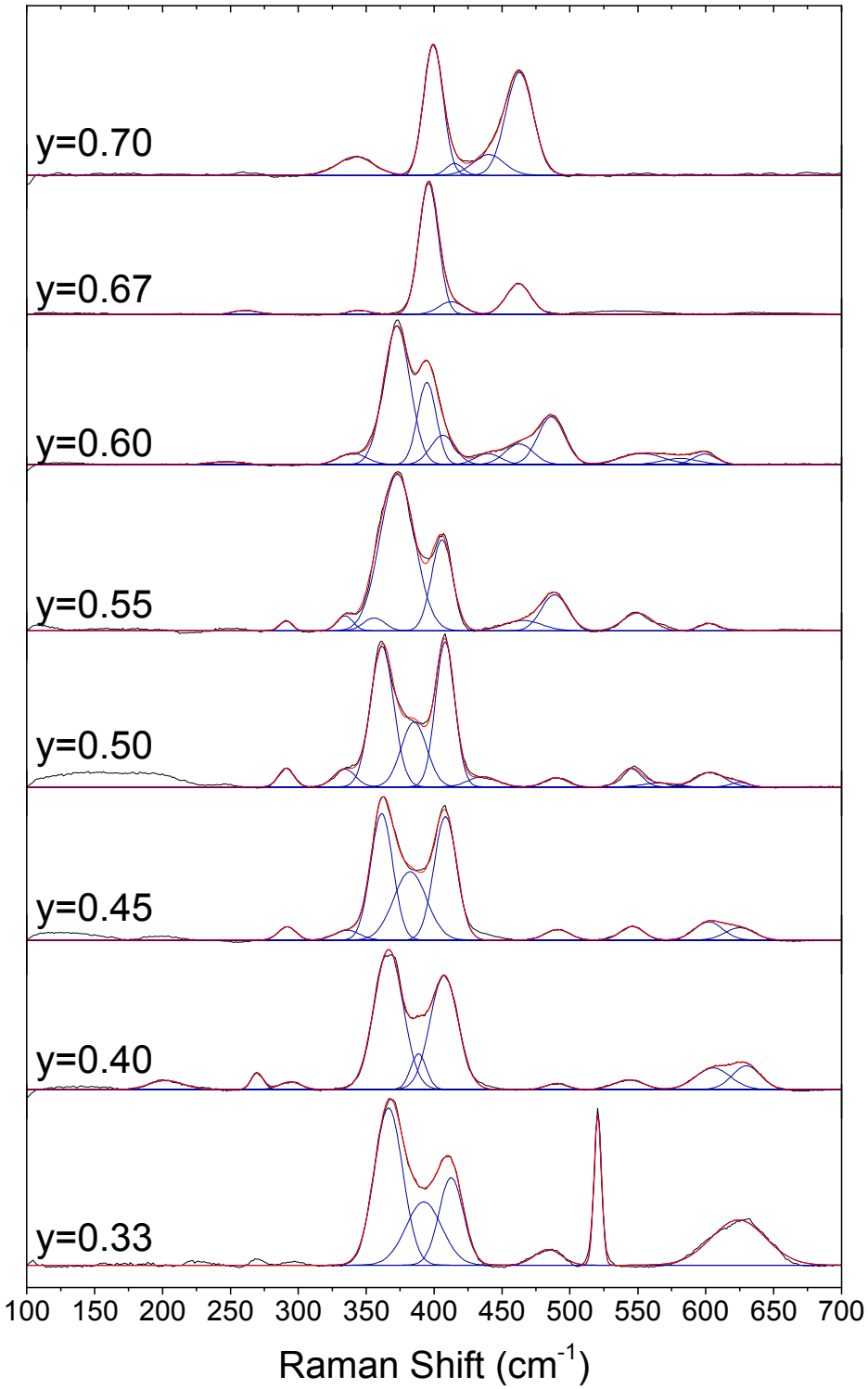

Figure 2.5 Deconvolution of Raman Spectra for $yNa_2S + (1-y)SiS_2$ glasses

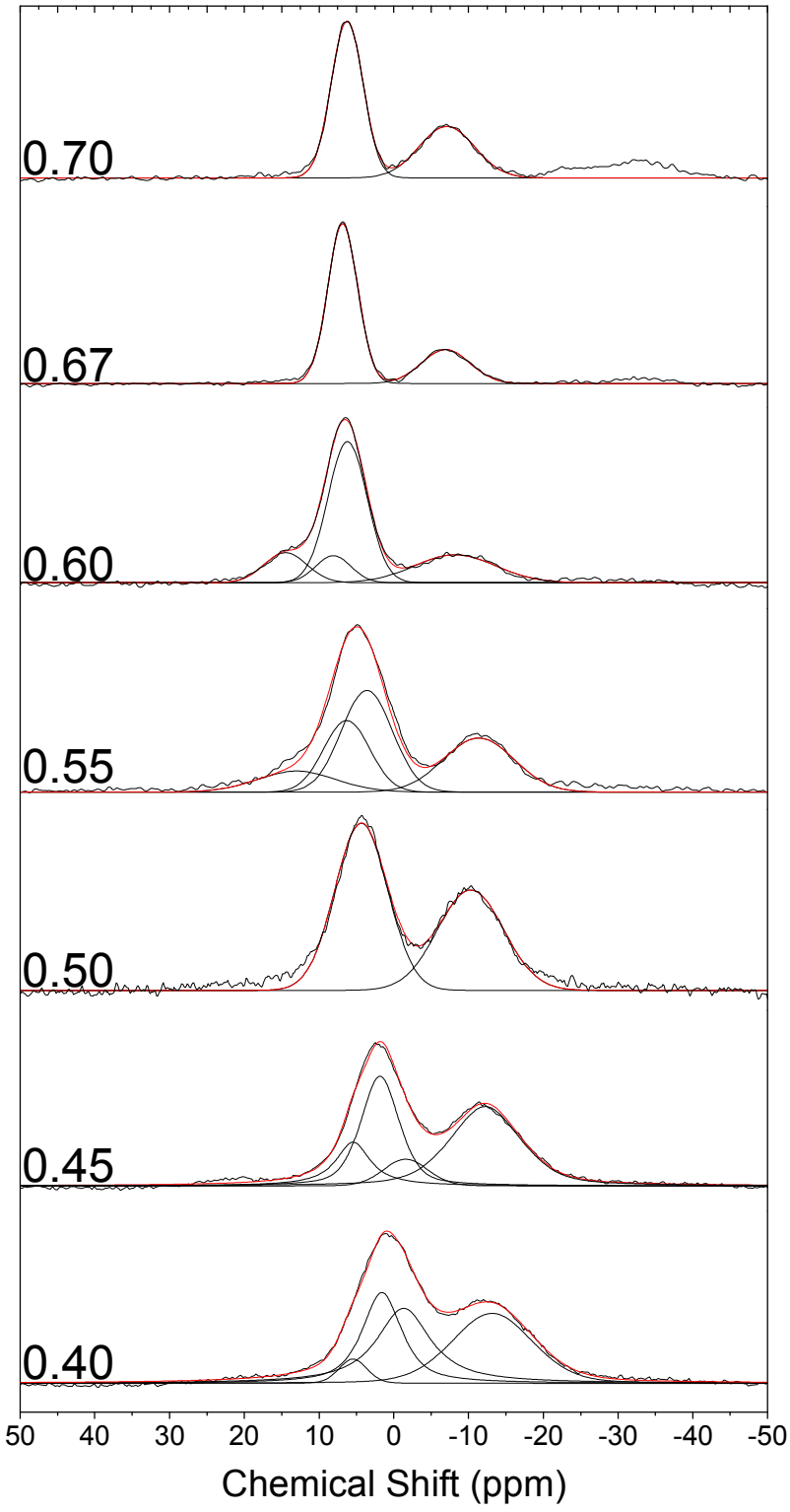

Figure 2.6 Deconvolution of ^{29}Si MAS NMR Spectra for $yNa_2S + (1-y)SiS_2$ glasses

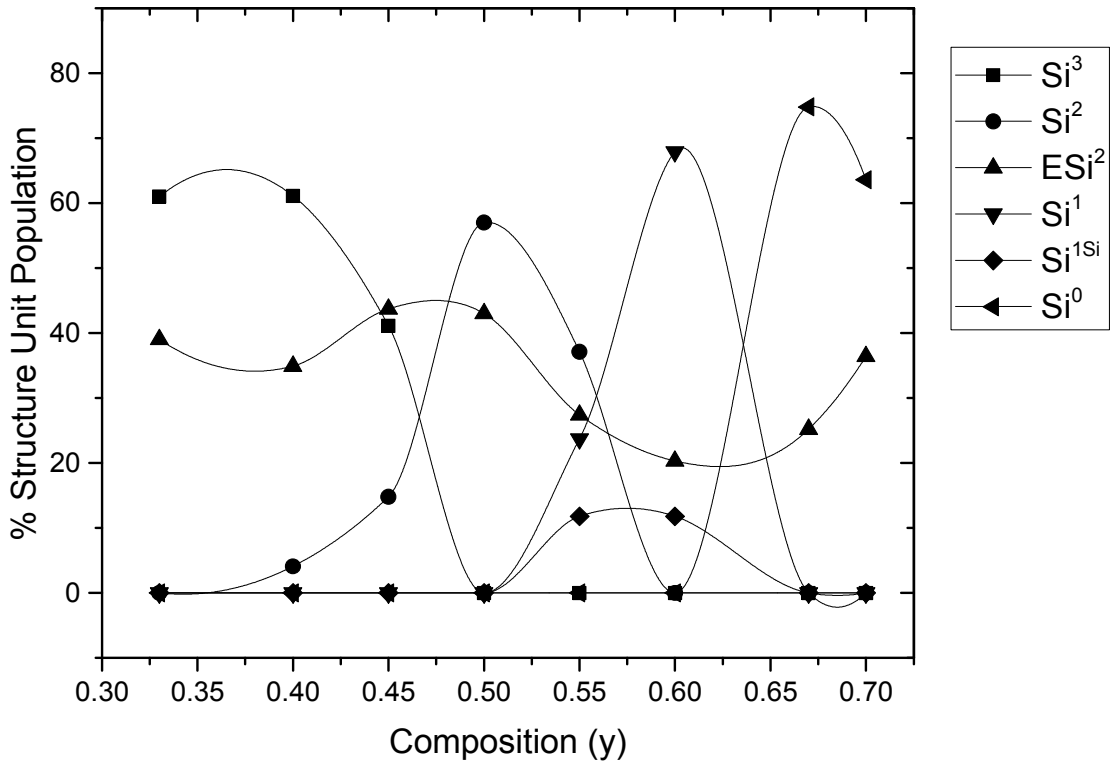

Figure 2.7 Composition Dependence of the SRO of $yNa_2S+(1-y)SiS_2$. Determined from ^{29}Si MAS NMR and Raman Spectroscopy analysis

2.8 References

1. Watson, D.E. and S.W. Martin, *Short range order characterization of the Na_2S + SiS_2 glass system using Raman, infrared and 29 Si magic angle spinning nuclear magnetic resonance spectroscopies.* Journal of Non-Crystalline Solids, 2017. **471**: p. 39-50.
2. Frede, B., et al., *Power Converters and Control of Renewable Energy Systems.* ICPE(ISPE)논문집, 2004: p. 2-20.
3. Hammerschlag, R., R. Pratt, and C.P. Schaber, *Energy Storage, Transmission, and Distribution*, in *Handbook of Energy Efficiency and Renewable Energy*. 2006, Taylor & Francis Group, LLC. p. 18-1 - 18-33.
4. Fuchs, E.F. and M.A.S. Masoum, *Introduction*, in *Power Conversion of Renewable Energy Systems*. 2011, Springer. p. 13-14.
5. Jacobson, M.Z. and C.L. Archer, *Saturation wind power potential and its implications for wind energy.* Proceedings of the National Academy of Sciences of the United States of America, 2012. **109**(39): p. 15679.
6. Khalil Amine, R.K.a.Y.T., *Rechargeable lithium batteries and beyond: Progress, challenges, and future directions.* MRS Bulletin, 2014. **39**(May 2014): p. 395-401.
7. Seddon, E., E. Tippett, and W. Turner, *The electrical conductivity of sodium meta-silicate-silica glasses.* J. Soc. Glass Technol, 1932. **16**(1641): p. 477.
8. Otto, K. and M.E. Milberg, *Ionic Conduction and Structure in Cesium and Thallium Silicate Glasses.* Journal of the American Ceramic Society, 1967. **50**(10): p. 513-516.
9. Ingram, M.D., *Ionic Conductivity in glass.* Physics and Chemistry of Glasses, 1987. **28**(6): p. 215-234.
10. Ribes, M., B. Barrau, and J.L. Souquet, *Sulfide Glasses - Glass Forming Region, Structure and Ionic-Conduction of Glasses in Na_2S-SiS_2, Na_2S-GeS_2, Na_2S-P_2S_5 and Li_2S-GeS_2 Systems.* Journal of Non-Crystalline Solids, 1980. **38-9**(May-): p. 271-276.
11. Martin, S.W. and C.A. Angell, *Dc and ac conductivity in wide composition range Li_2O ・P_2O_5 glasses.* Journal of Non-Crystalline Solids, 1986. **83**(1): p. 185-207.
12. Martin, S.W., et al., *Multiple frequency spin-lattice relaxation time and ionic conductivity measurements of Li_2S + SiS_2 glasses from 1 Hz to 40 MHz.* Journal of Non-Crystalline Solids, 1991. **131**: p. 1041-1045.
13. Dunn, B., H. Kamath, and J.-M. Tarascon, *Electrical energy storage for the grid: a battery of choices.* Science (New York, N.Y.), 2011. **334**(6058): p. 928.
14. Otto, K. and M.E. Milberg, *Ionic Conduction in Alkali and Thallium Silicate Glasses.* Journal of the American Ceramic Society, 1968. **51**(6): p. 326-329.
15. Ravaine, D. and J.L. Souquet, *A thermodynamic approach to ionic conductivity in oxide glasses. Part 1. Correlation of the ionic conductivity with the chemical potential of alkali oxide in oxide glasses.* Physics and Chemistry of Glasses, 1977. **18**(2): p. 27-31.
16. Ravaine, D., J.P. Diard, and J.L. Souquet, *Dielectric relaxation in alkali metal oxide conductive glasses studied by complex impedance measurements.* Journal of

the Chemical Society, Faraday Transactions 2: Molecular and Chemical Physics, 1975. **71**(0): p. 1935-1941.
17. Christensen, R., G. Olson, and S.W. Martin, *Ionic conductivity of Mixed Glass Former 0.35 Na_2O + 0.65 [xB_2O_3 + (1-x) P_2O_5] Glasses.* Journal of Physical Chemistry B, 2013. **117**: p. 16577-16586.
18. Angell, C.A., *Fast ion motion in glassy and amorphous materials.* Solid State Ionics, 1983. **9**: p. 3-16.
19. Angell, C.A., *Recent developments in fast ion transport in glassy and amorphous materials.* Solid State Ionics, 1986. **18&19**: p. 72-88.
20. Angell, C.A., *Mobile Ions in Amorphous Solids.* Annual Review of Physical Chemistry, 1992. **43**(1): p. 693-717.
21. Hayashi, A., et al., *Superionic glass-ceramic electrolytes for room-temperature rechargeable sodium batteries.* Nature Communications, 2012. **3**: p. 5.
22. Nagao, M., et al., *In situ SEM study of a lithium deposition and dissolution mechanism in a bulk-type solid-state cell with a Li_2S-P_2S_5 solid electrolyte.* Physical Chemistry Chemical Physics, 2013. **15**(42): p. 18600-18606.
23. Hayashi, A., et al., *Formation of superionic crystals from mechanically milled Li_2S–P_2S_5 glasses.* Electrochemistry Communications, 2003. **5**(2): p. 111-114.
24. Hayashi, A., et al., *Characterization of Li_2S–P_2S_5 glass-ceramics as a solid electrolyte for lithium secondary batteries.* Solid State Ionics, 2004. **175**(1–4): p. 683-686.
25. Minami, T., A. Hayashi, and M. Tatsumisago, *Recent progress of glass and glass-ceramics as solid electrolytes for lithium secondary batteries.* Solid State Ionics, 2006. **177**(26–32): p. 2715-2720.
26. Cho, J. and S.W. Martin, *Infrared spectra of lithium thioborate glasses and polycrystals.* Journal of Non-Crystalline Solids, 1994. **170**(2): p. 182-189.
27. Martin, S.W. and D.R. Bloyer, *Preparation and Infrared Characterization of Thioborate Compounds and Polycrystals.* Journal of the American Ceramic Society, 1991. **74**(5): p. 1003-1010.
28. Sills, J.A., S.W. Martin, and D.R. Torgeson, *^{11}B NMR studies of the short range order in K_2S+B_2S_3 glasses.* Journal of Non-Crystalline Solids, 1994. **175**(2,3): p. 270-277.
29. Sills, J.A., S.W. Martin, and D.R. Torgeson, *^{11}B NMR studies of the short range order in wide composition range xNa_2S + (1-x)B_2S_3 glasses.* Journal of Non-Crystalline Solids, 1994. **168**(1-2): p. 86-96.
30. Eckert, H., Z.M. Zhang, and J.H. Kennedy, *Glass-Formation in Non-Oxide Chalcogenide Systems Structural Elucidation of Li_2S-SiS_2-Lil Solid Electrolytes by Quantitative Si-29, Li-6 and Li-7 High-Resolution Solid-State Nmr Methods.* Journal of Non-Crystalline Solids, 1989. **107**(2-3): p. 271-282.
31. Eckert, H., et al., *Structural Transformation of Thiosilicate Glasses - Si-29 Mas Nmr Evidence for Edge-Sharing in the System Li_2S-SiS_2.* Journal of Non-Crystalline Solids, 1989. **113**(2-3): p. 287-293.
32. Pradel, A., et al., *Si-29 Nmr Structural Studies of Ionically Conductive Silicon Chalcogenide Glasses and Model Compounds.* Journal of Non-Crystalline Solids, 1995. **188**(1-2): p. 75-86.

33. Hayashi, A., et al., *Characterization of $Li_2S–SiS_2–Li_3MO_3$ (M=B, Al, Ga and In) oxysulfide glasses and their application to solid state lithium secondary batteries.* Solid State Ionics, 2002. **152–153**: p. 285-290.
34. Hayashi, A., et al., *Characterization of $Li_2S–SiS_2–Li_xMO_y$ (M=Si, P, Ge) amorphous solid electrolytes prepared by melt-quenching and mechanical milling.* Solid State Ionics, 2002. **148**(3–4): p. 381-389.
35. Tatsumisago, M., et al., *Preparation of amorphous solid electrolytes in the system $Li_2S–SiS_2–Li_4SiO_4$ by mechanical milling.* Solid State Ionics, 2000. **136–137**: p. 483-488.
36. Cho, J. and S.W. Martin, *Structures and Ionic Conduction of xNa_2S+ (1-x)SiS_2 Glasses.* Role of Ceramics in Advanced Electrochemical Systems: p. 85-99.
37. Ribes, M., et al., *Etude structurale de thiocomposés à groupement anionique de type tétrane $Na_4X_4S_{10}$ (X = Ge, Si) et $Ba_2Ge_4S_{10}$.* Journal of Solid State Chemistry, 1973. **8**(3): p. 195-205.
38. Tenhover, M., M.A. Hazle, and R.K. Grasselli, *Atomic Structure of SiS_2 and $SiSe_2$ Glasses.* Physical Review Letters, 1983. **51**(5): p. 404-406.
39. Tossell, J.A., *Theoretical Studies on the Structural and Spectral Properties of Silicon Sulfide Glasses.* Chemistry of Materials, 1994. **6**(2): p. 239-248.
40. Tenhover, M., M.A. Hazle, and R.K. Grasselli, *Raman-effect studies of Si_xS_{1-x} glasses.* Physical Review B, 1984. **29**(12): p. 6732-6735.
41. El Jaroudi, O., et al., *ChemInform Abstract: Raman Spectroscopy Study of the Reaction Between Sodium Sulfide or Disulfide and Sulfur: Identity of the Species Formed in Solid and Liquid Phases.* ChemInform, 1999. **30**(33): p. no-no.
42. Tenhover, M., et al., *Magic angle spinning ^{29}Si nuclear magnetic resonance of Si-chalcogenide glasses.* Solid State Communications, 1988. **65**(12): p. 1517-1521.
43. Kennedy, J.H., *Ionically conductive glasses based on SiS_2.* Materials Chemistry and Physics, 1989. **23**(1–2): p. 29-50.
44. Bischoff, C., *The Mixed Glass Former Effect in $0.5Na_2S + 0.5[xGeS_2 + (1-x)PS_{5/2}]$ glasses*, in *Materials Science and Engineering*. 2013, Iowa State University. p. 193.
45. Barrau, B., et al., *Glass formation, structure and ionic conduction in the Na_2S · GeS_2 system.* Journal of Non-Crystalline Solids, 1980. **37**(1): p. 1-14.
46. Mu¨ller, A., et al., *Spectroscopic studies of As_4O_6, Sb_4O_6, P_4S_{10}, $Ge_4S_{10}^{4-}$ and organometallic compounds containing the M_4X_6 cage. The Raman and i.r. spectrum of $Ge_4S_{10}^{4-}$.* Spectrochimica Acta Part A: Molecular Spectroscopy, 1976. **32**(1): p. 67-74.
47. Pradel, A. and M. Ribes, *Lithium chalcogenide conductive glasses.* Materials Chemistry and Physics, 1989. **23**(1-2): p. 121-142.
48. Pradel, A., et al., *Mixed glass former effect in the system $0.3Li_{(2)}S$-$0.7[(1-x)SiS_2$-$xGeS_{(2)}]$: A structural explanation.* Chemistry of Materials, 1998. **10**(8): p. 2162-2166.
49. Bischoff, C., et al., *Structural investigations of $yNa_2S + (1 - y)PS_{5/2}$ glasses using Raman and infrared spectroscopies.* Journal of Non-Crystalline Solids, 2012. **358**(23): p. 3216-3222.

CHAPTER 3. STRUCTURAL CHARACTERIZATION OF THE SHORT RANGE ORDER IN HIGH ALKALI CONTENT SODIUM THIO-SILICOPHOSPHATE GLASSES

A paper submitted to Inorganic Chemistry

Deborah E. Watson[3]*, Steve W. Martin*[4]

Department of Materials Science and Engineering, Iowa State University

Ames, Iowa 50010-2300

3.1 Abstract

The composition dependence of the short range order (SRO) structure in highly modified mixed glass former sodium thio-silicophosphate glasses, $yNa_2S + (1-y)[xSiS_2 + (1-x)PS_{5/2}]$ were investigated using infrared (IR), Raman, ^{29}Si and ^{31}P magic angle spinning nuclear magnetic resonance (MAS-NMR) spectroscopies. Both the y = 0.5 and 0.67 glasses undergo disproportionation reactions among the Si and P SRO structures which leads to various and complex SRO structural units for the Si and P as shown via the spectra used to characterize the glasses. In the y = 0.5 series, the compositionally expected and experimentally observed SRO units are the P^1 and Si^2 units in the two binary end-member glasses, where the superscript is the number of bridging sulfur atoms on the P or Si units. However, in the ternary mixed glasses, $0 < x < 1$, these units were found to react to form P^0 (more highly modified, y = 0.60) and Si^3 (less highly modified, y = 0.33) units indicating preferential association of Na^+ ions with the P SRO structures. The Raman spectra were used to resolve the heretofore incompletely studied Si^3 SRO unit, which was otherwise

[3] Primary researcher and author

[4] Corresponding author and principle investigator

difficult to elucidate using ^{29}Si MAS NMR alone. In the y = 0.67 series glasses, the expected P^0 and Si^0 SRO units were observed for the end member binary glasses. Like in the y = 0.5 series, the ^{29}Si MAS NMR showed that edge shared Si^2 (ESi^2, y = 0.5) structures were also present in these highly modified glasses which meant Na_2S was not completely incorporated in the network. Evidence of this was shown in the Raman spectra in the form of polysulfide structures Na_2S_x (x = 2, 4).

KEYWORDS Mixed Glass Former Effect, Fast Ion Conducting Glasses, MAS NMR, Short Range Order, Sodium Glassy Electrolyte

3.2 Introduction

The study of the mixed glass former effect (MGFE) has been a useful tool in probing the short-range order (SRO) and network structure behavior of mixed glass former (MGF) systems containing oxide glass formers such as SiO_2, GeO_2, P_2O_5, B_2O_3, and their sulfide analogues such as GeS_2 and P_2S_5 in ternary glass forming systems. In most studies to date, the ratio of one glass former, say SiO_2, to another, such as B_2O_3, has been kept constant while the amount of modifying oxide (or sulfide), such as Na_2O has been varied. In the MGF systems studied here, we have fixed the overall ratio of the modifier, Na_2S in this case, to total glass formers, $SiS_2 + PS_{5/2}$, and then varied the ratio, x, of the glass formers to each other from 0 to 1. In our previous studies of MGF systems[1-7], we have purposefully adjusted the compositions of the glass formers such that equal numbers of glass formers are present in the glass at any one composition. So, in this case here, we use $PS_{5/2}$ instead of the more common P_2S_5. Through our studies of such MGF systems, it becomes possible to examine the unique role that the mixing of the glass

formers has upon both the SRO structure of the resulting glasses and their physical properties, most notably the alkali ion conductivity. The MGFE has been explored in a number of different glass families and is found to produce non-linear, non-additive trends in their physical properties [5, 8-14]. In the case of the alkali ion conductivity, these glasses are finding important uses such as solid state electrolytes for use in solid state batteries [6, 15-18].

3.2.1 Structures of MGF Glasses

The majority of the studies of MGF glass-forming systems have been focused on understanding the ionic conduction in a glassy network. However, inherent to the study of this phenomena is an exploration and determination of the atomic level structures, the SRO, of these glasses as a function of a constant modifier concentration and a variable glass former ratio. So far, most of the studies of the MGFE have been done on the much easier to prepare and study oxide glass systems [5, 19-21]. For example, in the sodium borophosphate system $0.35\ Na_2O + 0.65[xB_2O_3 + (1-x)P_2O_5]$, Christensen et al.[22] have reported that as the sodium borate binary glass is added to the binary sodium phosphate glass, there is a preferential reaction of the strong Lewis acid trigonal boron units, B^3, where the superscript 3 refers to the number of bridging oxygens, with the strong Lewis base of the non-bridging oxygens in the binary sodium phosphate glass to form charge delocalized and hence energy stabilized tetrahedral boron (B^4) units. The Na^+ ion conductivity in these ternary Na B P O glasses reaches sharp a maximum above the expected value that would be achieved for simple mixing of the sodium phosphate and sodium borate glass structures at the same composition where the B^4 composition reaches a maximum value. Beyond this maximum in the Na^+ ion conductivity, $x > 0.5$, the SRO

structures in the glasses are again dominated by the minority glass former, P, which like B for $x < 0.5$, extracts a larger share of the Na^+ charge away from B to form more highly modified P SRO structures.

A similar behavior, where the minority glass former P extracts a disproportionate fraction of the mobile cation charge away from the majority glass former, has also been observed in the sodium thio-germanophosphate glass forming system $0.5Na_2S + 0.5[xGeS_2 + (1-x)PS_{5/2}]$ investigated by our group[23]. In this system, the negative charge per glass former, Ge and P, was expected to be -2. By careful Raman and ^{31}P MAS NMR measurements, it was found that for all compositions across this series, the expected P^1 groups, see Figure 3.1, were converted to the more charge dense P^0 groups, the amount of which was governed by the composition x. In this process, charge was removed from the expected Ge^2 SRO to form less charged Ge^3 SRO units. It was observed that this disproportionate sharing of charge towards the P centers was again strongest when the P was the minority glass former.

The majority of work in chalcogenide ternary MGF systems contain lithium, sodium or silver as the modifier species[24]. Pradel et al. has reported the Raman spectra and the composition dependence of the conductivity in the lithium thio-silicogermanate system $30Li_2S + (70-x)SiS_2 + xGeS_2$[10]. Using Raman spectroscopy and small angle x-ray scattering they found that the MGF system $0.3Li_2S + 0.7[(1-x)SiS_2 + xGeS_2]$ was phase separated within the compositional region $0.5 \leq x \leq 0.64$ where they had previously observed a positive MGFE in the Li^+ ion conductivity. Larink et al. have reported the infrared (IR), Raman and the ^{11}B and ^{31}P MAS NMR spectra of the sodium thio-borophosphate series $0.5Na_2S + 0.5[xB_2S_3 + (1-x)P_2S_5]$[25]. However, these authors report

that these glasses were heavily oxygen contaminated and new work in our group is in progress to prepare and characterize oxygen-free glasses in this system.

Through work on these different families, it is evident that the sulfide glasses possess unique bonding and network forming characteristics that do not often follow the same chemical ordering principles as in the oxide glasses. For example, sulfide glasses can possess S-S and glass former – glass former, such as P-P, homopolar bonding structures that are so far unseen in the oxide glasses. Therefore, structural knowledge of the comparable oxide systems does not always fully translate to understanding the sulfide-based glass forming systems. One example is the different network chemical bonding behavior between SiO_2 glass and SiS_2 glasses [11]. Glassy SiO_2 is well-known to be a three-dimensional network former, where all of the $SiO_{4/2}$ tetrahedra share corners. SiS_2, on the other hand, consists of long chains of edge sharing units, see Figure 3.2, which significantly reduce the dimensionality of the glass structure from 3D to essentially 2D[26]. As a result, SiO_2 is a well-known exceptionally strong glass former, while SiS_2 readily crystallizes on cooling.

In this paper, we present a structural investigation of two MGF sodium thio-silicophosphate series: $0.5Na_2S + 0.5[xSiS_2 + (1\text{-}x)PS_{5/2}]$ as a parallel study of our previously reported $0.5Na_2S + 0.5[xGeS_2 + (1\text{-}x)PS_{5/2}]$ system and the newer more highly modified glass $0.67Na_2S + 0.33[xSiS_2 + (1\text{-}x)PS_{5/2}]$ series. Significantly, the $y = 0.6$ system was not studied due to the fact that the sodium thiophosphate end member is not glass forming. The atomic structure of and glass networking behavior in binary sodium thiophosphate glasses have been studied recently through the work of Bischoff et al.[27] in this group. It was reported that the glass forming region of the sodium thiophosphate

system $yNa_2S + (1-y)PS_{5/2}$ extends from $0.33 \leq y \leq 0.55$ and $y = 0.65$, and ^{31}P MAS NMR, Raman, and IR spectroscopies were used to identify the different phosphorus SRO units in this binary system, again see Figure 3.1. Pradel et al. have studied the binary alkali thiosilicate glasses and have shown that the addition of a modifier species depolymerizes the network structure[28]. However, the edge sharing character of SiS_2 described above is maintained well into the high modifier end, $yM_2S > 0.5$, of the glass forming regime of the system as evidenced by their studies on the binary glasses $yM_2S + (1-y)SiX_2$ (M = Li, Na and X = S, Se).

In this study, we have purposefully not examined glasses with smaller amounts of Na_2S, $y < 0.5$, for three reasons; (1) these compositions are found to be only marginally glass forming, (2) they exhibit high vapor pressures at temperatures necessary to form a quenchable liquid, and (3) their Na^+ ion conductivity decreases sharply with decreasing Na_2S content. This latter property is a key driver for many of our studies of these glasses for use in solid-state Na batteries.

Using a combination of Raman, IR, ^{31}P and ^{29}Si MAS NMR spectroscopies, the SRO units of each glass former have been identified, characterized, and quantified as a function of the mixing ratio x. Special attention was given to analyzing the thiosilicate SRO units of this system because this is the very first study of this system and as such the thiosilicate SRO units are much less understood than the thiophosphate SROs units. Though ^{29}Si is a low sensitivity nuclide due to its low natural abundance, ^{29}Si MAS NMR was still useful for providing insight into specific thiosilicate SRO units present in the glass structure. Finally, with the identification and characterization of the P and Si SRO units, a model of the composition dependence of all of the SRO units present in the glass

was determined. The model satisfies both charge compensation and glass former fraction rules and will be used to contribute to our understanding of the overall structure of these glasses. In particular, we report one of the very first detailed studies of the Si^3 group, heretofore previously unreported, but is shown here to play an important role in the structures of these glasses. Like the $0.5Na_2S + 0.5[xGeS_2 + (1-x)PS_{5/2}]$ glasses studied by Bischoff et al.[7], disproportionate sharing of the Na away from Si and towards P is observed for all compositions in the 0.5 Si series and hence the Si^3 unit is formed in high concentrations. This is like the Ge^3 group as observed in the thio-germanophosphate glasses. From Figures 3.1 and 3.2, it is seen that the expected predominant SROs are the Si^2 and P^1 groups for the 0.5 series and are the Si^0 and P^0 groups for the 0.67 series. We will show that while these expectations are borne out by each of the end-member glasses, x = 0 and x= 1, respectively, significant disproportion away from these simple single SRO groups are seen in both series of glasses.

3.3 Experimental Methods and Materials

3.3.1 Sample preparation of glasses in the series $0.5Na_2S + 0.5[xSiS_2 + (1-x)PS_{5/2}]$

Sodium sulfide (Na_2S) was made via the thermal dehydration of crystalline sodium sulfide nonahydrate ($Na_2S•9H_2O$, 98% Alfa Aesar) by heating under ~ 3Pa roughing pump vacuum over a liquid nitrogen trap for a duration of 35 hours. Silicon sulfide (SiS_2) was made by combining stoichiometric amounts of silicon (99.999% Alfa Aesar) and sulfur (99.999% Alfa Aesar Puratronics) in a silica ampoule under vacuum and rotated and heated slowly to 970 ^oC and held over a 50-hour period. Phosphorus pentasulfide ($P_2S_5 = PS_{5/2}$) (99.99% Sigma Aldrich) was used as received, but it was mechanically milled as a pre-step to glass melting to decrease volatilization. We believe

this step converts the P_4S_{10} molecules in the material to more of a $PS_{5/2}$ molecular network.

The ternary sodium thio-silicophosphate glasses were prepared by combining stoichiometric amounts of the previously melted and quenched binary end member glasses, $0.5Na_2S + 0.5SiS_2$ and $0.5Na_2S + 0.5PS_{5/2}$, ranging from $0 \leq x \leq 1$. The binary glasses were made by combining stoichiometric amounts of Na_2S and SiS_2 for the sodium thiosilicate and Na_2S and $PS_{5/2}$ for the sodium thiophosphate. Binary and ternary glass samples were melted in covered vitreous carbon crucibles inside a tube furnace that was hermetically sealed to a nitrogen glove box. Each composition was melted in the temperature range of 680° to 795 °C for 3 to 5 minutes. The higher temperatures were used in the thiosilicate rich end, $x > 0.5$. Weight loss measurements were recorded after the first melt and if a loss of less than 1% was observed, the charge was melted a second time and splat quenched between two room temperature brass plates. The glassy samples were collected and stored in the nitrogen glove box. Powder x-ray diffraction and SEM EDS compositional analysis were performed on representative samples in this series and it was found that all samples were x-ray amorphous and their compositions were as batched to within a few percent.

3.3.2 Sample preparation of glasses in the series $0.67Na_2S + 0.33[xSiS_2 + (1-x)PS_{5/2}]$

The ternary glasses were made by milling stoichiometric amounts of Na_2S, SiS_2 and $PS_{5/2}$ together for 5 minutes inside a closed steel pot with a steel ball. Na_2S used in these glasses was obtained commercially (Alfa Aesar). It was observed that the commercial and ISU prepared (see above) versions of Na_2S had nearly identical IR and

Raman spectra and powder XRD patterns. The other components were the same as that used in the 0.5 glass series. The glass batch powders were then melted in the same manner as the 0.5 series of glasses. Melting temperatures ranged from 575 to 630°C for 3 to 5 minutes. Again, after the first melt, weight loss measurements were taken. Then after a second melt, the resulting liquid was cast between brass molds to create a splat quenched sample.

3.3.3 Raman and IR Spectroscopy

The Raman spectra were collected using a Renishaw InVia confocal micro-Raman spectrometer using a 488 nm Argon laser. A survey spectra was collected from 100 to 3000 cm^{-1} on each sample to determine the spectral range of interest. Co-added spectra of 10 accumulations for 20 seconds each were then collected for each sample over a range of 100 to 700 cm^{-1} using a 5x microscope objective. It is estimated the laser spot size on the glass sample for any one spectral accumulation was ~ $(100)^2$ μm^2. Multiple spots across the sample were examined to determine if there was any variation in the spectra, which would be suggestive of phase separation, crystallization and/or chemical contamination. All spectra were essentially identical and an example of this is shown in Figure 3.4 below. The Raman spectra were deconvoluted in Origin Lab 2016. The spectra of the binary end members were first deconvoluted in order to give a standard or basis for deconvolution of the ternary glasses. Pure Gaussians were used to deconvolute each spectrum. The peak positions were also compared to literature values available for known SRO structures. A tolerance of ±2 cm^{-1} was allowed for the peak position.

The IR spectra were collected using a Bruker 66v/s spectrometer using a KBr beam splitter. Samples were diluted in dried CsI at a concentration of <5% and pressed

into pellets. 32 scans were collected per sample at a resolution of 4 cm^{-1} from 400 to 4000 cm^{-1}. Spectra were collected in the far-IR (FIR) region as well using a Si-coated Ge beam splitter, but only a single mode associated with the Na^+ S^- NBS cation motion was observed that gave little new information about the SRO structural units, and as such, will not be reported here.

3.3.4 MAS-NMR Spectroscopy

The ^{31}P and ^{29}Si MAS-NMR spectra were collected using a Bruker Avance II 600 MHz Spectrometer employing a 14.1 T magnetic field. The samples were packed under nitrogen in to 4 mm zirconia rotors and spun at 12 kHz. Samples for the NMR measurements were doped with ~0.1 wt% manganese (II) sulfide (99.9% Alfa Aesar), a paramagnetic dopant, to shorten the spin-lattice relaxation time (T1) of the ^{29}Si nuclei. Comparative Raman and IR spectra of the doped and undoped glasses showed identical spectra and indicate that at the low concentration used, the MnS created no observable structural changes. The pulse widths for ^{31}P and ^{29}Si MAS NMR collections were 2 and 4.5 μsec, respectively corresponding to a 90° pulse, with a recycle delay time of 30 sec. The collected NMR spectra were analyzed and deconvoluted using MestRe Nova 10.0 software from the MestreLab Research S.L and Origin Lab 2016.

3.4 Results and Discussion

3.4.1 IR Spectra

3.4.1.1 $0.5Na_2S + 0.5[xSiS_2 + (1-x)PS_{5/2}]$ Glasses

The IR spectra of this glass system, $0 \leq x \leq 1$, are shown in Figure 3.3a. Minor peaks due to oxide contamination of just a few percent can be seen in the 900 to 1000 cm^{-1} range. The FIR spectra, while not shown here, contain the Na^+ ^-S- vibrations, but

provide no other significant information to the SRO of these glasses. The first mode of interest in the x = 0.0 sodium thiophosphate glass at 457 cm^{-1} is due to the BS of the P^1 unit (i.e. bridging P-S-P bending mode), see Figure 3.1. Throughout the thiophosphate rich region, x < 0.5, this mode decreases in intensity and shifts to 460 cm^{-1}. Also observed in this x = 0 composition, is the mode at 604 cm^{-1} which is attributed to the asymmetric stretch of the P^1 tetrahedral groups. This mode also decreases in intensity until the x = 0.4 composition and then shifts slightly toward higher wavenumbers until it is at 609 cm^{-1} in the x = 1 composition. This shift demonstrates a change in the SRO units from P dominated species to Si dominated species.

In the x = 1 sodium thiosilicate end-member glass, a mode is also at 609 cm^{-1} and is attributed to the BS Si-S-Si, vibration[29]. In conjunction with this peak in the 603 - 610 cm^{-1} region becoming more prominent, the 460 cm^{-1} mode for BS on the P^1 unit is (as expected) negligible. This is an indication that P^0 units are generated due to the conversion of P^1 units (as evident by the decrease in P^1 peak) into P^0 units by the simultaneous conversion of Si^2 units into Si^3 units. This is the first indication of the structural interaction between the Si and P SRO units where unequal sharing of the Na^+ ions is a major structural characteristic of these MGF glasses.

As the composition changes to the thiosilicate rich region of the series, x > 0.5, a shoulder mode at 460 cm^{-1} develops and is associated with edge-sharing ESi^2, see Figure 3.2, tetrahedra[30]. The mode at 505 cm^{-1} in the x = 1 glass is due to edge-sharing ESi^2 and corner-sharing Si^2 units that possess two NBSs. In the glasses with x = 0.5, towards the thiophosphate end, this mode decreases in intensity (and shifts to slightly higher wavenumbers) to the point that is barely visible in the IR spectra of the x = 0.1 and 0.2

glasses. This demonstrates the high sensitivity of IR spectra to the various SRO structural units in the glass. Another unique mode that appears for the addition of the sodium thiosilicate glass (x = 0.1) to the sodium thiophosphate glass is the appearance of a weak shoulder off of the P^1 SRO group at 550 cm^{-1}. Cho et al.[29], have previously assigned this mode to the Si^1 dimer, $Na_6Si_2S_7$, y = 0.6. However, given the stoichiometry of this composition, y = 0.5, giving rise to the expected predominant Si^2 SRO, this is unlikely. More likely, rather, is that it arises from the Si^3 unit which is formed in the ternary glasses from the disproportional sharing of the Na^+ towards the P units according to reaction Eq. (1). In the binary sodium thiosilicate glasses, there is a weak shoulder at ~534 cm^{-1} and this mode shifts to ~ 550 cm^{-1} in these ternary glasses.

$$P^1 + Si^2 \rightarrow P^0 + Si^3 \quad (1)$$

The intensity of the mode at 550 cm^{-1} reaches a maximum at x ~ 0.5, and decreases thereafter to 0 at x =1 consistent with the model here that Si^3 units are formed according to reaction (1). It is possible that this mode could be assigned to a cross networking P-S-Si unit such as Si^2-P^1, between the two glass formers. However, deconvolution of these spectra did not yield any new information because the Si and P IR modes are so close together in frequency (cm^{-1}), presumably because the atomic weight of P is close (31) to that of Si (28), and the modes are quite broad. Therefore, it is difficult to make any further significant interpretation of the SRO structure of these glasses from the IR spectra alone and for this reason, we will turn to the Raman spectra of the glasses after we examine the IR spectra of the xNa_2S = 0.67 series of glasses.

3.4.1.2 $0.67Na_2S + 0.33[xSiS_2 + (1-x)PS_{5/2}]$ Glasses

The IR spectra of the glasses in the 0.67 sodium thiosilicophosphate series, $0 \leq x \leq 1$, are given in Figure 3.3b. The P-S and Si-S modes typically lie in the 100 to 700 cm^{-1} region while the modes, Si-O and P-O, associated with minor oxide contamination lie at 800 cm^{-1} and higher. There is some oxide contamination seen in these glasses and the modes have some character to them. The three sharper modes at the higher wavenumbers in this range are associated with various $P^i(O)$ units, where i is likely to be small such as 0, 1, and 2, and are indicative of the high overall modifier content (y = 0.67) in these glasses. The broad mode in the lower wavenumber range is likely associated with $Si^i(O)$ units, again where i is also small. While not optimal, from various other measurements we estimate that the total concentration of oxide in these glasses to be less than 3 wt%.

The IR spectra of the x = 0.1 composition shows a prominent mode at 545 cm^{-1} with a shoulder at 505 cm^{-1}. These modes are due to P^0 and NBS on Si tetrahedra, respectively. As x increases, the intensity of the mode 505 cm^{-1} grows and becomes a separate peak along with the P^0 peak until it takes over in the x = 0.7 composition. There appear to be no peaks for BS units for the Si tetrahedra around 609 cm^{-1}, as seen in the y = 0.5 series, which would suggest that no networking sulfurs are being contributed by Si and it is therefore likely that these NBS vibrations are arising from Si^0 SRO units. Indeed, this is expected since at this modifier concentration, the glasses would be completely depolymerized to the Si^0 and P^0 units as well as contain excess Na_2S for x > 0.5. Eq. (2) shows that as x decreases, the amount of excess Na_2S in the composition decreases from ½ to 0 moles of Na_2S for every mole of $PS_{5/2}$ due to the fact that for x = 0, this corresponds to $2Na_2S + 1PS_{5/2} = Na_3PS_4 + ½Na_2S$.

$$0.67Na_2S + 0.33[xSiS_2 + (1\text{-}x)PS_{5/2}] = 2Na_2S + xSiS_2 + (1\text{-}x)PS_{5/2}$$

$$= xNa_4SiS_4 + (1\text{-}x)Na_3PS_4 + x½Na_2S \quad (2)$$

The FIR spectra does reveal the Na^+ ^-S- vibration around 200 cm^{-1}. Thus, the IR spectra agree with the prediction that these glasses are comprised primarily of P^0, Si^0 and excess Na_2S.

3.4.2 Raman Spectra

3.4.2.1 $0.5Na_2S + 0.5[xSiS_2 + (1\text{-}x)PS_{5/2}]$ Glasses

The Raman spectra of the $0.5Na_2S + 0.5[xSiS_2 + (1\text{-}x)PS_{5/2}]$ glass series are shown in Figure 3.4a. The sodium thiophosphate, x = 0, glass shows a strong mode at 398 cm^{-1}, characteristic of the P^1 SRO unit[27]. At 415 cm^{-1}, a weak shoulder on this P^1 peak is due to the presence of a small concentration of P^0 structural units in the glass. The IR spectrum of the x = 0 glass corroborates the Raman spectrum, having vibrational modes at 605 and 460 cm^{-1} which identifies the asymmetric stretch of the P tetrahedron and BSs on the P^1 SRO unit, respectively, see Figure 3a. Another shoulder on the low wavenumber side of the 398 cm^{-1} peak can be observed at 387 cm^{-1}. This may be associated with P^2 SRO units in the glass. The IR spectra do not show any modes related to this unit, nevertheless an argument could be made for their existence as they would charge balance the P^0 SRO units in this composition which should comprise solely of P^1 SRO units. The deconvolution of this spectrum gives (by percentage of area) 20% P^0, 22% P^2 and 57% P^1 SRO units, so this would seem to support this hypothesis. The 387 cm^{-1} mode is present throughout this series glasses in the deconvolution analysis, however the overall trend of the areas of these peaks does not have one consistent

behavior. Namely, it is seen that these populations decrease from x = 0 to 0.4, increase at x = 0.5 and continue to fluctuate out to the end of the series, x = 1.

Although the Raman spectra are not completely quantitative, this may indicate the presence of another type of SRO unit in these compositions. The corner shared Si^2 SRO unit has a peak at 388 cm^{-1}, as shown in the previous study of the sodium thiosilicate system using Raman spectroscopy by Watson[30]. When the spectra are fitted for both P^2 and Si^2 SRO units in this region, the trends are more consistent with the expected decrease in the P^2 SRO structures[27] as the composition moves from a P rich environment to a Si rich environment and more sodium becomes available to depolymerize the network and increase in Si^2 SRO structures. The mode at 398 cm^{-1} persists until the x = 0.6 glass. The shoulder at 415 cm^{-1} due to P^0 units appears to grow into a peak at x = 0.2 and continues to increase in relative intensity until x = 0.9, where after it decreases in intensity to zero as it is expected to for the x = 1, Si^0, composition. At the composition x = 0.4, a peak begins to grow in intensity at 361 cm^{-1} which becomes a well-defined peak at the x = 0.6 composition and has been assigned to BS units on Si^3 structural units, most likely found in an adamantane cage[30], see Figure 3.2. At the composition of x = 0.7, the peak arising from the P^1 group at 398 cm^{-1} is replaced by a shoulder that grows into a separate peak at 406 cm^{-1}. This peak has been assigned to NBS units on edge-sharing ESi^2 and corner-sharing Si^2 structural units, see Figure 3.2. There are minor peaks above 500 cm^{-1} for x > 0.6 glasses which are attributable to small amounts of oxide contamination in the glass as discussed above.

These results are consistent with the reaction of P^1 groups with Si^2 groups, both edge- and corner-sharing SROs, to form P^0 and Si^3 groups through the reaction given in

Eq. (1) above. This reaction shows an unequal sharing of the sodium ions, where P appears to have a higher affinity for the sodium ions than Si. Furthermore, as evidenced in the IR and Raman spectra, we have also seen such disproportionate reactions of the units in both the pure thiophosphate and thiosilicate glass members. In the case of the $0.5Na_2S + 0.5PS_{5/2}$, which should yield 100% P^1 SRO structures, P^1, P^0 and P^2 SRO units were detected in the Raman. The $0.5Na_2S + 0.5SiS_2$ is nominally the Si^2 composition, expected to yield all Si^2 SRO structures, yet the Raman showed the presence of Si^2, corner and edge shared, Si^3, and Si^1 SRO units. The deconvolution of these spectra proved powerful in revealing this diversity of structures.

3.4.2.2 $0.67Na_2S + 0.33[xSiS_2 + (1-x)PS_{5/2}]$ glasses

The Raman spectra of glasses in this series are shown in Figure 3.4b. In the x = 0 composition, a strong peak is observed at 422 cm^{-1}, which is assigned to the P^0 SRO structure. At x = 0.1, a shoulder on this P^0 peak is observed at 398 cm^{-1}, and is assigned to the Si^0 SRO structure[27]. The intensity of this peak grows as the compositions move toward the thiosilicate rich region, x → 1, until it is nearly the same intensity as the P^0 peak in the x = 0.7 glass. Deconvolution of these spectra confirm that there is nearly a 1:1 ratio between the areas of these peaks. Interestingly, at this composition, the peaks appear to match in intensity despite the fact that there should nominally be more Si structures than P, x = 0.7. This suggests that the Raman scattering cross-section of the P^0 unit is intrinsically greater than that of the Si^0 unit. Nevertheless, the uniqueness of the spectral features of these units is sufficient to clearly distinguish them in the Raman spectra. The Raman spectra are also very sensitive to the presence of polysulfide structures within the glass. This is primarily manifested as a peak at 460 to 470 cm^{-1} [31], but peaks at 217 cm^{-1}

and 275 cm^{-1} are also characteristic of sodium sulfide. Given the stoichiometry of this system, where the sodium thiophosphate introduces excess sodium sulfide, see Eq. (2) above, and the nature of these sulfide structures to eject free sulfur into the network, it is expected to have a considerable amount of excess sodium and sulfur in the glass. Note that as shown in Eq. (2), for x = 0, $0.67Na_2S + 0.33PS_{5/2}$ is equivalent to $2P^0 + Na_2S$.

3.4.3 ^{31}P MAS NMR Spectroscopy

3.4.3.1 $0.5Na_2S + 0.5[xSiS_2 + (1-x)PS_{5/2}]$ Glasses

The ^{31}P MAS NMR spectra of the $0.5Na_2S + 0.5[xSiS_2 + (1-x)PS_{5/2}]$ glass series from x = 0.0 to x = 0.9 is shown in Figure 3.5a.The spectrum of the x = 0 glass, the pure sodium thiophosphate end member, shows a prominent NMR resonance at 93 ppm, characteristic of the P^1 unit[7, 27]. However, the asymmetry of the peak indicates that more than one resonance contributes to this peak. As x increases towards the x = 1 pure thiosilicate glass, two new shoulders develop on this peak. The shoulder at 83 ppm is assigned to the P^0 SRO and the shoulder at 101 ppm is assigned to the P^{1P} SRO unit, see Figure 3.1, where 1P indicates a P SRO where the bond is a homonuclear bond between two P. Significantly, while the shoulder at 100 ppm decreases in intensity, the shoulder at 83 ppm grows steadily in intensity while the original main and central peak at 93 ppm decreases in intensity. The peak at 83 ppm assigned to the P^0 group becomes the dominant peak for the thiosilicate rich glasses and confirms the unequal sharing of the Na^+ ions to form the depolymerized P^0 SRO groups as found in the interpretation of the IR and Raman spectra and consistent with the disproportionation reaction given in Eq. (1).

At the x = 0.9 composition, the spinning side band contributions from P^{1P} and P^1 structures drop out completely and only spinning side bands of the P^0 group persist. Deconvolution of these spectra yield populations for the following SRO structures: P^1, P^0, P^{1P}, and P^2. In addition to these resonances, the superposition of the peaks for the P^1 (91 ppm), P^{1P} (100 ppm) and P^0 (82 ppm) SRO units can be observed using the deconvolution analysis. 2D ^{31}P - ^{31}P MAS NMR experiments are also in progress and will be reported in the future to confirm these assignments correspond to these structures.

3.4.3.2 $0.67Na_2S + 0.33[xSiS_2 + (1-x)PS_{5/2}]$ Glasses

The ^{31}P MAS NMR spectra of the $0.67Na_2S + 0.33[xSiS_2 + (1-x)PS_{5/2}]$ glasses in Figure 3.6a show two resonances; one at 83 ppm has been attributed to the P^0 SRO structure and one at 60 ppm has been attributed to $P^{:0}$ SRO units, see Figure 3.1 and reference[7]. However, through recent work in oxy-sulfides done in this group, this resonance may be associated with the P^0 oxy-sulfide structure PS_2O[32, 33]. This would corroborate the P-O linkages observed in the IR spectra. Two sets of spinning side bands of these resonances can also be observed at ~50 ppm from this peak in each direction. There are no apparent shifts in the P^0 resonance throughout the series. The deconvolution of the ^{31}P MAS NMR spectra shows that the P^0 population decreases for the x = 0.4 to 0.6 glasses, where the $P^{:0}/P^0_{OS}$ population is greatest. After this composition region, the P^0 population increases back to a population of ~97%. This would suggest that this unit is being generated in response to the formation of the Si^0 glass former SRO units.

3.4.4 ^{29}Si MAS-NMR Spectroscopy

3.4.4.1 $0.5Na_2S + 0.5[xSiS_2 + (1-x)PS_{5/2}]$ Glasses

As discussed above, the structures of thiosilicate glasses differ significantly from those of the oxide silicate glasses due to the fact that the thiosilicate glasses form edge-shared units, ESi^2, at the Si^2 composition of glasses studied here. Eckert et al.[26], who have studied the lithium thiosilicate glasses extensively, report that this edge-sharing propensity dominates the chemical shift behavior of the ^{29}Si nucleus. This effect is so strong that it apparently dominates over the normally observed effect of changing ratios of BS and NBS units. It appears that this is the case for the sodium thiosilicate glasses studied here as well.

The ^{29}Si MAS-NMR spectra of these glasses for x = 0.1 to 1 are shown in Figure 3.5. The two resonances centered at approximately 4.3 ± 0.35 ppm and -10.4 ± 2 ppm correspond to the E^0Si^2 and E^1Si^2 structural units, respectively, which are consistent with assignments found in the literature[26, 28] and expectations based on the stoichiometry of the composition. Here, the E^0Si^2 unit is the normal corner shared Si^2 SRO unit and the E^1Si^2 SRO unit is the edge-shared SRO unit, see Figure 3.2. Based on the ^{31}P MAS NMR results, where it was found that there was a shift from P^1 units to P^0 units as the series goes to the thiosilicate rich end, the expectation is that these edge- and corner-shared Si^2 units are losing the Na^+ ions to the P and therefore forming Si^3 units according to Eq. (1) above. The ^{29}Si MAS-NMR spectra, however, consistent with previous results by Eckert et al.[28], seem to show no significant changes in chemical shift nor intensity as the composition goes from x = 1 to 0.1. The lack of direct observation of a distinct ^{29}Si

MAS-NMR resonance for the Si^3 SRO unit is investigated in more detail through a careful deconvolution of the ^{29}Si MAS-NMR included below.

3.4.4.2 Deconvolution of ^{29}Si MAS-NMR Spectra

The presence of E^0Si^3 SRO units is proposed to account for the formation of the Si^3 SRO structural units, which is believed to be required to charge balance with the observed formation of the P^0 phosphorus SRO, structural units according to Eq. (1). The deconvolution and fitting of these spectra was done by assigning peaks to positions reported in the literature for particular Si SRO units[28, 30]. The E^1Si^3 unit has not so far been reported in the literature for the sodium or lithium thiosilicate glasses nor was evidence of its existence so far seen here. However, such corner-shared E^0Si^3 units are known to exist in adamantane like structures in the crystalline thiosilicates as $Na_4Si_4S_{10}$, where the Si^3 tetrahedra form a molecular anion cage[34]. In a previous study by Watson et al., the adamantane structure was proposed to exist in the binary y = 0.33 to 0.5 sodium thiosilicate glasses[30]. Figure 3.7 shows an example of one of these spectra deconvoluted and spectrally fit for corner-shared Si^1, Si^2 and Si^3 and edge-shared E^1Si^2 SRO units. As described above, both of the binary end members in this system experience a disproportionation reaction of the SRO units. In the case of the y = 0.5 sodium thiosilicate glasses, the Si^2 structure is expected to be the predominant unit, but Si^3 and Si^1 are also found. The deconvolution of the ^{29}Si MAS-NMR spectrum of the x = 1 glass shows that 62% of the population comes from Si^2 SRO units, both corner- and edge-shared, 27% from Si^1 and 20% from Si^3 units. This distribution gives a net charge of -2.07, quite close to the expected value of 2.0.

As seen in Figure 3.7, there is good agreement between the ^{29}Si MAS-NMR spectra and the fit which is comprised of Gaussians peaks for each of the units described above, E^1Si^2, E^0Si^2, and E^0Si^3. Figure 3.8 gives the compositional mapping of the various Si SRO structural units identified in this glass series.

3.4.4.3 $0.67Na_2S + 0.33[xSiS_2 + (1\text{-}x)PS_{5/2}]$ glasses

The ^{29}Si MAS NMR spectra of the 0.67 sodium thiosilicate system $0.1 \leq x \leq 1$ are shown in Figure 3.6b. For x = 1, the thiosilicate end member, two resonances are observed at 6.8 ppm and at –6.7 ppm. These resonances are assigned to the Si^0 and E^1Si^2 SRO structures, respectively. At y = 0.67 modifier concentration, it is expected to have Si^0 and therefore a completely depolymerized network, i.e. no BS units. The presence of ESi^2 structures at this modifier concentration has been discussed in a previous study on the $yNa_2S + (1\text{-}y)SiS_2$ by this group[30]. In brief, the edge-sharing structures appear to be quite stable, persisting out to y = 0.7 when their structure corresponds to only y = 0.5. Throughout the entire series, the Si^0 resonance is maintained into the Si poor samples. There is no apparent change in its chemical shift or width after the x = 1 composition that would suggest the presence of another SRO structure. The intensity of the E^1Si^2 resonance, however, appears to decrease as the composition approaches the P rich region, $x \rightarrow 1$. This behavior is different from that observed in the pure sodium thiosilicate binary system and the y = 0.5 sodium thiosilicophosphate ternary system where the ESi^2 population appears unaffected by the change in modifier concentration or the introduction of the competing P SRO structures in the latter system. The majority of the chemistry in these systems occurred between the corner shared SRO structures. This behavior in this $0.67Na_2S + 0.33[xSiS_2 + (1\text{-}x)PS_{5/2}]$ system would suggest that at this modifier

concentration there is an interaction between the P and Si SRO structures that lead to the depolymerization of the ESi^2 units. This will be discussed in more detail through the analysis of the composition dependence of the various SRO units in these glasses. The composition dependence of these Si and P SRO structures is shown in Figure 3.9.

3.4.4.4 Deconvolution of ^{29}Si MAS NMR Spectra

The deconvolution of the ^{29}Si MAS-NMR spectra was performed to determine the population fractions of the Si^0 and E^1Si^2 SRO units. Due to the simplicity of the spectra, fitting was accomplished with only one or two Gaussian peaks per composition – one peak corresponding to the Si^0 structure and the other to the ESi^2 structure. There was no change in the chemical shift or width for each peak throughout the series that would indicate the presence or evolution of addition SRO structures.

3.4.5 Composition Dependence of the various SRO units in the $0.5Na_2S + 0.5[xSiS_2 + (1-x)PS_{5/2}]$ Glasses.

As determined from all of the methods and analyses as described above, the composition dependence of the various SRO units in the y = 0.5 series is shown in Figure 3.8. These results come from the deconvolution analysis of the ^{31}P and ^{29}Si MAS-NMR spectra described above and the analysis of the Raman spectra. In this series, P^1, P^0, Si^2 and Si^3 SRO units are the expected SRO structures to be present in these glasses. However, because of the disproportionation reactions as described above in both the binary and ternary glasses, we observe additional SRO structures in this composition series such as P^{1P}, Si^1 and Si^{1Si}. Additionally, the Si^2 SRO structure can occur in two forms, as an edge-sharing, E^1Si^2 or corner-sharing structure, E^0Si^2. The trend of the E^1Si^2 SRO units is nearly linear, appearing only to decrease due to the relative concentration of $Na_2S + SiS_2$ in the composition. From previous studies of the sodium thiosilicate

glasses[30], it is known that this structure is very stable and in the presence of high modifier concentration, i.e. y = 0.7, a population of E^1Si^2 SRO units will remain in the glass. This suggests that the E^1Si^2 unit is unresponsive or unreactive with the P SRO units or environments in general. This further suggests that the Si SRO units participating in the reactions are only the corner-shared structures.

If Eq. (1) is followed across the series from x = 0 to 1, the concentration of Si^3 SRO units should reach a maximum. It starts at a non-zero value on the Si rich end (due to disproportionation in the binary glasses) and then it should reach a maximum at x = 0.5 and then decrease due to Si being the minority glass former in this composition range. If the Si^3 SRO structure exists in adamantane cages, it would take 2 moles of Na_2S to break up the cage to form Si^2 corner-shared structures. However, since we have found that in this composition (x) range, the P structures are unequally sharing the Na^+ and therefore form P^0 units according to Eq. (1) above, it is believed that these caged Si^3 structures will remain unaffected. If Si^3 units are being formed from the reaction of P^1 and Si^2 SRO units, where P takes the Na^+, it would have to come from the corner sharing E^0Si^2 structures. Because of this, the Si^3 units have the potential to exist in two forms, similar to the Si^2 -a networking Si^{3B} and a caged Si^{3M}, where the superscripts B and M refer to bridging and molecular, respectively see Figure 3.2. We have seen and quantified such behavior in the analogous $0.5Na_2S + 0.33[xGeS_2 + (1\text{-}x)PS_{5/2}]$ series[8] for the Ge^{3B} and Ge^{3M} units, where the former are the branched, corner-shared, and networked Ge^3 unit and the latter is the molecular adamantane Ge^3 unit.

3.4.6 Composition Dependence of the Various SRO Units in the $0.67Na_2S + 0.33[xSiS_2 + (1-x)PS_{5/2}]$ Glasses.

For the y = 0.67 series and Eq. (2) above, it is expected that there is sufficient Na_2S to completely depolymerize the glass network and even have left over unreacted Na_2S for x > 0 glasses. According to Eq. (2), in this series, the sodium thiosilicate glass would have a ratio of 4 Na to 1 Si, thereby yielding a pure Si^0 SRO unit at x = 1. The sodium thiophosphate glass would also have a ratio of 4 Na to 1 P, which would give the P^0 SRO unit and ½ mole of excess Na_2S. As a result, unlike the y = 0.5 glass series, there would seem to be no opportunity for P or Si to take Na from the other glass former or the glass network because all the available S sites are NBS sites and thereby change the various SRO units to anything other than Si^0 and P^0. Therefore, the expected evolution of SRO structures over this series would simply be the exchange of (1-x) moles of P^0 units for x moles of Si^0 units. However, as was shown above, the structural evolution is more complicated than this and more SRO units are observed in this series of glasses.

While the ^{31}P MAS-NMR spectra are indeed consistent with this simple model with concentration of the P^0 units decreasing to zero for $x \rightarrow 1$, the ^{29}Si MAS NMR spectra, Figure 3.6b, show that both Si^0 and ESi^2 SRO structures are observed in all of the spectra for x > 0.2. It is presumed that the relatively low sensitivity of the ^{29}Si MAS NMR signal is the reason that the ESi^2 units are not observed in the x = 0.1 and 0.2 glasses. Indeed, even with scans lasting more than 24 hrs, the resonance due to the main Si^0 species in these glasses has a signal to noise ratio of no more than about 5 to 1. Therefore, the structural evolution of the glasses in this series appears to be that the presumably small fraction of the energetically favored ESi^2 units formed in the x = 1 glass continue to be present even when P^0 units (x < 1) are added to glass. This reaction,

Eq. (3), would produce an additional amount of 1 mole of Na_2S for every mole of ESi^2 SRO units formed. Since we have already determined the relative proportions of the Si^0 and ESi^2 units in these glasses, Figure 3.9, we can determine the amount of additional Na_2S added to the glass structure from Eq. (3). Furthermore, as described above, there is already an additional amount of Na_2S coming from the excess Na_2S from the (1-x) moles of Na_2S added for every (1-x) moles of P^0 added to the composition. We have combined these two calculations in Figure 3.10 where we show the fraction of this "free" Na_2S as a fraction of the total moles of Na_2S, 0.67, added to the glass. As can be seen from Figure 3.10, the amount of "free" Na_2S in these glasses is quite high for all of the glasses. The value is high for the pure thiophosphate glass since the amount of extra added Na_2S is greatest for this glass, Eq. (2). The value is high for the pure thiosilicate glass because the disproportionation reaction, Eq. (3), produces the most Na_2S for this composition. The fraction of Na_2S passes through a minimum between these two compositional limits at x =0.3 composition. We are in the process of making a new series of glasses where the expected stoichiometric reaction should be $Si^0 \rightarrow P^0$ without any extra Na_2S and we will report on these glasses in the future, $0.67Na_2S + 0.33[xSiS_2 + (1\text{-}x)4/3PS_{5/2}]$.

$$Si^0 \rightarrow ESi^2 + Na_2S \qquad \text{Eq. (3)}$$

3.5 Conclusions

The structures of the sodium thiosilicophosphate glass series $yNa_2S + (1\text{-}y)[xSiS_2 + (1\text{-}x)4/3PS_{5/2}]$ at $yNa_2S = 0.5$ and $y = 0.67$ were examined through a combination of Raman, IR, and ^{31}P and ^{29}Si MAS-NMR spectroscopies. Through these studies, it was shown that the SRO structures arising from both glass formers are quite complex. In the y = 0.5 series, disproportionation reactions of structures for both the P and Si end members

led to the formation of P^2, P^1, P^0 and P^{1P} SRO units for P and Si^3, Si^2, and Si^1 SRO units for Si SRO. It was demonstrated that there is unequal sharing of the Na^+ ions between the two glass formers; P taking additional Na^+ to form P^0 SRO units and Si giving up Na to form Si^3 structures. In the 0.67 series, disproportionation reactions were also seen where the Si SRO structures were Si^0 and ESi^2, while P had two P^0 species present. In this series, due to the formation of under modified ESi^2 units and the over modified $0.67Na_2S + 0.33PS_{5/2}$ units, there appears to be a significant concentration of unreacted Na_2S for all compositions. This structural analysis will prove instrumental in explaining the physical properties studied in these two systems.

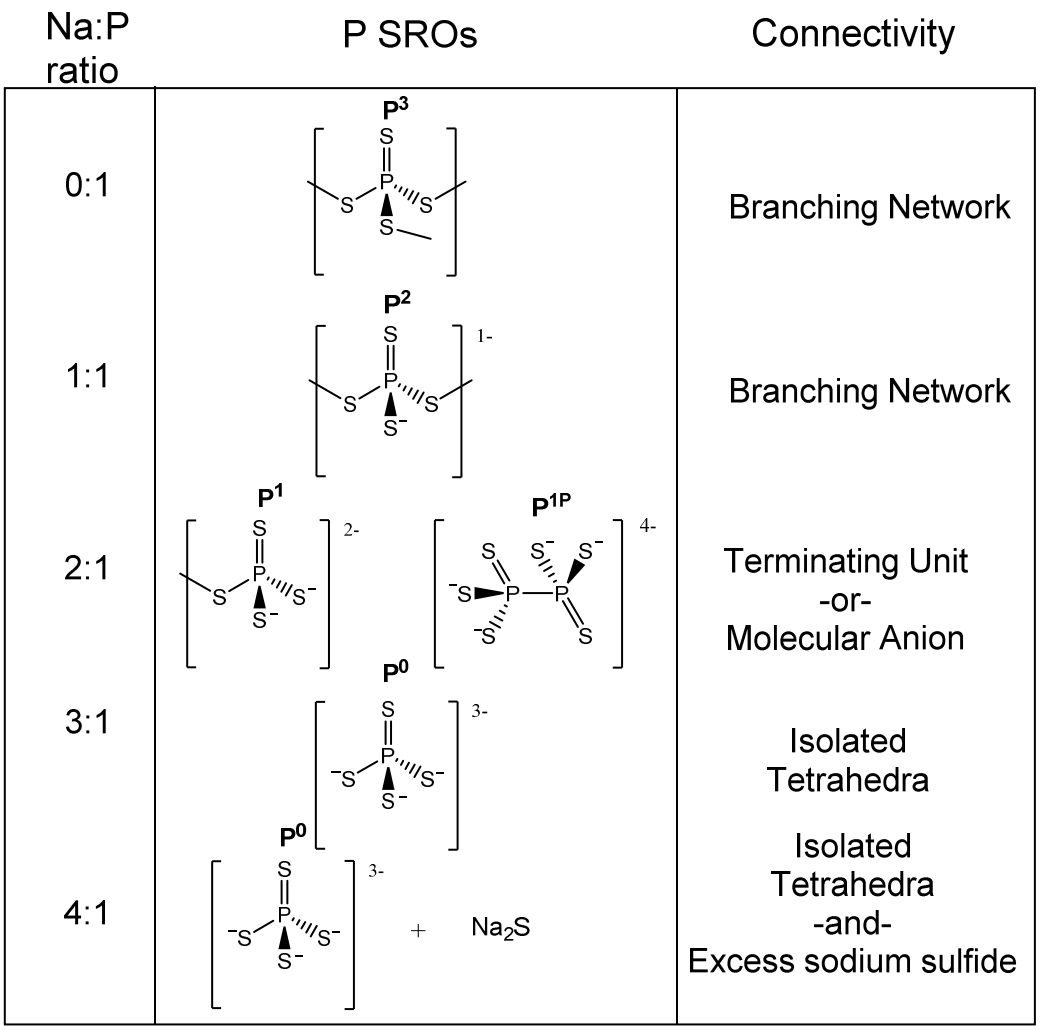

Figure 3.1 Phosphorus SRO structures in the sodium thiophosphate system

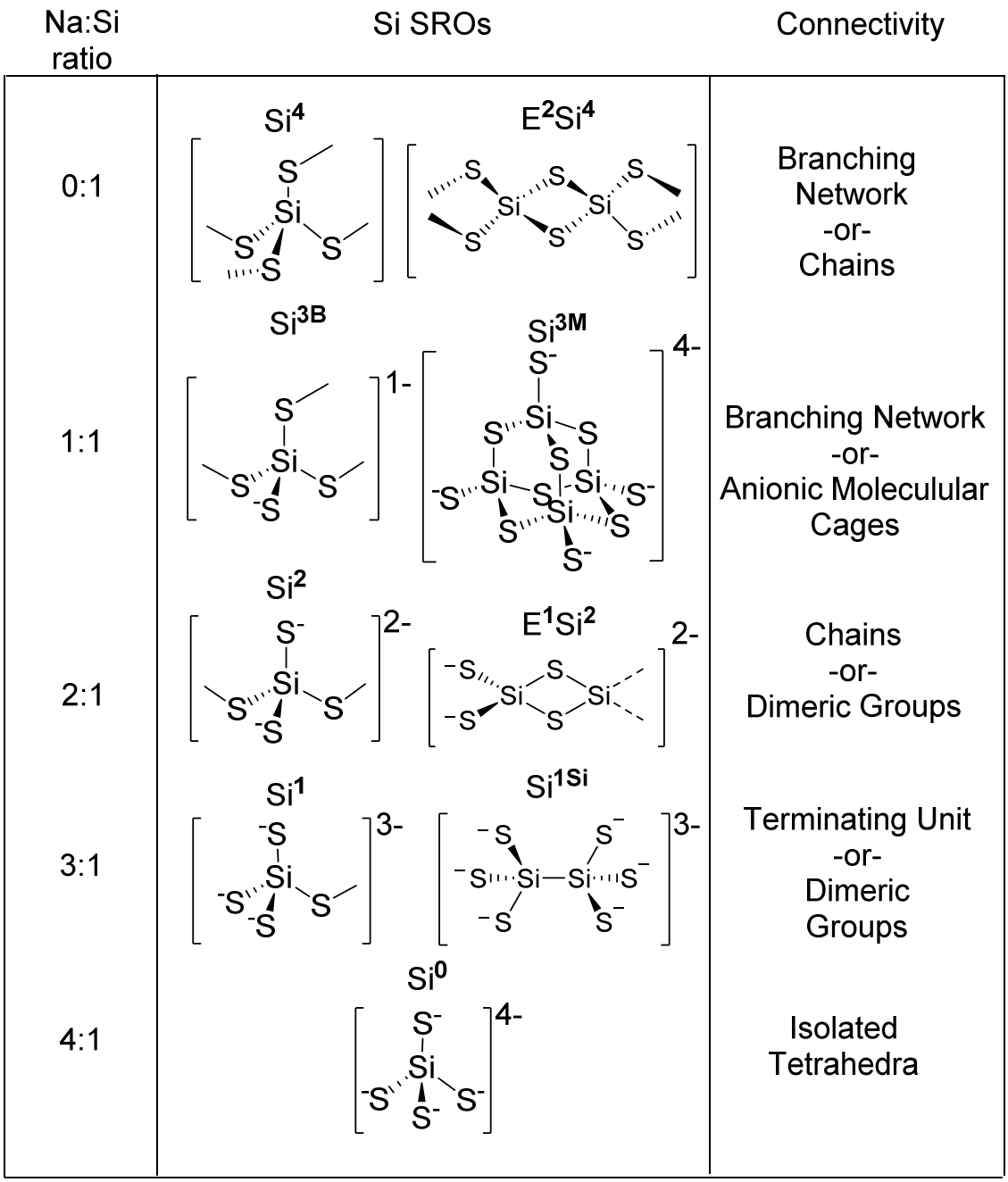

Figure 3.2 Silicon SRO Structures in the sodium thiosilicate system

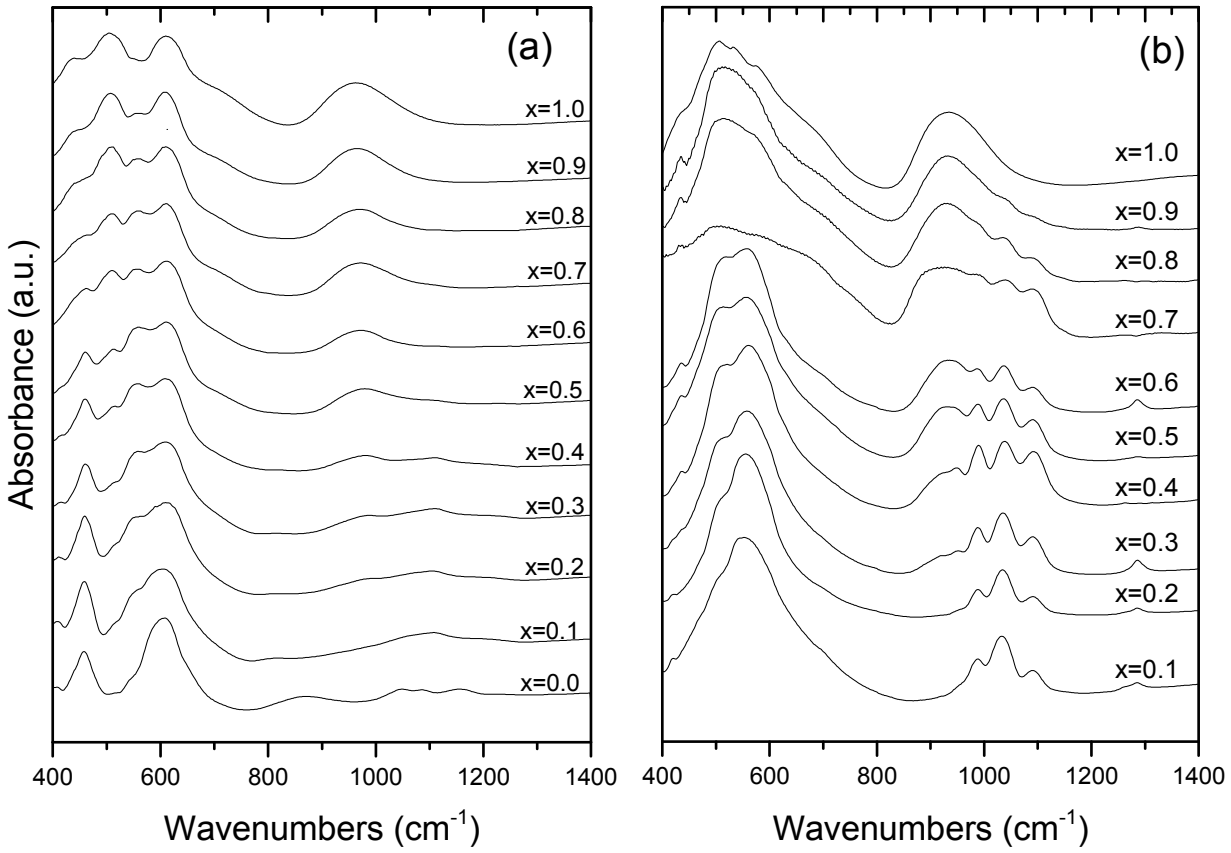

Figure 3.3 IR spectra of $yNa_2S + (1-y) [xSiS_2 + (1-x) PS_{5/2}]$ (a) y = 0.5 and (b) y = 0.67 glass series

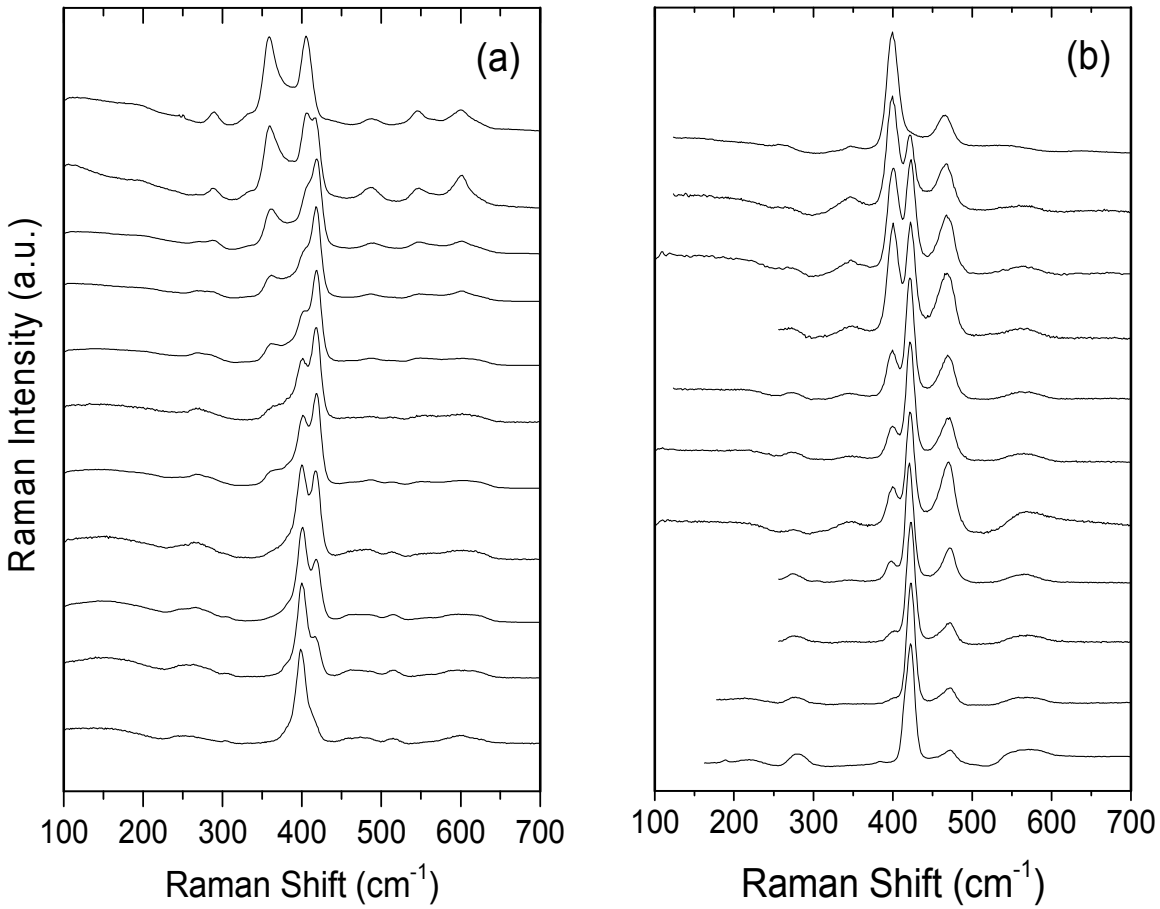

Figure 3.4 Raman spectra of $yNa_2S + (1-y) [xSiS_2 + (1-x) PS_{5/2}]$ (a) y = 0.5 and (b) y = 0.67 glass series

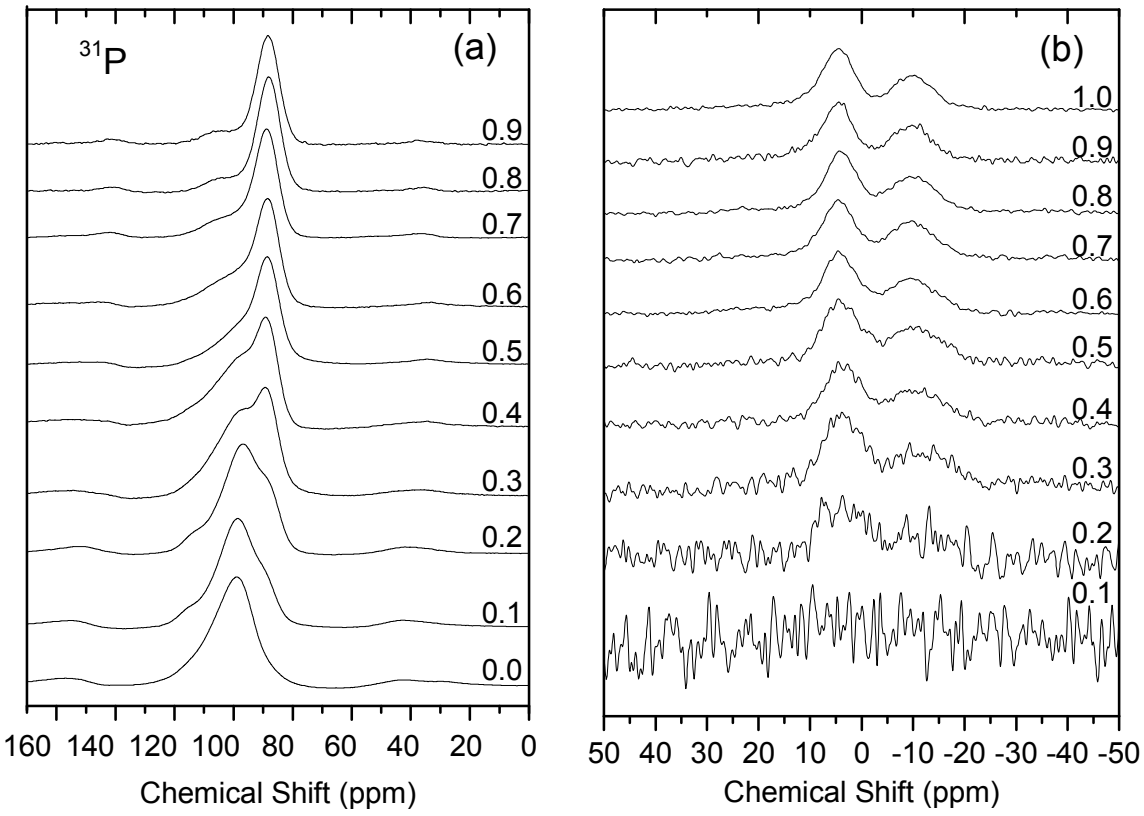

Figure 3.5 $0.5Na_2S + 0.5[xSiS_2 + (1\text{-}x)\ PS_{5/2}]$ (a) ^{31}P MAS NMR spectra x = 0.0 – 0.9 and (b) ^{29}Si MAS NMR spectra x = 0.1 to 1.0

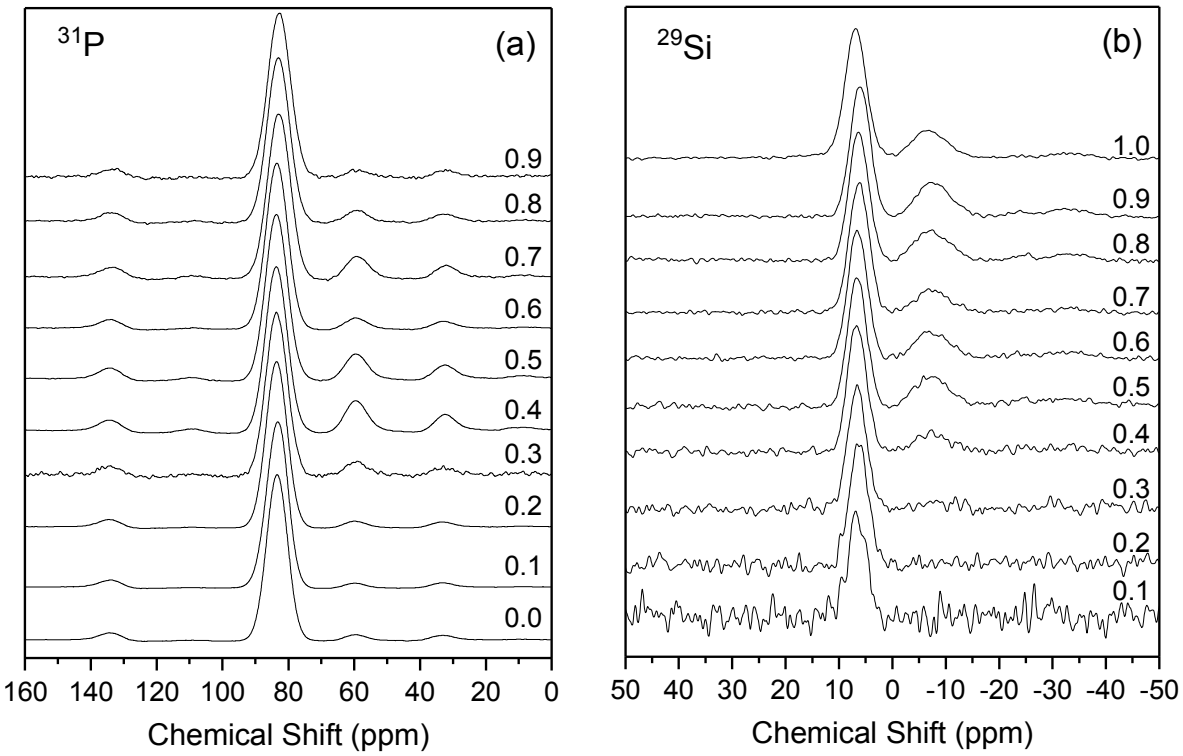

Figure 3.6 $0.67Na_2S + 0.33[xSiS_2 + (1\text{-}x)\ PS_{5/2}]$ (a) ^{31}P MAS NMR spectra x = 0.0 – 0.9 and (b) ^{29}Si MAS NMR spectra x = 0.1 to 1.0

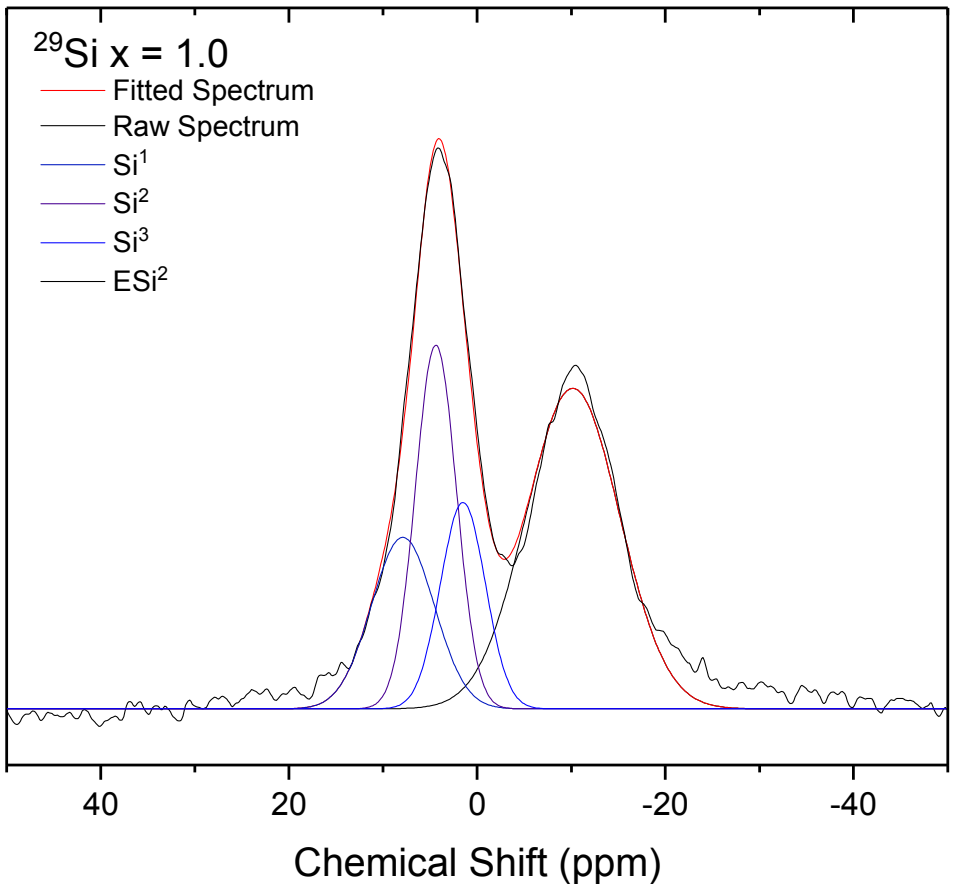

Figure 3.7 Deconvolution of ^{29}Si MAS NMR spectrum of $0.5Na_2S+0.5[xSiS_2 + (1-x)PS_{5/2}]$ x=1.0

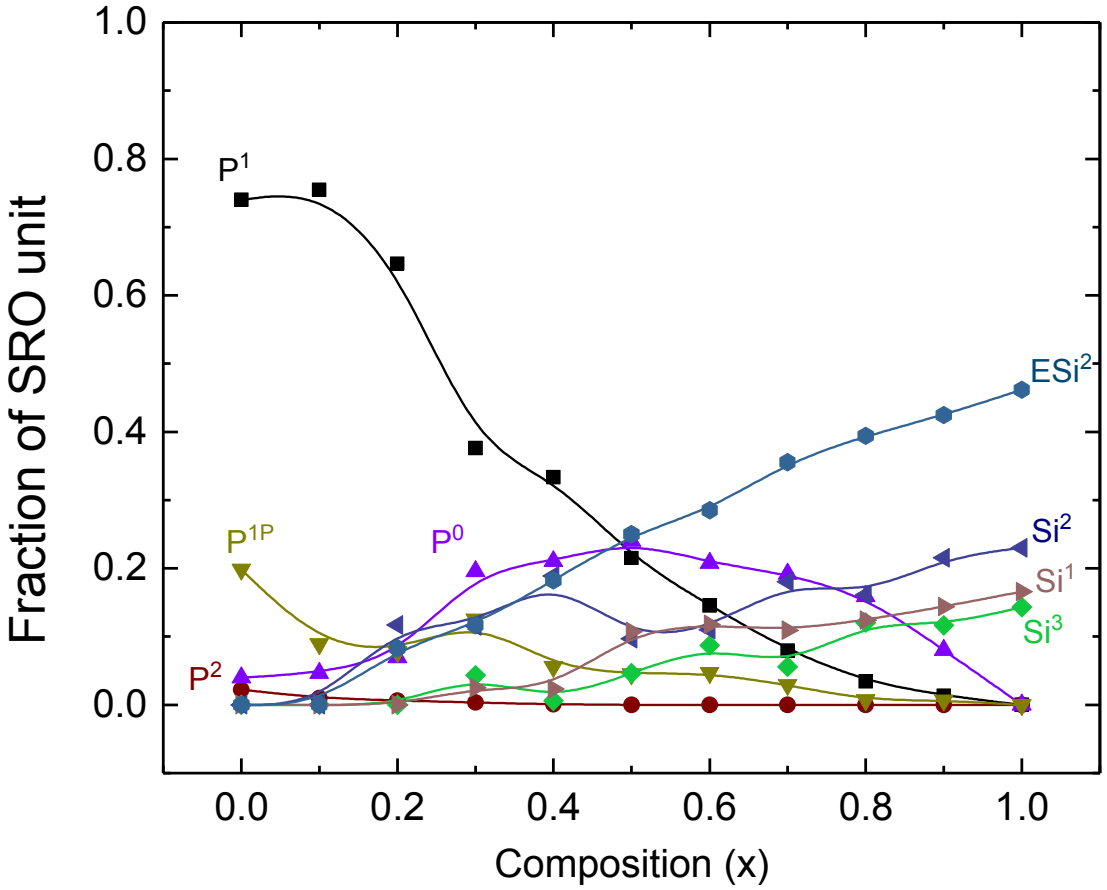

Figure 3.8. Composition Dependence of SRO structures in the $0.5Na_2S + 0.5[xSiS_2 + (1-x)\ PS_{5/2}]$ glass system

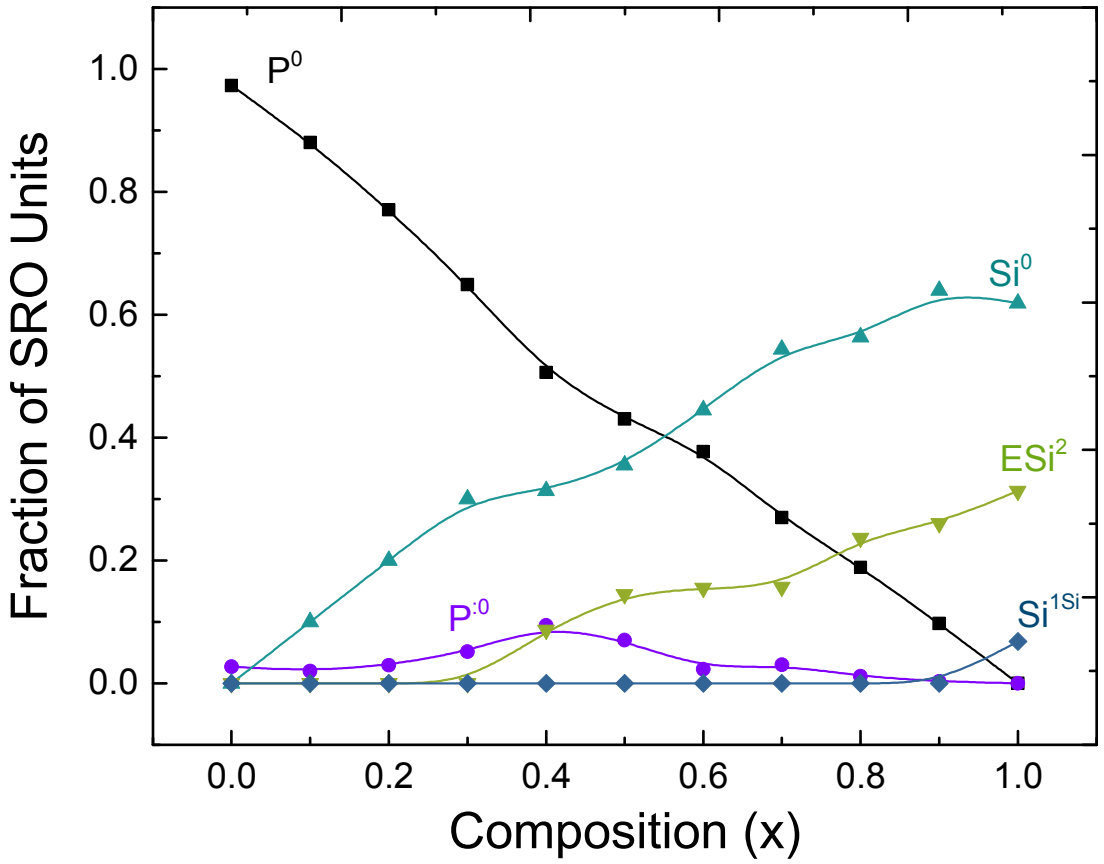

Figure 3.9. Composition Dependence of SRO structures in the $0.67Na_2S + 0.33[xSiS_2 + (1\text{-}x)\ PS_{5/2}]$ glass system

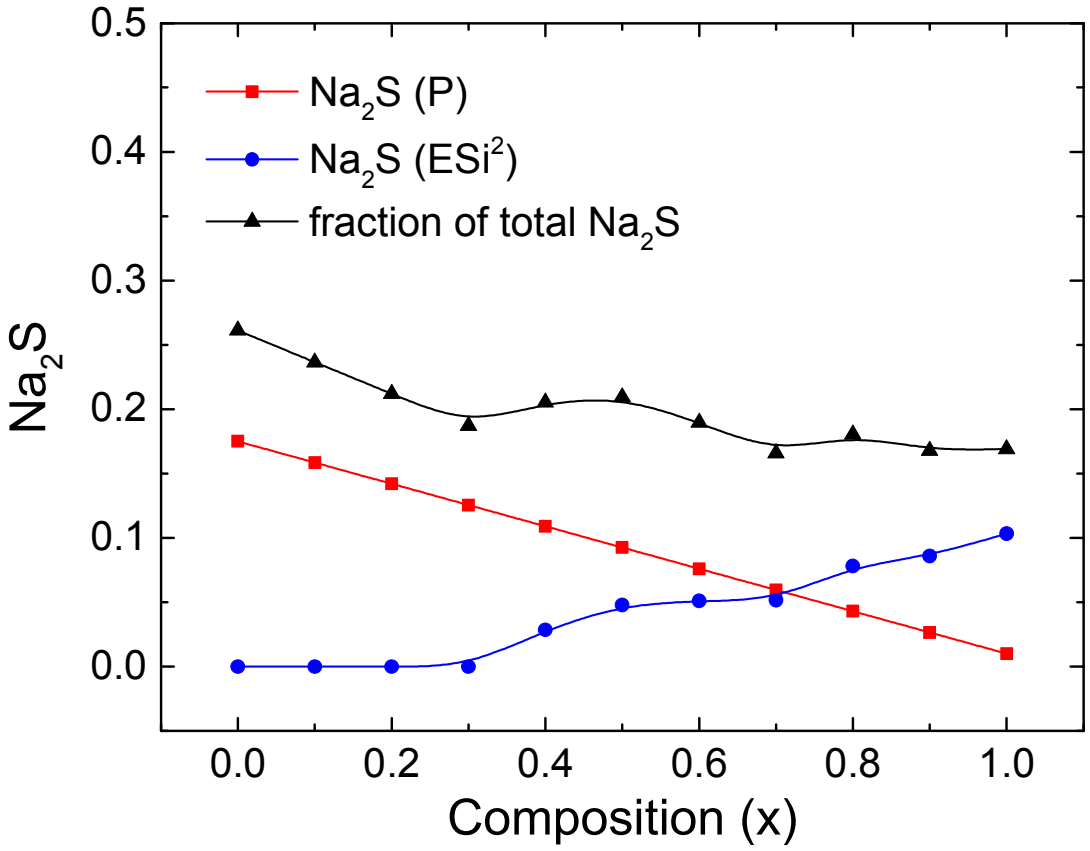

Figure 3.10. Composition (x) dependence of the excess Na_2S added to the glass from $0.67Na_2S$ +0.33 $PS_{5/2}$, from the formation of ESi^2 from Si^0 groups, and the total added Na_2S as a fraction of the total Na_2S in the glass, 0.67. The former two amounts are absolute mole numbers.

3.6 Acknowledgements

This research was supported by NSF grants DMR 0710546 and DMR 1304977. Iowa State University is gratefully acknowledged for support of Deborah Watson through their AGEP graduate fellowship program. Steven Kmiec is thanked for his help in collection of the Raman spectroscopy data and Sarah Cady and the Chemical Instrumentation Facility at Iowa State University are thanked for the use of their solid state NMR spectrometer and expertise. Thank you to Emma White of Ames National Lab for reading and editing this manuscript.

ABBREVIATIONS

SRO – Short Range Order

IR – Infrared

MAS-NMR – Magic Angle Spinning Nuclear Magnetic Resonance

3.7 References

1. Christensen, R.; Byer, J.; Kaufmann, T.; Martin, S. W. Structure–Property Relationships in the Mixed Glass Former System Na_2O–B_2O_3–P_2O_5. *Phys. Chem. Glasses – Eur. J. Glass Sci. Technol. B* **2009,** 50, 237.
2. Christensen, R.; Byer, J.; Olson, G.; Martin, S. W. The Densities of Mixed Glass Former 0.35 Na_2O + 0.65 [xB_2O_3 + (1 – x)P_2O_5] Glasses Related to the Atomic Fractions and Volumes of Short Range Structures. *J. Non-Cryst. Solids* **2012,** 358, 583.
3. Schuch, M.; Christensen, R.; Trott, C.; Maass, P.; Martin, S. W. Investigation of the Structures of Sodium Borophosphate Glasses by Reverse Monte Carlo Modeling to Examine the Origins of the Mixed Glass Former Effect. *J. Phys. Chem. C* **2012,** 116, 1503.
4. Christensen, R.; Olson, G.; Martin, S. W. Ionic conductivity of Mixed Glass Former 0.35 Na_2O + 0.65 [xB_2O_3 + (1-x) P_2O_5] Glasses. *J.Phys.Chem. B* **2013,** 117, 16577-16586.
5. Haynes, M. J.; Bischoff, C.; Kaufmann, T.; Martin, S. W. The mixed glass former effect on the thermal and volume properties of Na_2S-B_2S_3-P_2S_5 glasses. *Phys. Chem. Glasses – Eur. J. Glass Sci. Technol. B* **2009,** 50, 144-148.
6. Martin, S. W.; Bischoff, C.; Schuller, K. Composition Dependence of the Na+ Ion Conductivity in 0.5Na_2S + 0.5[xGeS_2 + (1 – x)$PS_{5/2}$] Mixed Glass Former Glasses: A Structural Interpretation of a Negative Mixed Glass Former Effect. *J. Phys. Chem. B* **2015,** 119, 15738.
7. Bischoff, C.; Schuller, K.; Dunlap, N.; Martin, S. W. IR, Raman and NMR Studies of the Short-Range Structures of 0.5Na_2S + 0.5[xGeS_2 + (1-x)$PS_{5/2}$] Mixed Glass Former Glasses. *J. Phys. Chem. B* **2014,** 118, 1943-1953.
8. Bischoff, C.; Schuller, K.; Martin, S. W. Short Range Structural Models of the Glass Transition Temperatures and Densities of 0.5Na_2S + 0.5[xGeS_2 + (1 – x)$PS_{5/2}$] Mixed Glass Former Glasses. *J. Phys. Chem. B* **2014,** 118, 3710.
9. Deshpande, V. K.; Pradel, A.; Ribes, M. The Mixed Glass Former Effect in the Li_2S-SiS_2-GeS_2 System. *Mater. Res. Bull.* **1988,** 23, 379-384.
10. Pradel, A.; Rau, C.; Bittencourt, D.; Armand, P.; Philippot, E.; Ribes, M. Mixed glass former effect in the system 0.3$Li_{(2)}S$-0.7[(1-x)SiS_2-x$GeS_{(2)}$]: A structural explanation. *Chem. Mater.* **1998,** 10, 2162-2166
11. Schuch, M.; Müller, C. R.; Maass, P.; Martin, S. W. Mixed Barrier Model for the Mixed Glass Former Effect in Ion Conducting Glasses. *Phys. Rev. Lett.* **2009,** 102, 145902.
12. Schuch, M.; Trott, C.; Maass, P. Network Forming Units in Alkali Borate and Borophosphate Glasses and the Mixed Glass Former Effect. *RSC Adv.* **2011,** 1, 1370.
13. Schuch, M.; Christensen, R.; Trott, C.; Maas, P.; Martin, S. W. Investigation of the Structures of Sodium Borophosphate Glasses by Reverse Monte Carlo Modeling to Examine the Origins of the Mixed Glass Former Effect. *J Phys Chem C* **2012,** 116, 1503-1511.
14. Bischoff, C.; Schuller, K.; Martin, S. W. Short range structural models of the glass transition temperatures and densities of 0.5Na_2S + 0.5[xGeS_2 + (1 - x)$PS_{5/2}$] mixed glass former glasses. *J Phys Chem B* **2014,** 118, 3710-9.

15. Martin, S. W. In *Handbook of solid state batteries*; 2 ed.; Dudney, N. J., West, W. C., Nanda, J., Ed.; World Scientific Pub.: New Jersey, 2016; Chapter 14, Vol. 6, pp 433-501.

16. Wang, W.; Christensen, R.; Curtis, B.; Hynek, D.; Keizer, S.; Wang, J.; Feller, S.; Martin, S. W.; Kieffer, J. Elastic properties and short-range structural order in mixed network former glasses. *Phys. Chem. Chem. Phys.* **2017**

17. Lee, Y.-I.; Lee, J.-H.; Hong, S.-H.; Park, Y. Li-ion conductivity in Li_2O–B_2O_3–V_2O5 glass system. *Solid State Ion.* **2004,** 175, 687-690

18. Lee, C. H.; Joo, K. H.; Kim, J. H.; Woo, S. G.; Sohn, H. J.; Kang, T.; Park, Y.; Oh, J. Y. Characterizations of a new lithium ion conducting Li_2O–SeO_2–B_2O_3 glass electrolyte. *Solid State Ion.* **2002,** 149, 59-65.

19. Christensen, R.; Byer, J.; Olson, G.; Martin, S. W. The densities of mixed glass former 0.35 Na_2O + 0.65 [xB_2O_3 + (1-x) P_2O_5] glasses related to the atomic fractions and volumes of short range structures. *J. Non-Cryst. Solids* **2012,** 358, 253-589.

20. Christensen, R.; Byer, J.; Olson, G.; Martin, S. W. The glass transition temperature of mixed glass former 0.35 Na_2O + 0.65 [xB_2O_3 + (1-x) P_2O_5] glasses. *J. Non-Cryst. Solids* **2012,** 358, 826-831.

21. Estournes, C.; Owens, A. P.; Menetrier, M.; Levasseur, A.; Rao, K. J.; Elliott, S. R. A Structural Study of Li_2S-B_2S_3 Glasses by Neutron-Diffraction. *J. Non-Cryst. Solids* **1994,** 171, 80-86

22. Christensen, R.; Olson, G.; Martin, S. W. Structural studies of mixed glass former 0.35 Na_2O + 0.65 [xB_2O_3 + (1-x) P_2O_5] glasses by Raman and ^{11}B and ^{31}P Magic Angle Spinning Nuclear Magnetic Resonance Spectroscopies. *J Phys Chem B* **2013,** 117, 2169-2179.

23. Bischoff, C. The Mixed Glass Former Effect in 0.5Na_2S + 0.5[xGeS_2 + (1-x)$PS_{5/2}$] glasses. Dissertation, Iowa State University, 2013.

24. Larink, D.; Ren, J. J.; Eckert, H. Spectral editing based on scalar spin-spin interactions: New results on the structure of metathiophosphate glasses. *Solid State Nucl. Magn. Reson.* **2012,** 45-46, 30-35

25. Larink, D.; Eckert, H.; Martin, S. W. Structure and Ionic Conductivity in the Mixed-Network Former Chalcogenide Glass System [Na_2S](2/3)[(B_2S_3)(x)(P_2S_5)(1-x)](1/3). *J Phys Chem C* **2012,** 116.

26. Eckert, H.; Kennedy, J. H.; Pradel, A.; Ribes, M. Structural Transformation of Thiosilicate Glasses - Si-29 Mas Nmr Evidence for Edge-Sharing in the System Li_2S-SiS_2. *J. Non-Cryst. Solids* **1989,** 113, 287-293

27. Bischoff, C.; Schuller, K.; Haynes, M.; Martin, S. W. Structural investigations of yNa_2S + (1 − y)$PS_{5/2}$ glasses using Raman and infrared spectroscopies. *J. Non-Cryst. Solids* **2012,** 358, 3216-3222

28. Pradel, A.; Taillades, G.; Ribes, M.; Eckert, H. Si-29 Nmr Structural Studies of Ionically Conductive Silicon Chalcogenide Glasses and Model Compounds. *J. Non-Cryst. Solids* **1995,** 188, 75-86

29. Cho, J.; Martin, S. W. *Structures and ionic conduction of xNa_2S + (1-x)SiS_2 glasses*. American Ceramic Society, Westerville, OH (United States): 1996; p Medium: X; Size: pp. 85-99.

30. Watson, D. E.; Martin, S. W. Short range order characterization of the $Na_2S + SiS_2$ glass system using Raman, infrared and ^{29}Si magic angle spinning nuclear magnetic resonance spectroscopies. *J. Non-Cryst. Solids* **2017,** 471, 39-50

31. El Jaroudi, O.; Picquenard, E.; Gobeltz, N.; Demortier, A.; Corset, J. Raman Spectroscopy Study of the Reaction between Sodium Sulfide or Disulfide and Sulfur: Identity of the Species Formed in Solid and Liquid Phases. *Inorg Chem* **1999,** 38 , 2917-2923.

32. Powell, D. B.; Scott, J. G. V. Infrared spectra of the thiophosphates of trisethylenediamine cobalt (III). *Spectrochim Acta A Mol Spectrosc* **1972,** 28 , 1067-1074.

33. Larink, D.; Ren, J.; Eckert, H. Spectral editing based on scalar spin–spin interactions: New results on the structure of metathiophosphate glasses. *Solid State Nucl. Magn. Reson.* **2012,** 45, 30-35.

34. Ribes, M.; Olivier-Fourcade, J.; Philippot, E.; Maurin, M. Etude structurale de thiocomposés à groupement anionique de type tétrane $Na_4X_4S_{10}$ (X = Ge, Si) et $Ba_2Ge_4S_{10}$. *J. Solid State Chem.* **1973,** 8 , 195-205

CHAPTER 4. THE COMPOSITION DEPENDENCE OF THE GLASS TRANSITION TEMPERATURE AND DENSITY IN MGF SODIUM THIOSILICOPHOSPHATE GLASSES: A STRUCTURAL PERSPECTIVE

A paper to be submitted to the Journal of Physical Chemistry B

Deborah E. Watson[5]*, Steve W. Martin*[6]

Department of Materials Science and Engineering, Iowa State University

Ames, Iowa 50010-2300

4.1 Abstract

The glass transition temperature and density are two physical properties known to exhibit the mixed glass former effect (MGFE), a nonlinear non-additive increase or decrease from a linear mixing behavior, in ternary systems where the two glass forming species are varied while the modifier remains constant across the system. The T_g(s) of $0.5Na_2S + 0.5[xSiS_2 + (1\text{-}x)\ PS_{5/2}]$ and $0.67Na_2S + 0.33[xSiS_2 + (1\text{-}x)PS_{5/2}]$ glasses were examined and determined to have a negative MGFE in the former and little evidence of such behavior in the latter system. Interestingly, the densities of the y = 0.5 system do not appear to have a distinct effect, showing both a maximum and minimum while in the y = 0.67 system there is a strong negative MGFE with two minima at the x = 0.2 & 0.6 compositions. Using the short range order structure model for each system, the number of bridging and non-bridging sulfurs were calculated and analyzed alongside these physical properties. In this analysis, a relationship between the T_g and the bridging sulfurs is evident in both systems. In the case of the densities, the molar volumes were calculated

---

[5] Primary researcher and author

[6] Corresponding author and principle investigator

for each systems and its behavior compared to the SRO model. In both cases the Si structures lead in an increase in molar volume, appearing to open up the structure. In the y = 0.5 system, the presence of Si^2 and Si^3 structures increases as the molar volume increase. In the y = 0.67 system, the maxima seen in the molar volume produced are related to the concentration of free Na_2S in the system.

4.2 Introduction

Renewable energy resources and the energy storage systems which accommodate them have gained importance in a society that is becoming ever more dependent on the use of electricity for everyday living[1, 2]. In an initiative going beyond batteries for phones, computers and electric vehicles (eV), advanced battery technologies, like the Li ion battery, are being explored as energy storage systems for grid level electrical storage applications[3]. Of the many advanced battery designs being consider, new solid state sodium batteries have recently regained interest as an alternative to lithium. Taking advantage of the similar technology and mechanism of Li batteries, but capitalizing on its natural abundance[4] and equal accessibility to the global community[5], sodium solid state batteries have the potential to address the needs of this particular niche. In order for the goals to be fully reached and encourage the progression of sodium solid state battery design, research to find electrolyte materials that can accommodate a sodium metal anode (or similar materials) and cathode materials with the best energy density and capacity is imperative and the field has responded to that demand[6]. Sodium mixed glass former systems are being investigate as one viable option to this task.

The study of the mixed glass former effect in ternary alkali glasses is the analysis of a nonlinear, non-additive increase or decrease in the physical properties as a result of

varying two glass formers while holding the alkali (modifier) concentration constant. The properties under which this behavior is typically observe in addition to ionic conductivity are the glass transition temperature and density [7-12]. By controlling the ratio of a glass forming species to another, it is possible to link the changes in these physical properties with the changes at the atomic short range order. The $0.5Na_2S + 0.5[xGeS_2 + (1-x)PS_{5/2}]$ MGF system, analogous to this sodium thiosilicophosphate systems, was shown to have a negative MGFE in the T_g while the densities did not show a strong MGFE in the densities[7]. Bischoff modeled the experimental T_g and molar volumes using the atomic short range order analysis from ^{31}P MAS NMR and was able to show that the proposed Ge^{3M} structure was causing the depression in the T_g and molar volume trends. This model was then modified to analyze the molar volumes of these glasses.

In a recent paper, the network structure of these sodium thiosilicophosphate MGF systems were proposed. In the y = 0.50 modified system, disproportionation reactions on both the phosphorus and silicon end members led to a complex diversity of short range order structures. Similar to the Na Ge P S, where non-equal sharing of Na^+ lead to the depolymerization of P^1 to P^0, P^1 were converted to P^0 as Si^2 were polymerized to Si^3. The Raman and ^{29}Si MAS NMR analysis showed the possibly presence of Si^{3M} structures like the Ge^{3M} proposed in Bischoff's work. In the y = 0.67 system, the network was nearly completely depolymerized. The $0.67Na_2S + 0.33PS_{5/2}$ sodium thiophosphate is above the P^0 composition (y = 0.60) and therefore contains both P^0 and ½ mole of Na_2S. A small population of the defect structure $P^{:0}$ was also found. The 0.67 sodium thiosilicate is the Si^0 composition but also disproportionates into Si^0 and ESi^2 dimers. As a result of this modifier concentration, there are no new SRO structures generated from Na^+ exchange

between these structures. However the presence of the $P^{:0}$ and ESi^{2} structures lead to the formation of Na_2S and Na_2S_2.

The goal of this paper is to tie the measured physical properties with the atomic structure that is known about the glass. Glass transition temperature has been used to describe various characteristics of a glass such as strength, network connectivity, and when compared with the crystallization temperature, it's resistant to crystallization, or otherwise the working range of the glass. These elements are very important to electrolyte design as it provides information on the potential stability of the material in an electrochemical environment. The density of a glass when connected to the atomic SRO structure can aid in the understanding of the packing behavior and potentially show how freely a Na^+ can move throughout the network.

4.3 Experimental Methods

4.3.1 Sample preparation

4.3.1.1 $0.5Na_2S + 0.5[xSiS_2 + (1\text{-}x)\ PS_{5/2}]$ glass system

Sodium sulfide (Na_2S) was synthesized by a low temperature thermal dehydration process of sodium sulfide nonahydrate under vacuum for 24 hour period. After the dehydration process, the product was mechanically milled in a N_2 glove box and then heat treated in a tube furnace for 10 minutes. The sodium sulfide was characterized using mid and far infrared spectroscopy (IR) and X ray diffraction spectroscopy.

Silicon sulfide (SiS_2) was synthesized by combining stoichiometric amounts of silicon and sulfur in a quartz ampoule which was after evacuated and sealed under a vacuum. The reactants are undergo a solid state process during a 48 hour heating schedule from 50 to 970°C. The ampoule is opened inside a N_2 atmosphere and the

product is mechanically milled to produce a powder for glass batching. IR, Raman and XRD were used confirm the target composition and determine phase purity.

4.3.1.2 $0.67Na_2S + 0.33[xSiS_2 + (1\text{-}x)PS_{5/2}]$ glass system

Commercial sodium sulfide (Alfa Aesar) and phosphorus pentasulfide (Sigma Aldrich) was used for the synthesis of these glasses. Silicon sulfide was made via the process described in the earlier section.

4.3.2 Glass Transition Temperature – Differential Scanning Calorimetry

The glass transition temperature (T_g) was measured using differential scanning calorimetry on a Perkin Elmer Diamond differential scanning calorimeter. Bulk pieces of glass were packed in aluminum pans and cold welded shut using a DSC pan press. Temperature scans over the range of 50 – 400 °C were done to survey the thermal properties of each sample at 20°C per minute. After determining the T_g and crystallization temperature (T_x) from these survey scans, the glass were then cycled at 20 °C through the T_g but before the T_x three times to establish good thermal history for the sample and test the reproducibility of the T_g values.

4.3.3 Density – Archimedes Principle

Density measurements were taken inside an argon atmosphere using Archimedes Principle. The submersion fluid used was paraffin oil (ρ=0.82 g/cc). Three to four measurements per composition were done. The densities were calculated using the following formula:

$$\rho = \frac{A}{A - B}(\rho_0 - \rho_L) + \rho_L$$

4.1

where ρ is the density, A is the mass of the sample in air, B is the mass of the sample in the auxiliary liquid, ρ_0 is the density of the auxiliary liquid and ρ_L is the density of argon.

4.4 Results

4.4.1 Glass Transition Temperatures of the $0.5Na_2S + 0.5[xSiS_2 + (1-x) PS_{5/2}]$ glasses

The composition dependence of the glass transition temperature in the 0.5 series are shown in Figure 4.1. The x = 0.0, sodium thiophosphate glass, has a T_g of 194 °C while the x = 1.0, sodium thiosilicate glass has a T_g of 272 °C. The ternary glasses exhibit a negative MFGE in this trend with the maximum deviation from linear mixing occurring at x = 0.4.

4.4.2 Glass Transition Temperatures of the $0.67Na_2S + 0.33[xSiS_2 + (1-x)PS_{5/2}]$ glasses

The glass transition temperatures of the 0.67 series is shown in Figure 4.2. The sodium thiophosphate's T_g is 162 °C and the sodium thiosilicate is at 247 °C. The ternary glasses exhibit a modest negative MGFE but experiencing two maxima at x = 0.4 and 0.6. The Tg(s) of this compositions are close to the temperatures expected for an ideal mixing linear behavior.

4.4.3 Densities of the $0.5Na_2S + 0.5[xSiS_2 + (1-x) PS_{5/2}]$ glasses

The composition dependence of the densities are shown in Figure 4.3. The density of the x = 0.0 glass is 2.02 g/cm^3 while the x = 1.0 glass has a density of 2.03 g/cm^3. Across the composition the thiophosphate rich glasses increase in density having a maximum at x = 0.2 with a density of 2.07 g/cm^3. When $x \geq 0.5$ the densities decrease experiencing a minimum at x =0.8 with a density of 1.99 g/cm^3. Nevertheless the average density of this system is 2.02 g/cm^3 and therefore the change is ± 0.05 g/cm^3.

4.4.4 Densities of the $0.67Na_2S + 0.33[xSiS_2 + (1-x)PS_{5/2}]$ glasses

The densities of the 0.67 series is shown in Figure 4.4. The densities of the end members differ only by ~0.01 g/cm^3 with the thiophosphate binary glass has a density of 1.96 g/cm^3 and the thiosilicate end member having a density of 1.97 g/cm^3. A negative MGFE is observed where two minima are experience at compositions at x= 0.2 and 0.6, having densities of 1.89 and 1.85 g/cm^3 respectively.

4.5 Discussion

4.5.1 Glass Transition Temperature

While the glass transition temperatures of the $0.5Na_2S + 0.5[xSiS_2 + (1-x)\ PS_{5/2}]$ system experience a negative deviation from linear mixing, the increase to the thiosilicate end is expected. From the ^{29}Si and ^{31}P MAS NMR analysis, the x = 0 glass consists of P^1, small populations of P^0 and P^2 (which charge balance) and a P^{1P} dimers. Therefore this glass mainly consists of molecular anions. The sodium thiosilicate contains Si^2, ESi^2, Si^3 and Si^1 structures. The Si^2 and Si^3 SRO are the main contributors for networking in this glass. As the composition goes from x = 0.0 to 1.0, the unequal sharing of Na^+ on the P leads to the formation of P^0 from P^1; as a result Si^3 structures form from Si^2 thus increasing the network bonding in the glass. This network bonding can be further understood by relating it to number of bridging sulfurs (bS) per composition. Table 1 lists the SRO structures of this system with their corresponding number of bS and non-bridging sulfurs (nbS). The P^1 structure has 0.5 bS while the Si^2 has 1 bS. Using the atomic fraction of SRO structures from the ^{29}Si and ^{31}P MAS NMR results, it is possible to calculate the total amount of bS and non-bridging sulfurs (nbS) in each glass and thus

investigate what effect it may have on the T_g. The N_{bS} (x) can be calculated using the following equation:

$$N_{bS} = \sum_j f(x) N_{bS_j} \qquad 4.2$$

Figure 4.5 shows the composition dependence of the T_g with the change in fraction of bS across the system. The trend of the glass transition temperatures in the y = 0.5 system appears to trend with the increase in bS. This translates to a ~ 78 °C increase in T_g from x = 0 to 1, the majority of that increase occurring after x = 0.4. Though the minimum in the T_g occurs at x = 0.4, the minimum in the bS occurs at x = 0.5. The reason for this is not yet understood however the difference in bS concentration between the 0.4 and 0.5 is 0.013, roughly 2% change. The N_{bS} in the thiophosphate rich glasses are controlled by the P^0 formation and perhaps this is what gives rise to the suppression of the T_g in these glass. At x = 0.4 the contribution of bS from P SRO units and Si SRO units are nearly equal (ΔN_{bS} =0.014), but at x = 0.5 the bS from Si increases above P (ΔN_{bS} =0.086). This shift could likely explain the significant increase in the T_g.

In the y = 0.67 system, the T_g decreased ~ 30 °C on each member below that of the y = 0.5 system. As in the y = 0.5 glasses, the T_g in the y = 0.67 glasses increases toward the thiosilicate rich end member, but here in a nominally linear fashion, perhaps suggesting weak to no presence of the MGFE. The increase over all between the end members is ~ 85 °C. At this high modifier concentration, there is a small concentration of glass formers, all of which's units are fully depolymerized SRO structures or molecular anions. The sodium thiophosphate contains P^0 and $P^{:0}$ structures while the sodium

thiosilicate contains Si^0 and ESi^2 structures. Both the P^0 and Si^0 change in a linear trend. In the Raman spectra, it appears that there is a simple exchange of P^0 for Si^0 as the composition changes. Again the NbS can be calculated from the atomic fraction of SRO structures from ^{29}Si and ^{31}P MAS NMR analysis. Table 2 lists the SRO structures of this system along with the number of bS and nbS corresponding to each. Figure 4.6 shows the composition dependence of T_g plotted with the change in fraction of bS. The trends of these curves behave similarly but show a weak connection between the two. Another interesting feature is the fraction of bS, which come only from the ESi^2 dimers, shifts only from 0 in the x = 0.0 glass to 0.31 in the x = 1.0 unlike in the y = 0.5 glasses, where the bS goes from 0.5 in the x = 0.0 to 1.0 in the x =1.0. Yet the T_g increase across the system surpass that of the y = 0.5 system by 7 °C. This raises the question of what else is effecting the T_g?

4.5.2 Density and Molar Volume

Like in the T_g of the $0.5Na_2S + 0.5[xSiS_2 + (1\text{-}x)\ PS_{5/2}]$ system there seems to some significant shift occurring between the x = 0.4 and 0.5 compositions. While the T_g increases from 196 to 217 °C, the density decreases from 2.02 g/cm^3 to 1.99 g/cm^3. While this change might not seem significant, it might give insight into the change in packing efficiency of the SRO structures which could be understood by analyzing the molar volume composition dependence.

The molar volume can be calculated by simply dividing the molecular mass of the glass by the measured density. The result of these calculations are shown in Figure 4.7. The x = 0.0 sodium thiophosphate has a molar volume of 46.9 cm^3/mol and the x = 1.0 sodium thiosilicate has a molar volume of 41.9 cm^3/mol. Figure 4.8 shows the decrease in

molar volumes as x → 1 while the fraction of bS, also compared in the T_g, increases. This seems to imply that as the Si SRO structures of this system increase the networking, they are tightening up the network, perhaps drawing the SRO structures closer together. The sodium phosphate rich glasses ($0.0 \leq x \leq 0.4$) initially shows a negative deviation from the linear trend ($0.0 \leq x \leq 0.2$), a densification in the glasses and almost plateaus in the molar volume from x = 0.2 to 0.5. In this region, the behavior may be dominated by the P^0 formation. In the x = 0.0 to 0.2, the P^0 concentration is low and begins to change quickly after x = 0.2. Here the molar volume decreases as the number of bS increase. From x = 0.2 to 0.5, the molar volumes plateau over the same region where the number of nbS created from P^0 is almost equal to the number of bS in the system (Figure 4.9). Then when the P^0 population decrease in the sodium thiosilicate rich region, the number of bS are no longer cancelled out by the nbS from P^0 and thus the molar volume decreases again as the number of bS increases. The positive deviation in the molar volume in the sodium thiosilicate rich glasses is due to a deficiency in bridging sulfurs. The majority of SRO structures in this region are molecular anions, such as ESi^2, P^0, P^{1P}, P^1 and Si^1, which decrease the connectivity.

The density of y = 0.67 sodium thiosilicophosphate systems decrease from that of the y = 0.5 system. These glasses exhibit an average density of 1.93 g/cm^3 compared to 2.02 g/cm^3 in the y = 0.5. The system exhibits a negative MGFE but has two minima are seen in the x = 0.2 and x = 0.6 glasses with densities at 1.89 and 1.85 g/cm^3. The SRO structure composition dependence may be used to understand this behavior. Initially the addition of SiS_2 appears to lower the density for compositions 0.1 and 0.2 where the P^0 population decrease proportionally with the increase of Si^0 population. In the y = 0.5 it

was shown that the addition of bS results in an increase in the density. Conversely, the lack of bS or increase of nbS may lead to a decrease in the density due to the extent of depolymerization. This can be seen by the molar volume composition dependence in Figure 4.10. Also at x = 0.2, the population of $P^{:0}$ begins at ~3%. As it rises to 9% at x = 0.4, the density also rises from 1.89 g/cm^3 to 1.94 g/cm^3. The ESi^2 population also begins to contribute to the network at x = 0.4. Then as the composition approaches x = 0.6, the density decrease to 1.86 g/cm^3 as the $P^{:0}$ population to 2.3%. Beyond this glass, the $P^{:0}$ population decreases as the Si SRO population begin to dominate the glass. At composition x = 0.7 to x = 1.0 increase again ending at 1.97 g/cm^3. Here the densities increase also with increasing ESi^2 population. Though the bS of the ESi^2 does not contribute to networking, the increase in bS does follow the increase in densities as also demonstrated in the y = 0.5 system.

4.6 Conclusions

The $0.5Na_2S + 0.5[xSiS_2 + (1\text{-}x)\ PS_{5/2}]$ and the $0.67Na_2S + 0.33[xSiS_2 + (1\text{-}x)PS_{5/2}]$ systems showed a negative MGFE in the T_g that is controlled by the amount of bS in the structure. In the thiophosphate rich glasses of the y = 0.5 system, the T_g remained fairly constant until the x = 0.5 composition where the T_g increased rapidly with each thiosilicate addition. This is proposed to be impart due to the bS from networking SRO structures such as Si^2 and Si^3 structures. In the y = 0.67 system, the T_g composition dependence trends with the amount of bS in the system, despite the fact that these bS are in ESi^2 dimers. ESi^2 structures are the known structure of the HT-Na_2SiS_3 phase that have shown to be stable and consistently formed in the thiosilicate glasses despite its seemingly high strain geometry in a 4-membered ring. Not all bridging sulfurs

are created equal. It may be that due to the edge shared conformation, the energy associated with this bS might be higher than that of a bS in a corner shared confirmation.

The $0.5Na_2S + 0.5[xSiS_2 + (1\text{-}x)\ PS_{5/2}]$ system did not show a particular MGFE behavior, having an increase in density in the thiophosphate rich glasses and then a decrease in density for the thiosilicate rich glasses. The $0.67Na_2S + 0.33[xSiS_2 + (1\text{-}x)PS_{5/2}]$ system showed a negative MGFE, but had two minima at x =0.2 and x=0.6 which had densities of 1.89 and 1.86 g/cm^3. These minima are proposed to be occurring with the changes in free Na_2S concentration ($\rho(Na_2S)$ = 1.86 g/cm^3). Thus far, these results suggest that the ionic conductivity for the sodium thiosilicophosphates may exhibit a negative MGFE. This will be the topic of future work.

4.7 Acknowledgements

This research was supported by the National Science Foundation under DMR grants 1304977 and 0710564. The authors would like to than the Iowa State Glass and Optical Materials research group for conversations and the careful proofing of this manuscript. Kah Loong Hoh is also thanked for his contribution to this project.

Table 4.1 Number of bridging and non-bridging sulfurs per SRO structure in the $0.5Na_2S + 0.5[xSiS_2 + (1-x)PS_{5/2}]$

P^n/Si^n	Net Bridging Sulfur P^n/Si^n	Net Non-Bridging Sulfur P^n/Si^n
P^2	1	2
P^1	0.5	3
P^0	0	4
P^{1P}	0.5	3
Si^3	1.5	1
Si^2	1	2
Si^1	0.5	3
ESi^2	1	2

Table 4.2 Number of bridging and non-bridging sulfurs per SRO structure in the $0.67Na_2S + 0.33[xSiS_2 + (1-x)PS_{5/2}]$

P^n/Si^n	Net Bridging Sulfur/ P^n/Si^n	Net Non-Bridging Sulfur P^n/Si^n
P^0	0	4
$P^{:0}$	0	3
Si^0	0	4
ESi^2	1	2

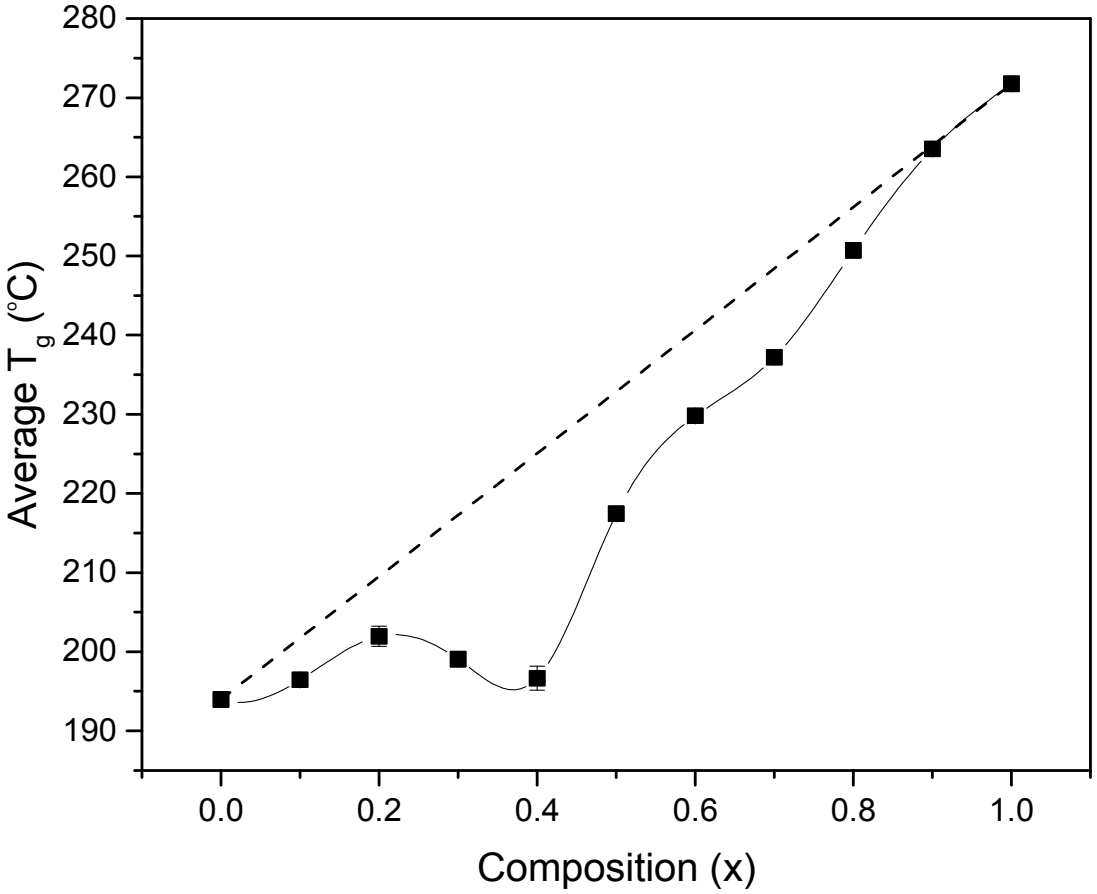

Figure 4.1: Composition Dependence of the glass transition temperature in the $0.5Na_2S + 0.5[xSiS_2 + (1-x)\ PS_{5/2}]$ system.

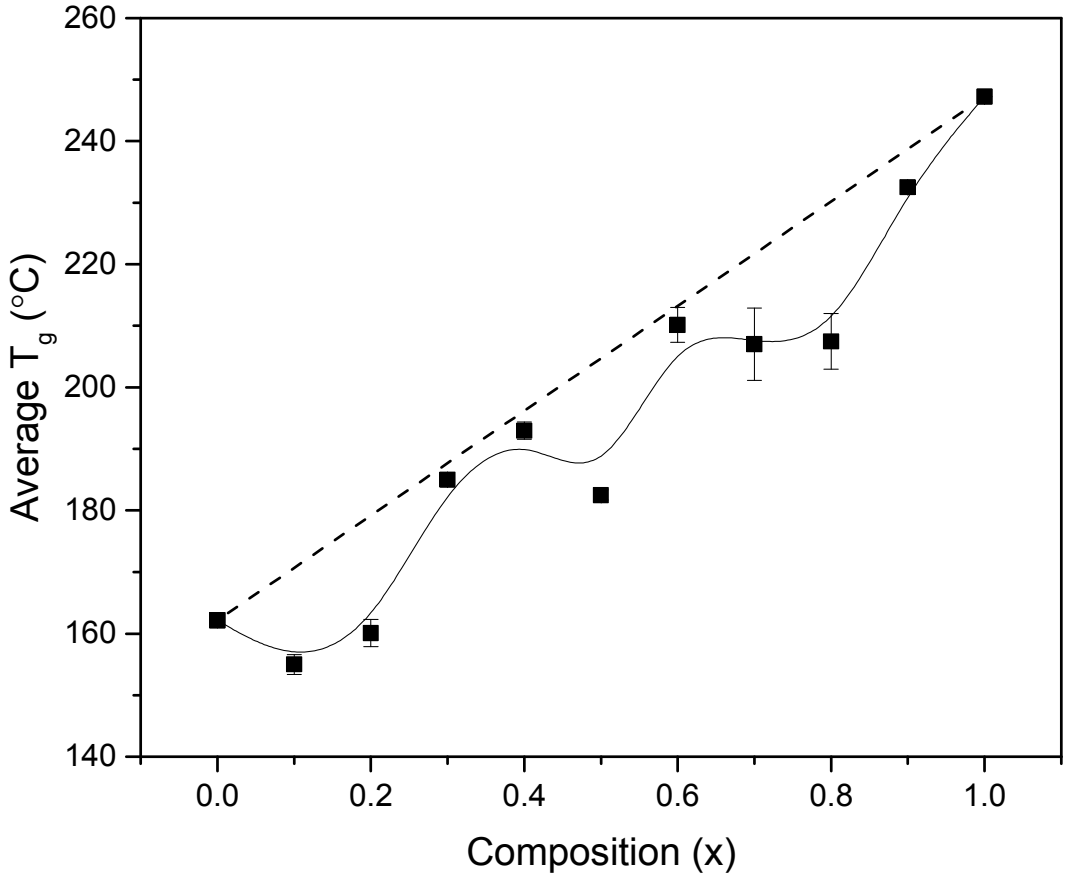

Figure 4.2: Composition Dependence of the glass transition temperature in the $0.67Na_2S + 0.33[xSiS_2 + (1\text{-}x)\ PS_{5/2}]$ system.

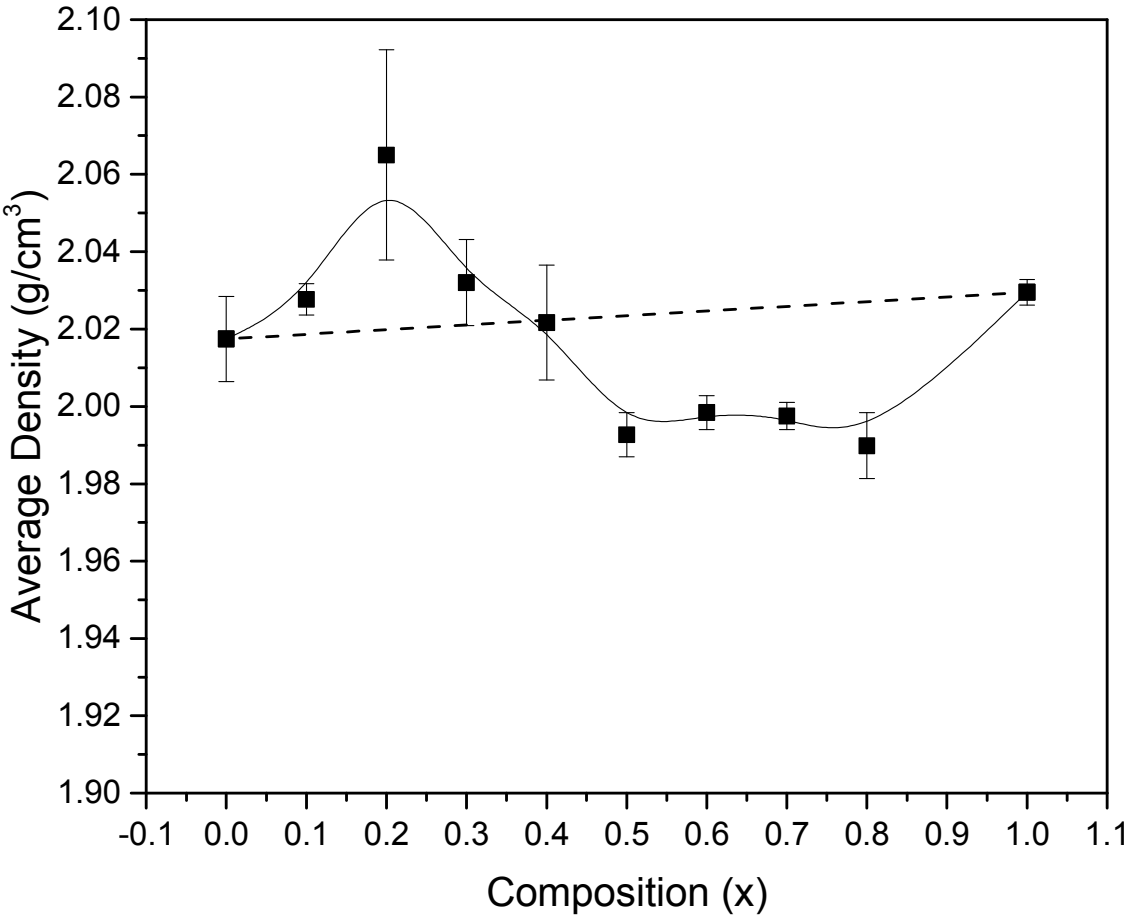

Figure 4.3: Composition Dependence of the densities in the $0.5Na_2S + 0.5[xSiS_2 + (1\text{-}x) PS_{5/2}]$ system.

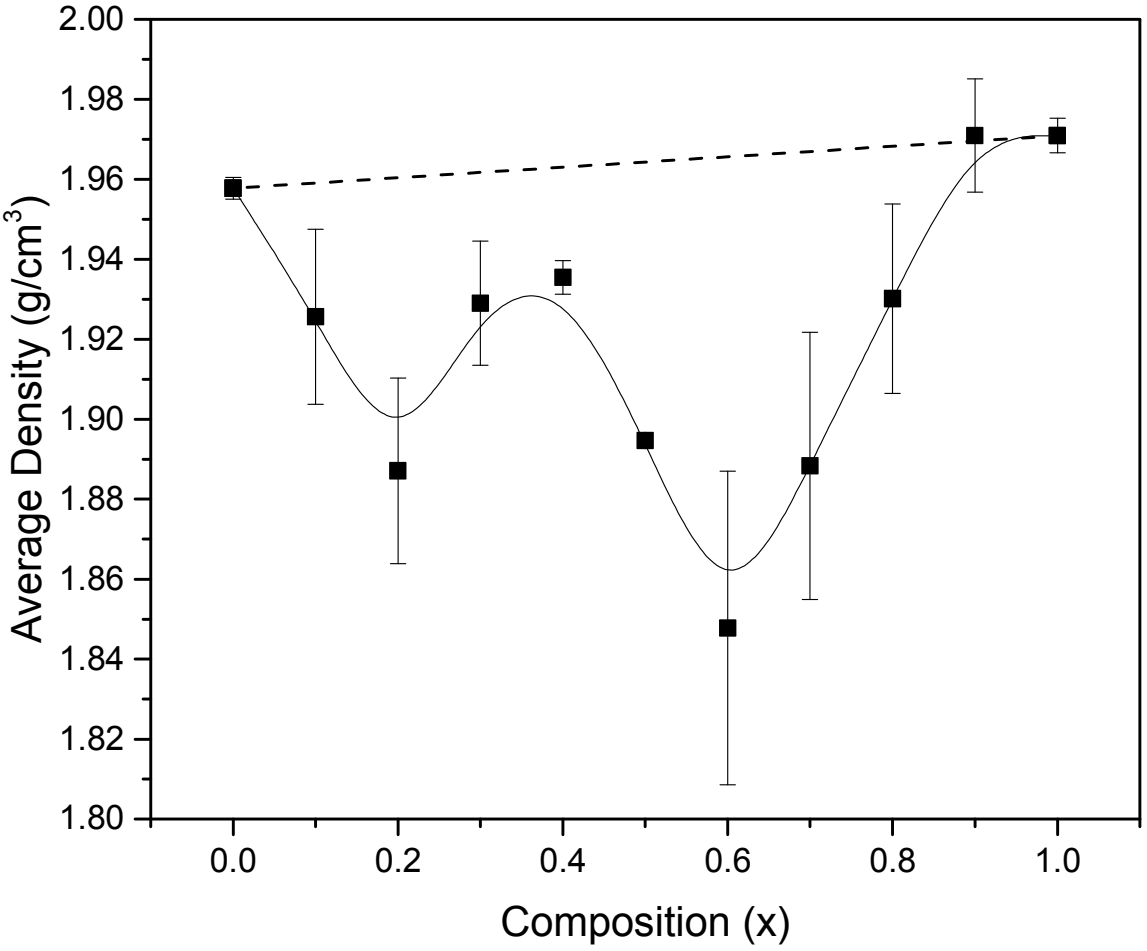

Figure 4.4: Composition Dependence of the densities in the $0.67Na_2S + 0.33[xSiS_2 + (1-x) PS_{5/2}]$ system.

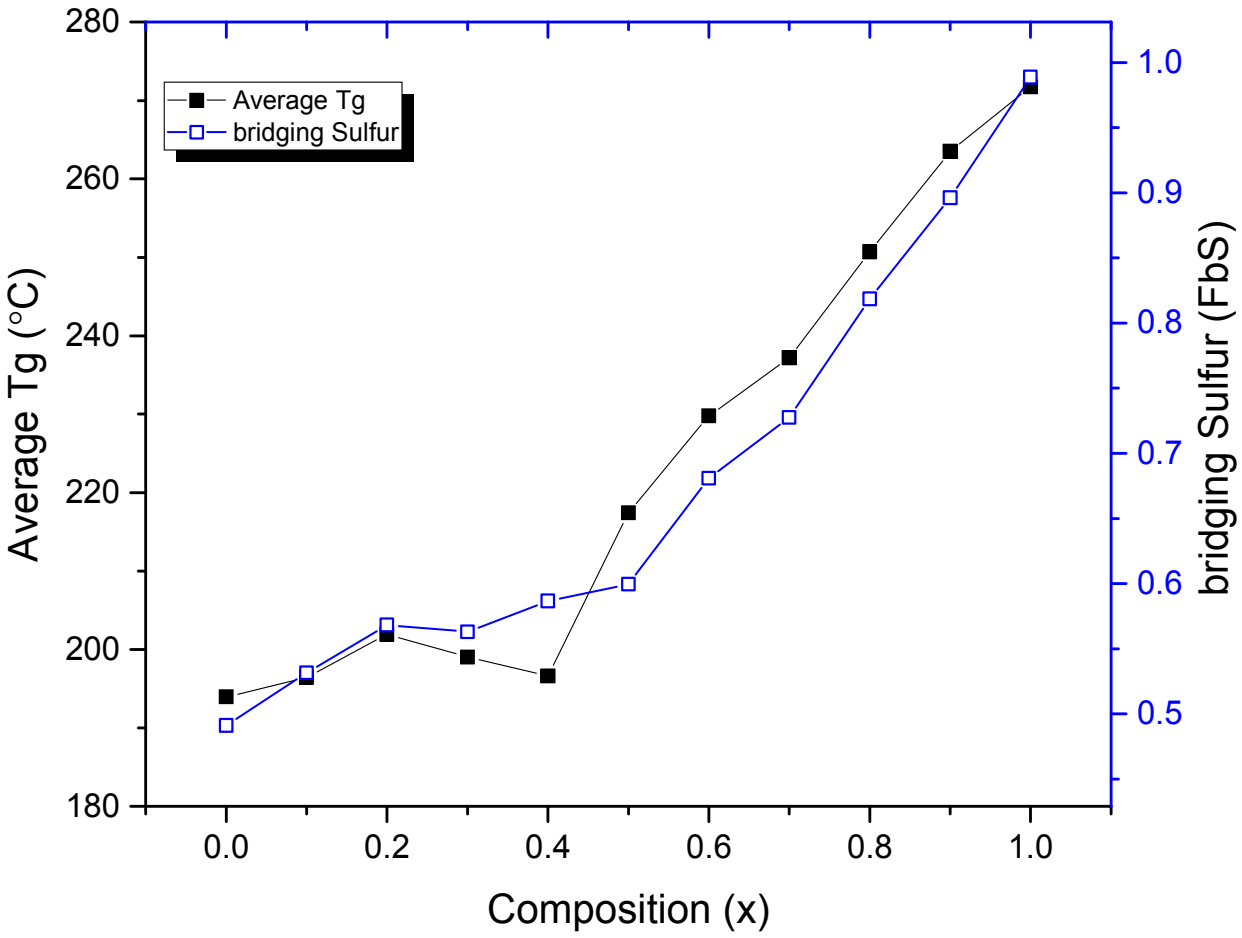

Figure 4.5: Composition Dependence of the T_g in the $0.5Na_2S + 0.5[xSiS_2 + (1\text{-}x)\ PS_{5/2}]$ system and the fraction of bridging sulfurs across the system

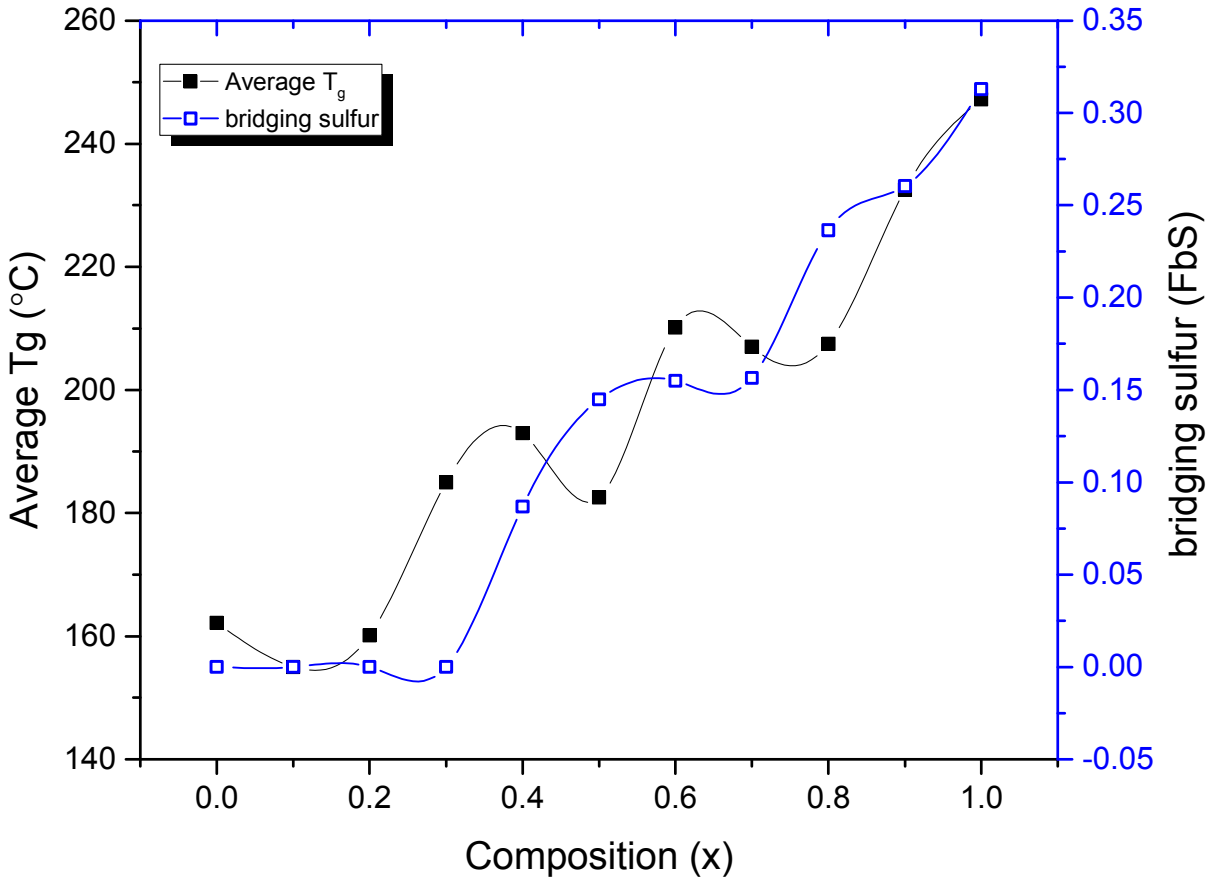

Figure 4.6: Composition Dependence of the T_g in the $0.67Na_2S + 0.33[xSiS_2 + (1\text{-}x) PS_{5/2}]$ system and the fraction of bridging sulfurs across the system

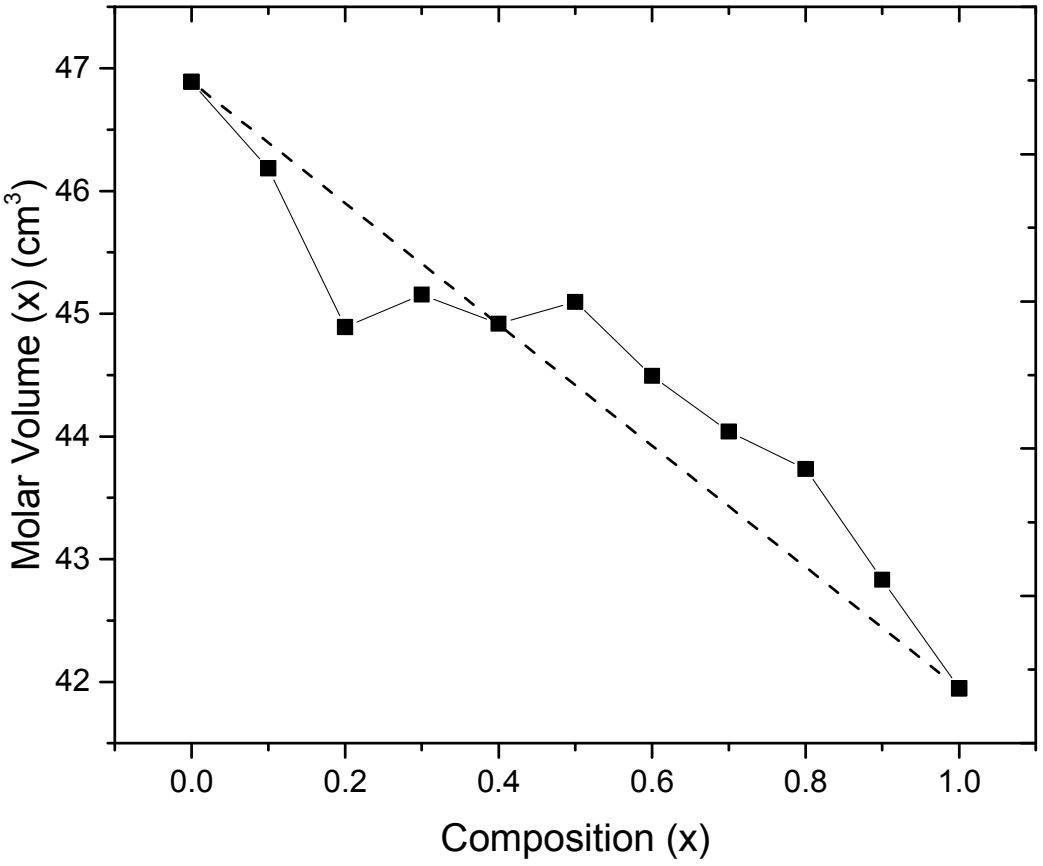

Figure 4.7: Composition Dependence of the Molar Volume in the $0.5Na_2S + 0.5[xSiS_2 + (1\text{-}x)\ PS_{5/2}]$ system

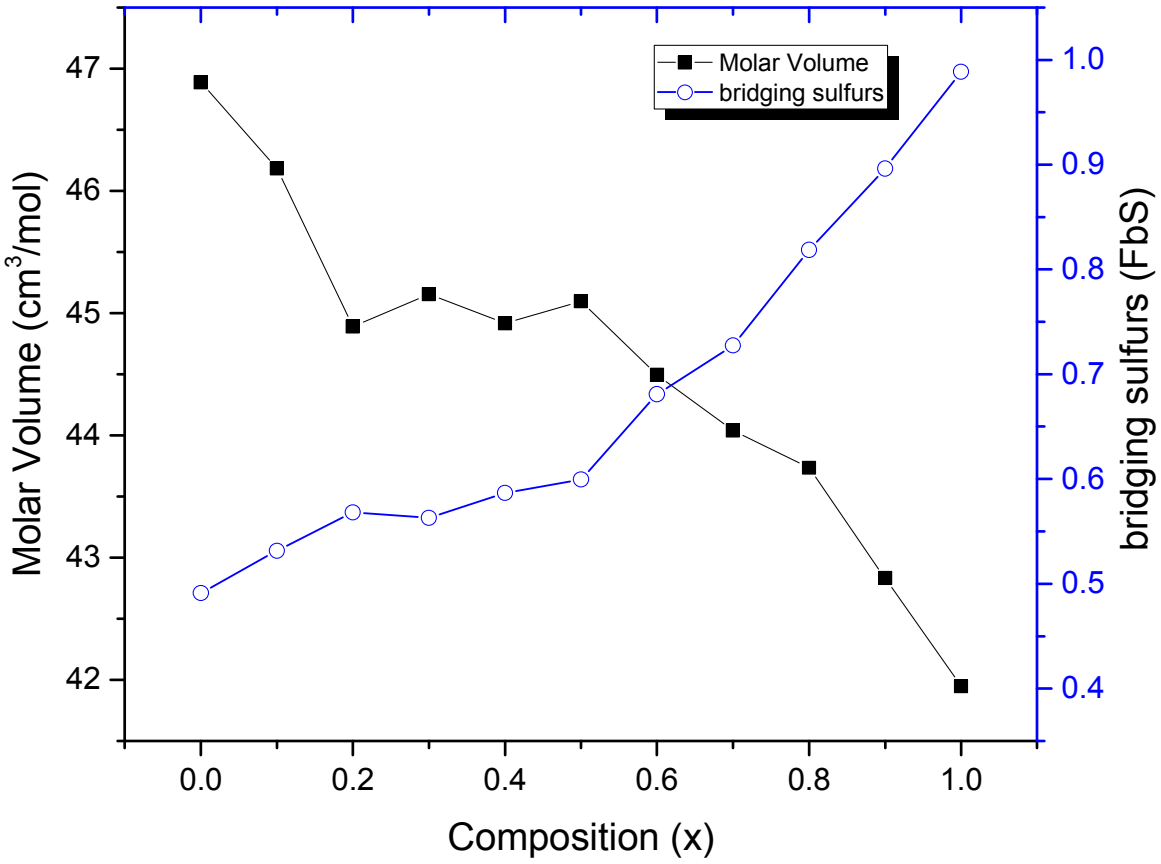

Figure 4.8: Composition Dependence of the Molar Volume and the fraction of bridging sulfurs in the $0.5Na_2S + 0.5[xSiS_2 + (1\text{-}x)\ PS_{5/2}]$ system

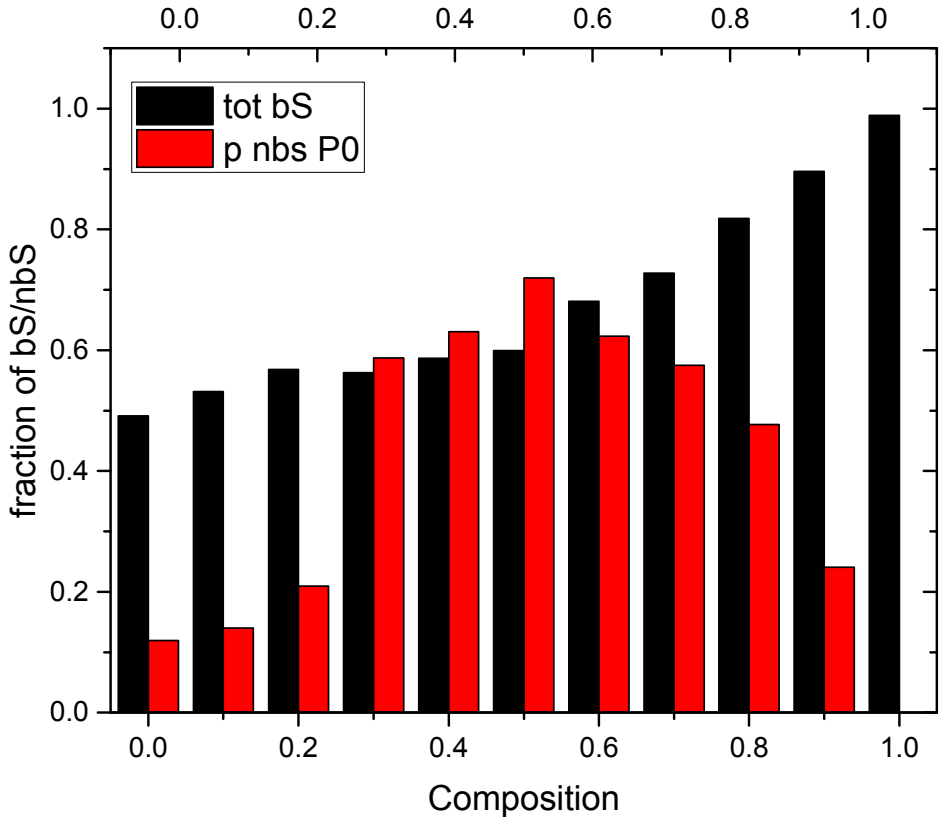

Figure 4.9: Total fraction of bS in the $0.5Na_2S + 0.5[xSiS_2 + (1\text{-}x)\ PS_{5/2}]$ system compared with the fraction of nbS from P^0 structures

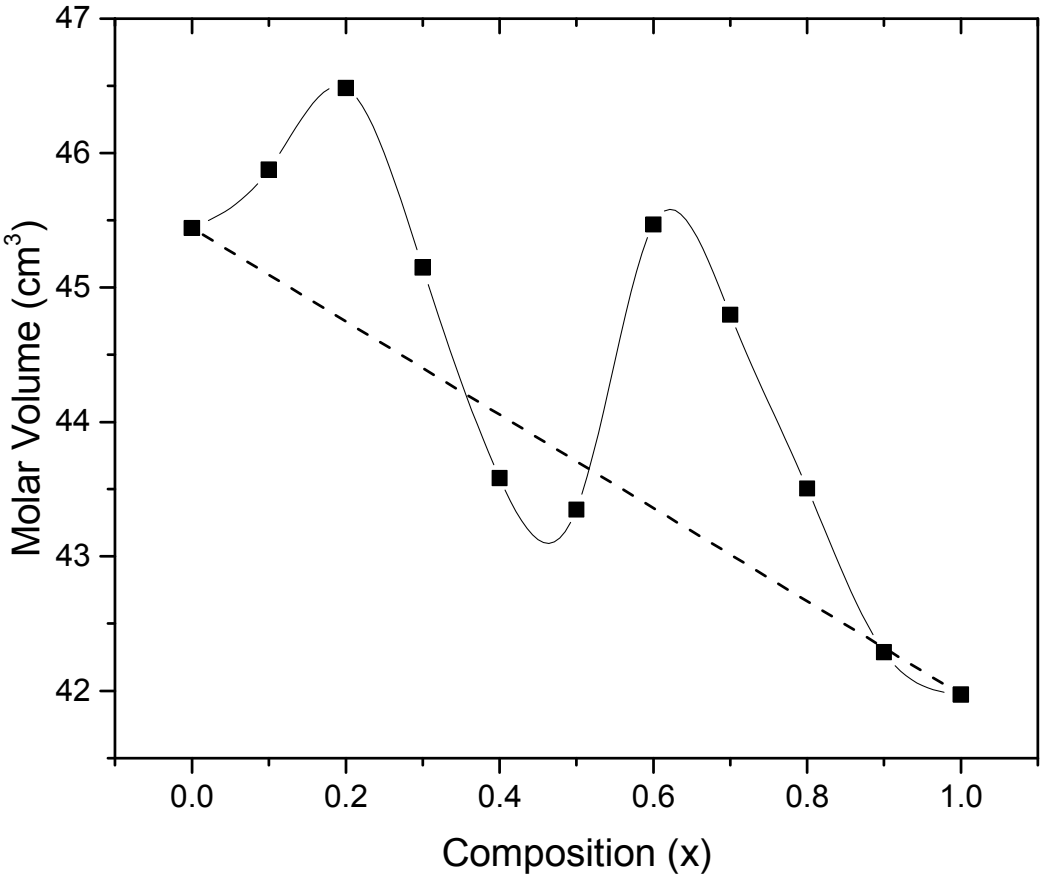

Figure 4.10: Composition Dependence of the Molar Volume in the $0.67Na_2S + 0.33[xSiS_2 + (1\text{-}x)\ PS_{5/2}]$ system

4.8 References

1. Galen, L.B., *U.S. Renewables Portfolio Standards: 2017 Annual Status Report*. 2017.
2. Energy, U.S.D.o., *Grid energy storage.* Grid Energy Storage, 2013.
3. Khalil Amine, R.K.a.Y.T., *Rechargeable lithium batteries and beyond: Progress, challenges, and future directions.* MRS Bulletin, 2014. **39**(May 2014): p. 395-401.
4. Vignarooban, K., et al., *Current trends and future challenges of electrolytes for sodium-ion batteries.* International Journal of Hydrogen Energy, 2016. **41**(4): p. 2829-2846.
5. Tang, J., A.D. Dysart, and V.G. Pol, *Advancement in sodium-ion rechargeable batteries.* Current Opinion in Chemical Engineering, 2015. **9**(Supplement C): p. 34-41.
6. Fergus, J.W., *Ion transport in sodium ion conducting solid electrolytes.* Solid State Ionics, 2012. **227**(Supplement C): p. 102-112.
7. Bischoff, C., K. Schuller, and S.W. Martin, *Short range structural models of the glass transition temperatures and densities of $0.5Na_2S + 0.5[xGeS_2 + (1 - x)PS_{5/2}]$ mixed glass former glasses.* J Phys Chem B, 2014. **118**(13): p. 3710-9.
8. Haynes, M.J., et al., *The mixed glass former effect on the thermal and volume properties of Na_2S-B_2S_3-P_2S_5 glasses.* Physics and Chemistry of Glasses-European Journal of Glass Science and Technology Part B, 2009. **50**(3): p. 144-148.
9. Martin, S.W., C. Bischoff, and K. Schuller, *Composition Dependence of the Na+ Ion Conductivity in $0.5Na_2S + 0.5[xGeS_2 + (1 – x)PS_{5/2}]$ Mixed Glass Former Glasses: A Structural Interpretation of a Negative Mixed Glass Former Effect.* J. Phys. Chem. B, 2015. **119**: p. 15738.
10. Christensen, R., et al., *The Densities of Mixed Glass Former $0.35 Na_2O + 0.65 [xB_2O_3 + (1 – x)P_2O_5]$ Glasses Related to the Atomic Fractions and Volumes of Short Range Structures.* J. Non-Cryst. Solids, 2012. **358**: p. 583.
11. Christensen, R., et al., *The glass transition temperature of mixed glass former $0.35 Na_2O + 0.65 [xB_2O_3 + (1-x) P_2O_5]$ glasses.* Journal of Non-Crystalline Solids, 2012. **358**: p. 826-831.
12. Christensen, R., G. Olson, and S.W. Martin, *Ionic conductivity of Mixed Glass Former $0.35 Na_2O + 0.65 [xB_2O_3 + (1-x) P_2O_5]$ Glasses.* Journal of Physical Chemistry B, 2013. **117**: p. 16577-16586.

CHAPTER 5. THE MIXED GLASS FORMER EFFECT IN THE IONIC CONDUCTIVITY OF $0.67NA_2S + 0.33[XSIS_2 + (1\text{-}X)PS_{5/2}]$ GLASSY ELECTROLYTES

A paper to be submitted to the Journal of Physical Chemistry B

Deborah E. Watson[7]*, Steven J. Kmiec*[8]*, Steve W. Martin*[9]

Department of Materials Science and Engineering, Iowa State University

Ames, Iowa 50010-2300

5.1 Abstract

New solid state electrolytes have been explored to change the landscape of advanced batteries for energy storage systems. The ionic conductivities of the mixed glass former $0.67Na_2S + 0.33[xSiS_2 + (1\text{-}x)PS_{5/2}]$ are thus investigated. The system exhibits a negative mixed glass former effect (MGFE) with the exception of one ternary composition, x = 0.7, having a DC conductivity of 1.29×10^{-5} S cm^{-1} at 30 °C. The Anderson Stuart model was used to calculate the Coulombic binding energy (E_b) and volumetric strain energy (E_s) to compare the predicted activation energy (E_A) with the experimental values calculated from the conductivity results. The model reproduced the trend of the experimental values which then allow the ability to make a connection between the E_b and E_s and the proposed short range order structure for the system. The structural model proposes the expected P^0 and Si^0 structures, with the $P^{:0}$ and ESi^2 structures which were found using ^{31}P and ^{29}Si MAS NMR. These NMR results also supported the Raman

---

[7] Primary researcher and author

[8] Graduate research assistant

[9] Corresponding author and principle investigator

spectroscopy which showed the presence of excess Na_2S and polysulfide structures in the network. These defect structures and the influence on the ionic conductivity was examined.

5.2 Introduction

5.2.1 Background

Interest in solid state batteries has increased significantly over the past few years. With the advent of technologies requiring fast and reliable energy storage devices, research into the alkali ion and alkali metal batteries have become one of many available technologies to address this demand. Research of the well-known and understood Li ion battery has been directed to the development of new battery chemistries and designs for advancement in vehicle innovation, electronic devices such as computers and cellular phones, etc. However, this technology has the potential to impact other areas such as large scale energy storage for grid systems, buildings and other stationary systems needing quick power turnover. For these applications, a portion of the research has shifted to the study of sodium solid state batteries.

Sodium has electrochemical properties that are analogous to lithium and its mechanism for ion conduction. Though slightly larger in size, which would lead to slower conduction speeds than lithium, sodium has the advantages of a greater natural abundance and even global distribution [1, 2] making it much more accessible to many countries and much cheaper than the cost of lithium. However one of the drawbacks sodium research faces is stability issues with sodium metal against commercial electrolytes. Therefore a unique opportunity exist for researching new solid electrolyte

materials that can accommodate sodium metal and achieve performances levels necessary to make this a viable option.

5.2.2 Glassy Solid State Electrolytes

Solid electrolyte research in both Li and Na based systems have explored the potential of crystalline and ceramic materials [1, 3]. Tatsumisago et al have done extensive research on Li_2S systems using mechanical milled glasses and glass ceramics [4-13]. Glassy electrolytes have also been introduced as potential materials. The Martin et al group has done research in Na based systems using melt quenched and mechanically milled glasses[14-18].

5.2.3 The Mixed Glass Former Effect

Our most recent work is in ternary glass systems which may exhibit a phenomena called the mixed glass former effect (MGFE) where one glass former is varied with another glass former while the alkali concentration is held constant across the series. This is done to isolate which glass former is responsible for enhancing an increase or decrease of the ionic conductivity of these glasses. The ionic conductivity of MGF glass systems have been studied extensively over the past decade in both oxide and sulfide systems[19-23]. The most recent systems studied in this group has included $0.5Na_2O + 0.5[xB_2O_3 + (1-x)P_2O_5]$, $0.67Na_2S + 0.33[xB_2S_3 + (1-x)P_2S_5]$ and $0.5Na_2S + 0.5[xGeS_2 + (1-x)PS_{5/2}]$.

The $0.67Na_2S + 0.33[xSiS_2 + (1-x)PS_{5/2}]$ system is the highest modified MGF system studied so far which can be regarded as an invert glass. This composition system is of interest due to the potential of high ionic conductivity.

5.3 Materials and Methods

5.3.1 Sample Preparation

Due to the susceptibility of sulfide compounds to moisture, all materials and samples were prepared in a N_2 glove box. Silicon sulfide (SiS_2) was synthesized by combining stoichiometric amounts of silicon and sulfur and mechanically milling the compounds to ensure good mixing. The mixture is then sealed under vacuum in a silicon coated quartz ampoule and reacted over a 48 hour heating period from 50 – 970 °C to form SiS_2. After the reaction process, the ampoule was opened inside the N_2 glove box and mechanically milled to acquire a powder for batching. Stoichiometric amounts of sodium sulfide (Alfa Aesar 99%), silicon sulfide and phosphorus pentasulfide (Sigma Aldrich 99.999%) were combined and mechanically milled in stainless steel pots to mix powders together and help decrease the volatilization of phosphorus pentasulfide. Samples were melted in vitreous carbon crucibles inside a tube furnace hermetically sealed to the N_2 glove box. The samples were melted for 3 – 7 minutes at 620 – 700 °C as the composition went from x = 0 to x = 1. After a first melt, a weight loss measurement was taken. If the weight losses were less than 2%, the sample went through a second melt, after which the glass was cast into brass molds to form bulk discs of 23 mm in diameter and 2 mm in thickness for conductivity measurements. The bulk disc samples were cast at an annealing temperature 30 – 50 °C below their respective glass transition temperature (T_g) and held at the annealed temperature for 45 minutes. After this hold period, the casted disc was slow cooled to room temperature at a rate of 1°C/min.

The bulk disc samples were hand polished first with 400 grit paper up to 4000 grit polishing paper. Electrodes were painted on each face with silver paint for electrical

connection with the instrumentation. Samples were tested in cells contain brass electrodes to make contact with the silver electrodes on the glass.

5.3.2 Impedance Spectroscopy

The impedance spectroscopy was performed on the annealed bulk discs. Samples were first hand polished and then painted with silver paint to make contact with brass electrodes inside impedance cell. The impedance was measured in a Novocontrol dielectric spectrometer over frequencies 10^7 to 10^{-1} Hz over a temperature range of 25 – 150 °C. Complex impedance plots were fitted to find the DC conductivity of the sample.

5.4 Results

The D.C. conductivity of a material can be calculated using the following relation (5.1):

$$\sigma_{D.C.} = \frac{1}{R} \cdot \frac{t}{A} \tag{5.1}$$

where the inverse of the resistance, R, of the glass multiplied by the thickness, t, of the disc sample over the area, A, of the disc. R can be determined by fitting the complex impedance plot like the one shown in Figure 5.1. The fitting of the complex impedance was based on a circuit model were a resistor and capacitor are in parallel with each other. The relationship between the impedance, Z, and the resistance in this circuit model is as follows:

$$Z = \frac{R}{1 + RQ(i\omega)^n} \tag{5.2}$$

where Q is the constant phase element, *i* the imaginary component $\sqrt{-1}$, ω is the angular frequency and *n* is an exponent between 0 and 1. In these samples, there are two arcs, the first arc which is due to the bulk material response as the electric field is applied across the glass and the second due to the interface between the sample and the silver painted electrodes. The tail at the end is due to space polarization when the Na^+ build up against the electrode balancing the negative charge on the blocking electrode. The arcs are fitted based on Equation 5.2 and the space polarization tail is modeled using the Warburg element. The ionic conductivities of the $0.67Na_2S + 0.33[xSiS_2 + (1-x)PS_{5/2}]$ at 30 °C from these calculations are given in Figure 5.2.

5.5 Discussion

5.5.1 The Composition Dependence of the Ionic Conductivity

The composition dependence of the ionic conductivities of the $0.67Na_2S + 0.33[xSiS_2 + (1-x)PS_{5/2}]$ at 30 °C is shown in Figure 5.2. A b-spline curve is used to highlight the trend of the conductivities. These are the averages of multiple data sets. Measurements were repeated on samples that showed anomalous behavior. The error bars represent the minimum and maximum values of these measurements. The x = 0.0 sodium thiophosphate end member glass has a conductivity measured at 3.55×10^{-6} S cm^{-1}. As x → 1, the conductivities experience a slight positive deviation from a linear interpolation based on the end member glasses, with the exception of compositions x = 0.2, 0.5, 0.8 and 0.9. These glasses fall on the linear mixing trend between the binary end member glasses. The highest conductivity of the ternary glasses occurs at x = 0.6, having a conductivity of 2.08×10^{-5} S cm^{-1}.

The activation energies of each composition were calculated by taking the slope from the Arrhenius plot of the natural log of the conductivities versus 1000 K over the temperature, as shown in Figure 5.3. The activation energy is calculated as shown below

$$\sigma_{D.C.} = \frac{\sigma_0}{T} exp\left[-\frac{\Delta E_{Act}}{RT}\right] \quad 5.3$$

Figure 5.4 shows the activation energy of each composition calculated from the experimental data. The activation energies decreases in what appears to be a step wise trend as silicon is added to the system. The activation energy for the sodium thiophosphate measured at 52.8 kJ/mol while the sodium thiosilicate glass had a lower activation energy at 45.6 kJ/mol.

5.5.2 Ionic Conduction in Glass and the Anderson Stuart Model

The ionic conduction in glassy materials is a function of the concentration of charge carriers and their mobility. The Nernst Einstein relation describes this mechanism a thermally activated diffusion process in the equation (5.4) as follows

$$\frac{\sigma_{D.C.}}{D} = \frac{n(Ze)^2}{k_b T} \quad 5.4$$

where D is the diffusivity, n is the number of charge carriers, k_b is the Boltzmann constant and T is the temperature. The Anderson Stuart model. The Na^+ hops for one non-bridging sulfur site to another which is controlled by an activation energy at each site. The model holds that there are two contributions to the activation energy for ionic hopping in a glass: the Coulombic binding energy and the volumetric strain energy. The

Coulombic binding energy is the attractive potential between the non-bridging sulfur and the Na^+ and therefore controls the availability of ions to participate in conduction. The Coulombic binding energy can be calculated using the following equation

$$E_b = \frac{Z_{Na} Z_S e^2}{4\pi\varepsilon_0\varepsilon_\infty}\left(\frac{1}{r_{Na} + r_S} - \frac{2}{\lambda}\right) \quad 5.5$$

where Z is the valence of each element, e is the electric charge, ε_0 is the permittivity of free space, ε_{hf} is the high frequency relative permittivity of the material, r_{Na} is the radius of Na, r_S, and λ is the jump distance. The permittivity can be measured as a function of temperature over the same frequency range the impedance measurements were performed. The permittivity of the material was taken from the plateau of the permittivities at low temperatures, an example of which is shown in Figure 5.5. The distribution can be fitted to extract the real (ε') and imaginary permittivity (ε") in order to calculate the ε_{hf} where

$$\varepsilon = \varepsilon' - i\varepsilon'' \quad 5.6$$

The composition dependence of the permittivities is shown in Figure 5.6. The binding energies calculated for the system is shown in Figure 5.7. The E_b of the x = 0 sodium thiophosphate glass is 54.69 kJ/mol and decreases to 44.23 kJ/mol in the x = 1 glass. Though the E_b of the ternary glasses vary a bit, as P is exchanged for Si the E_b decreases. This behavior is reasonable considering P due to its electronic structure will bind Na^+ tighter its Si counterpart. However it is worth noting the behavior occurring over the regions of x = 0.3 – 0.5 and 0.7 – 0.9. The E_b starts at a minimum (at 0.3 and

0.7), goes through a maximum (at 0.4 and 0.8) and then decrease again afterward (0.5 and 0.9). To understand this behavior the structure model for this system is revisited. At x = 0.4 and 0.8 where the E_b reaches a maximum, the ESi^2 population goes from being constant to experiencing a substantial increase. Why would the ESi^2 increase the binding energy? What else is occurring when ESi^2 is introduced into the system? It was established in a previous paper that when ESi^2 is present in this system, free Na_2S also accommodates it (Figure 5.9). It is plausible that the Na_2S would increase the binding energy rather than the ESi^2. It was just established the Si structures in general would lower the binding energy while P structures would increase it. If anything, one could imagine the E_b of the ESi^2 would be low in comparison to the other species in the glass. The P^0 and Si^0 are completely depolymerized with sodium concentrating all the charge while perhaps in an ESi^2 the charge is delocalized to the bridging sulfur making the Na^+ at the nbS less tightly bound. The Na^+ in the Na_2S would be very tightly bound and nearly immobile. The immediate decrease of the E_b after this Na_2S introduction could be due to the continue exchange of P^0 for Si^0 and therefore a structure with a higher E_b for one with a lower E_b.

The volumetric strain energy in the energy necessary to create a doorway radius through which the Na^+ can conduct and therefore controls the mobility of the Na^+. The volumetric strain energy can be calculated using the following equation

$$E_s = \pi G \frac{\lambda}{2}(r_{Na} - r_D)^2 \qquad 5.7$$

where G is the shear modulus and r_D is the doorway radius. Since the G of these glasses are unknown in literature, we can calculate a theoretical value based on the following calculation:

$$G(x) = \frac{3e^2}{4\pi(r_{Na} - r_S)\alpha} \tag{5.8}$$

where α is the polarizability of the material. The calculation for the polarizability is as follows:

$$\alpha = \frac{3\varepsilon_0(\varepsilon_\infty - 1)}{N(\varepsilon_\infty + 2)} \tag{5.9}$$

The results of the volumetric strain energy calculation is shown in Fig 5.8. The x = 0.0 binary end member composition has an E_s of 3.92 kJ/mol which is lower than that of the x = 1.0 binary end member composition at 4.16 kJ/mol. This is reasonable considering the sodium thiosilicate has a lower molar volume than the sodium thiophosphate, hence more packed and therefore effecting the mobility of the ion through the network. The E_s reaches minima at the x = 0.3 and 0.7, and a maximum at x = 0.4, just as was observed in the E_b energies. The minimum at 0.7 seen here in the E_s is also where the highest conductivity in the experimental data for the ternary glasses is observed. If the model holds, this shows that the increase in conductivity is due to a lowering of the volumetric strain energy contribution of the activation energy. Using the structural model, the decrease in the E_s can be related to change with the total

concentration of free Na_2S. Figure 5.10 shows the concentration of free Na_2S in the system plotted with the E_s.

The E_A from the Anderson Stuart model is plotted in Figure 5.9 with the experimental E_A. It can be seen that there is good agreement between the experimental data and model, with the maximum agreement in the silicon rich glasses.

5.5.3 Evaluation of the MGFE

From the results there does not seem to be strong evidence of a MGFE in these glasses, perhaps a slight positive MGFE. Based on previous studies, the MFGE appears to be evident when there is a chemical reaction between the SRO structures of each glass former, either a P or Si taking or giving Na^+ to form new structures. The generation of these resultant structures is normally tied to the MGFE witnessed in the physical properties. However in this system, at the y = 0.67 modifier concentration we are supersaturating the system with sodium sulfide so that the SRO are completely depolymerized. There is no giving or taking of Na^+ from another glass former. Instead there is an exchange of P^0 for Si^0 as x $\rightarrow$ 1.0. However the defect structures, $P^{:0}$ and ESi^2 have more of an effect on the properties due to their production of free S and polysulfides.

In a previous paper, the population of each SRO structures was determined using 1D MAS NMR for the silicon-29 and phosphorus-31 nuclei (Chapter 3). With this information, we could calculate the amount of sodium and sulfur associated with each unit. When the amount of sodium and sulfur associated with SRO units was subtracted from the theoretical amount of sodium and sulfur based on the stoichiometry of the composition, the results showed that there was an unaccounted amount of sodium and

sulfur in the system. This is not surprising, given that the expected SRO from this system, having P^0 and ½ mol of Na_2S to Si^0 as x goes from 0 to 1, differs from the experimental data which shows these structures and presence of defect structures such as $P^{:0}$ and ESi^2. These defect structures motivate the formation of Na_2S and Na_2S_x. The ratio of the leftover sodium to the left over sulfur produces a "compound" $Na_{2.06}S$ for the x = 0 composition. If 2 Na and 1 S form the sodium sulfide compound, this 2.06:1 Na:S may signify the following:

$$\frac{2.06 - 2}{2.06} \times 100 = \ [2.91\%]$$

where 2.91% is the amount of Na in the x = 0 glass is not associated with the Na_2S compound. Interestingly the population of the $P^{:0}$ structure is 2.69%. It is proposed that the Na^+ may be loosely associated with a partial negative charge of the lone pair of electrons on the $P^{:0}$ structure. If this is the case, maybe the $P^{:0}$ population would have a slight effect on the conductivity of these compositions.

5.6 Conclusion

The ionic conductivity of the $0.67Na_2S + 0.33[xSiS_2 + (1\text{-}x)\ PS_{5/2}]$ system exhibited a weak negative MGFE although a short maximum was observed at x = 0.7. The Anderson Stuart was able to model the trend of the experimental E_A. As a result, E_b and E_s for each composition could be calculated. The E_b showed maxima at the x = 0.4 and 0.8 compositions. Using the SRO analysis, it was seen at the first change in ESi^2 population from a constant trend, the E_b would increase and then in the next compositions decrease while the ESi^2 population plateaus. The reason for this is believed to be the effect of Na_2S brought in with each spike in ESi^2. When ESi^2 is increased the amount of

Na_2S increase which likely has a higher binding energy than the SRO structures in the glass. Then once stabilized the E_b decreases and perhaps reflects the E_b of the SRO structures. The E_s across the system correlates with the trend of the free sodium sulfide across the series. Minima in the E_s were observed at x = 0.3 and 0.7, which are proposed to be tied to the minima points in the total fraction of free Na_2S. In general the E_s decreased with each addition of SiS_2, perhaps implying that the higher conductivity in the thiosilicate rich glasses is due to easier transport through the created network. Overall, the ionic conductivity did not improved in this MGF system. There is also the question of whether the behavior shown in this series could truly be called the MGFE when it lacks reaction or interaction between glass formers. The defect structures from disproportiation appear to have more bearing on the conductivity than the expected P^0 and Si^0 structures. Further investigation is being done where the composition is adjusted to have the exchange of the binary y =0.60 Na P S (the P^0 composition) and the y = 0.67 Na Si S (the Si^0 composition.) In doing this, perhaps the formation of free Na_2S and polysulfides could be avoided, thus enabling an analysis of behaviors strictly based on the glass forming tetrahedra.

5.7 Acknowledgements

This research was supported by the National Science Foundation under DMR grants 1304977 and 0710564. The authors would like to take this time to thank the other members of the Iowa State Glass and Optical Materials research group for conversations and the careful proofing of this manuscript.

Table 5.1 Parameters for the calculation of the Coulombic binding energy

x	$\bar{V}$ **(cm^3/mol)**	**λ (Å)**	**r_s (Å)**	**ε_{hf}**
0.0	45.44	3.57	2.21	13.87
0.1	45.88	3.58	2.22	13.43
0.2	46.48	3.60	2.23	13.69
0.3	45.15	3.56	2.21	16.33
0.4	43.58	3.52	2.18	13.50
0.5	43.35	3.51	2.18	14.89
0.6	45.47	3.57	2.21	14.77
0.7	44.80	3.55	2.20	16.65
0.8	43.50	3.52	2.18	14.50
0.9	42.29	3.48	2.16	15.63
1.0	41.97	3.48	2.16	16.64

Table 5.2 Parameters for the calculation of the volumetric strain energy

x	**G (GPa)**	**λ (Å)**	**r_D**
0.0	11.17	3.57	0.37
0.1	10.83	3.58	0.37
0.2	10.90	3.60	0.37
0.3	10.88	3.56	0.37
0.4	11.82	3.52	0.36
0.5	11.67	3.51	0.36
0.6	11.03	3.57	0.37
0.7	10.99	3.55	0.37
0.8	11.68	3.52	0.36
0.9	11.92	3.48	0.36
1.0	11.90	3.48	0.36

Table 5.3 Calculated Anderson Stuart Model Activation Energies and experimental activation energies

X	E_b (kJ/mol)	E_s (kJ/mol)	E_{Act} (A-S)	E_{Act} (kJ/mol)
0.0	52.88	3.92	56.80	52.80
0.1	54.38	3.80	58.28	53.35
0.2	53.03	3.82	56.86	51.67
0.3	45.06	3.82	48.89	50.91
0.4	55.40	4.14	59.54	53.04
0.5	50.35	4.09	54.44	48.42
0.6	49.65	3.87	53.52	49.21
0.7	44.35	3.85	48.20	45.14
0.8	51.64	4.09	55.73	49.94
0.9	48.52	4.17	52.70	47.27
1.0	45.74	4.16	49.91	45.56

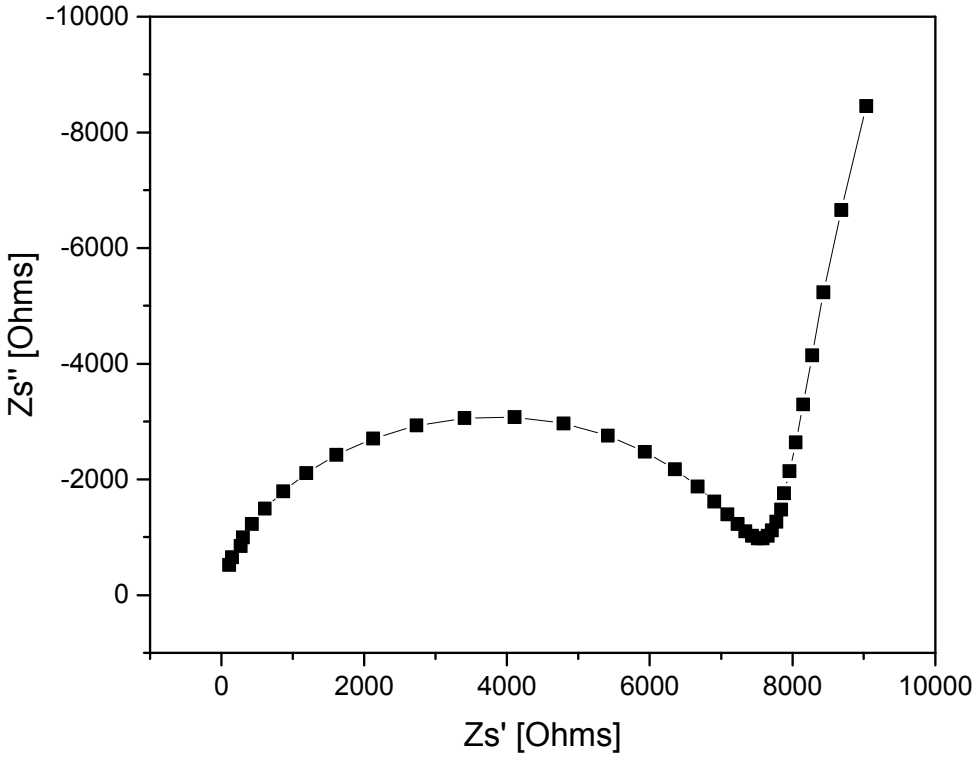

Figure 5.1 Complex Impedance Plot of x = 0.1 $0.67Na_2S + 0.33[xSiS_2 + (1-x)PS_{5/2}]$

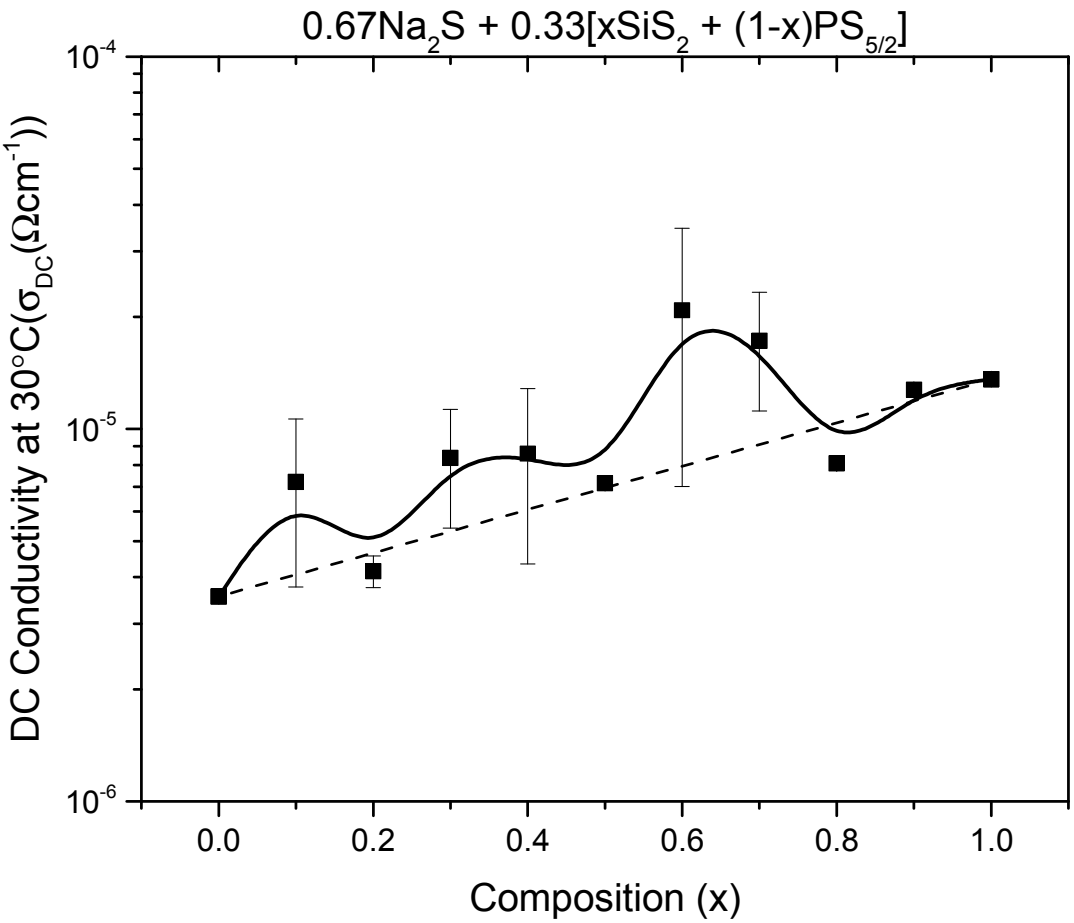

Figure 5.2 Composition Dependence of the Ionic Conductivities in the $0.67Na_2S + 0.33[xSiS_2 + (1-x)PS_{5/2}]$

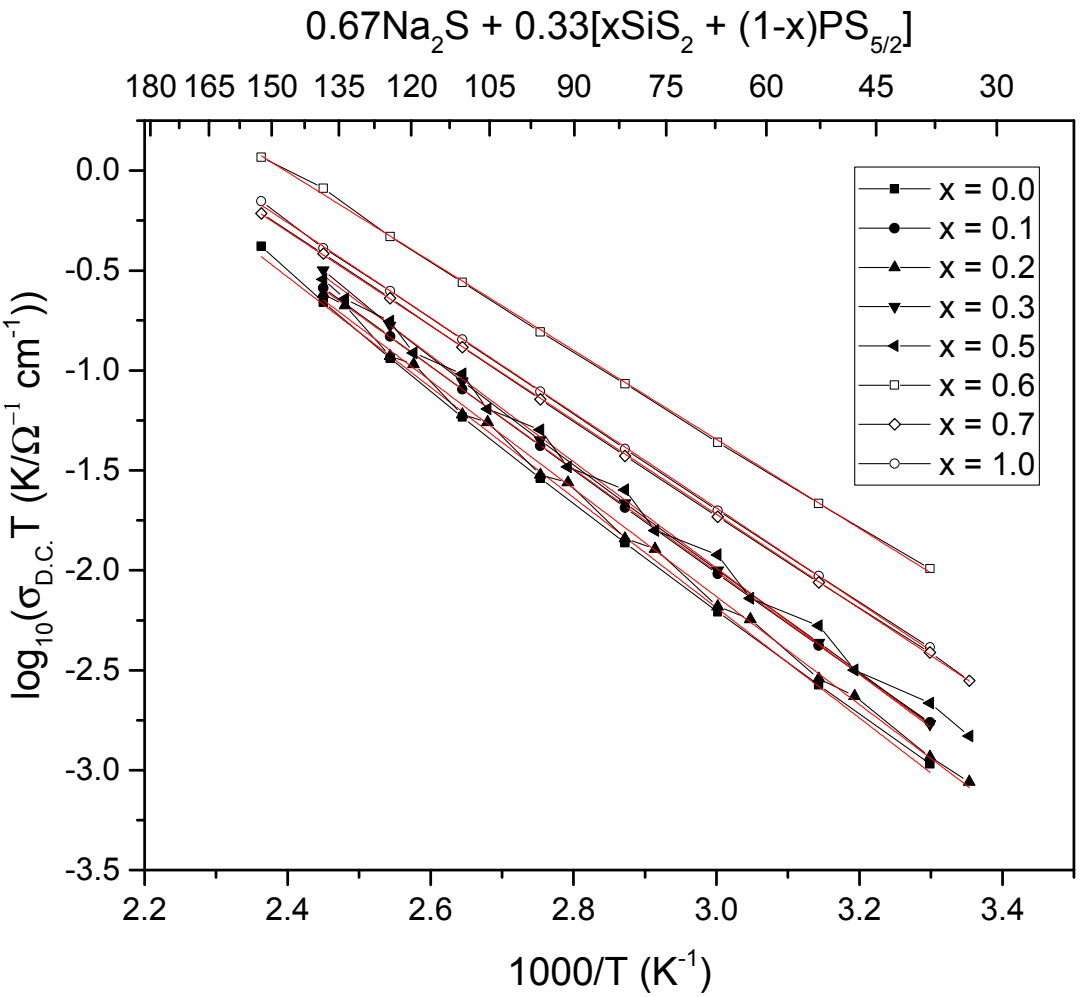

Figure 5.3 Arrhenius Plots of the $0.67Na_2S + 0.33[xSiS_2 + (1-x)PS_{5/2}]$ glasses

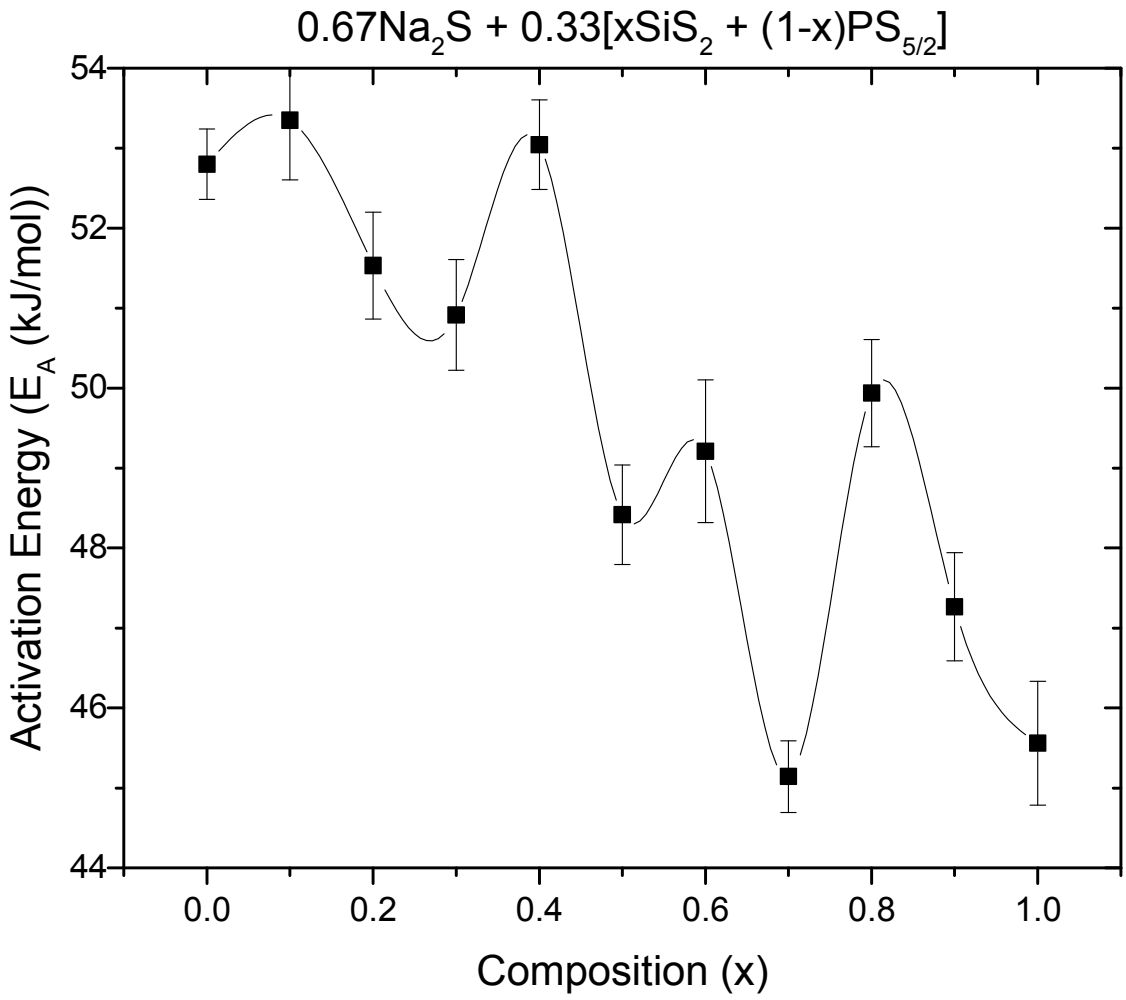

Figure 5.4 Experimental Activation Energies of the $0.67Na_2S + 0.33[xSiS_2 + (1-x)PS_{5/2}]$ system

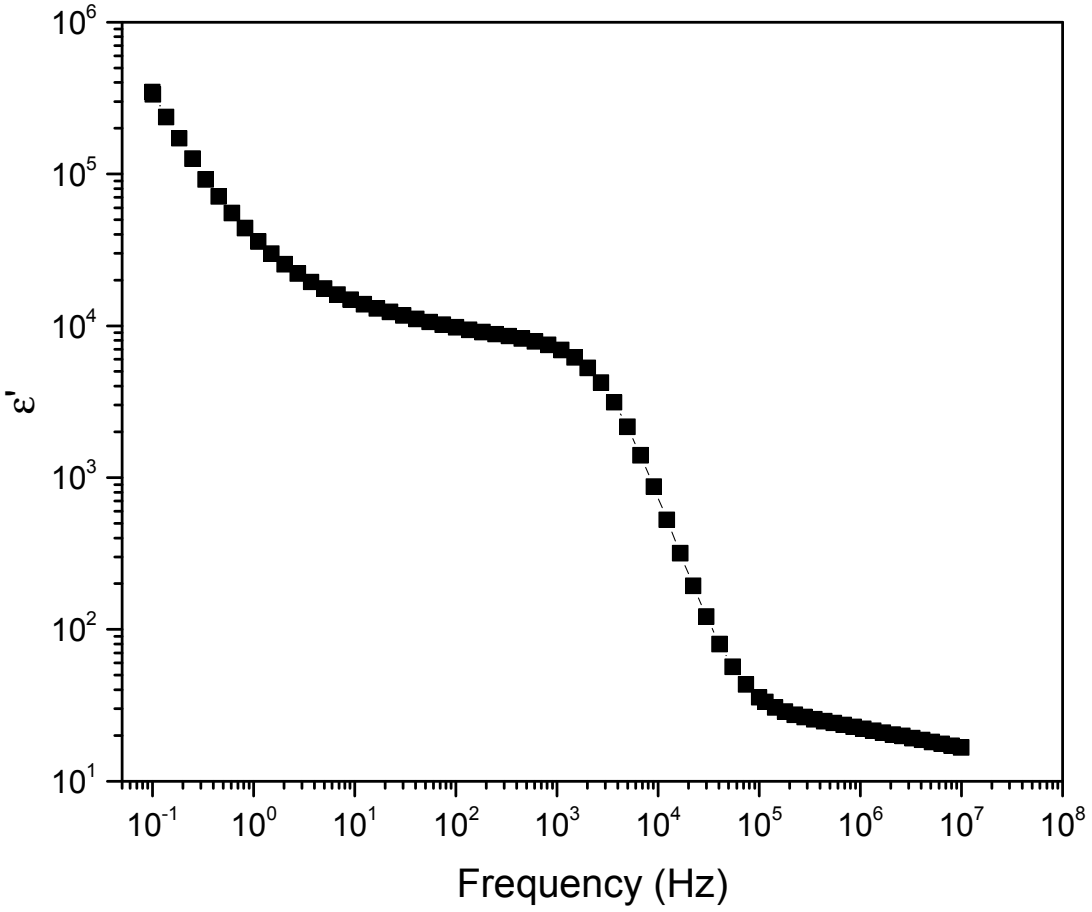

Figure 5.5 Measurement of the high frequency permittivity of x = 0.0 $0.67Na_2S + 0.33[xSiS_2 + (1-x)PS_{5/2}]$

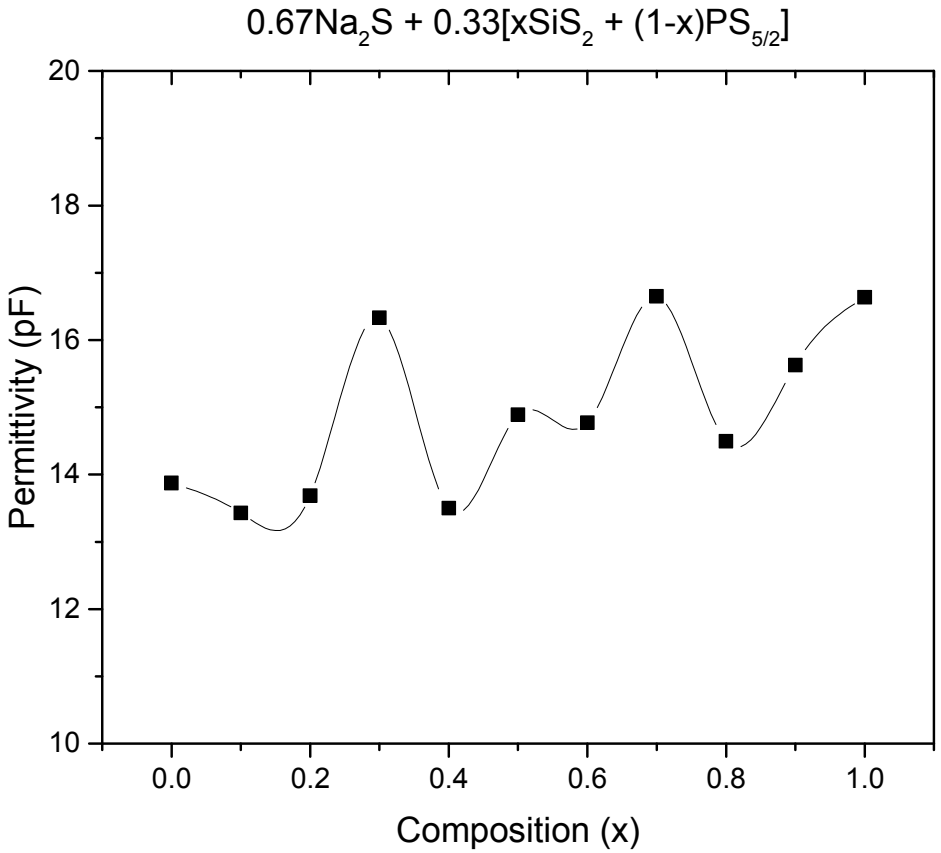

Figure 5.6 Composition Dependence of the High Frequency Permittivity in the $0.67Na_2S + 0.33[xSiS_2 + (1-x)PS_{5/2}]$ system

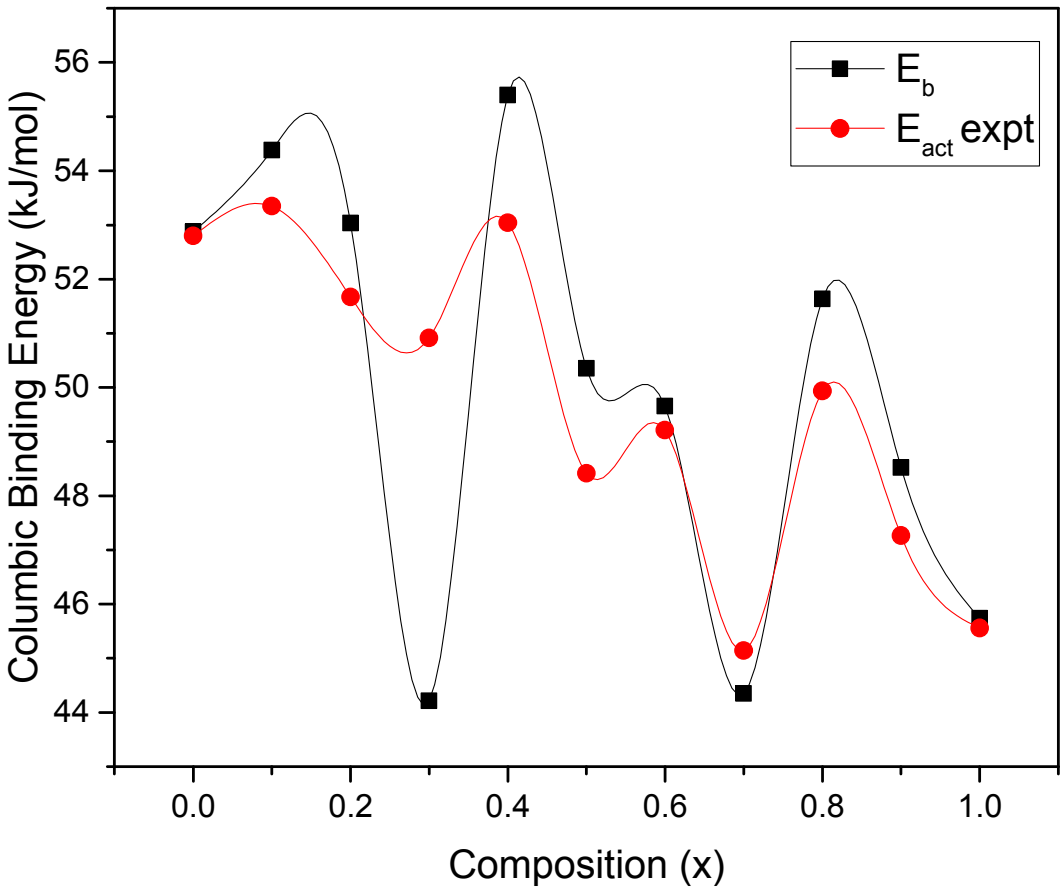

Figure 5.7 Composition Dependence of the calculated Coulombic binding energy

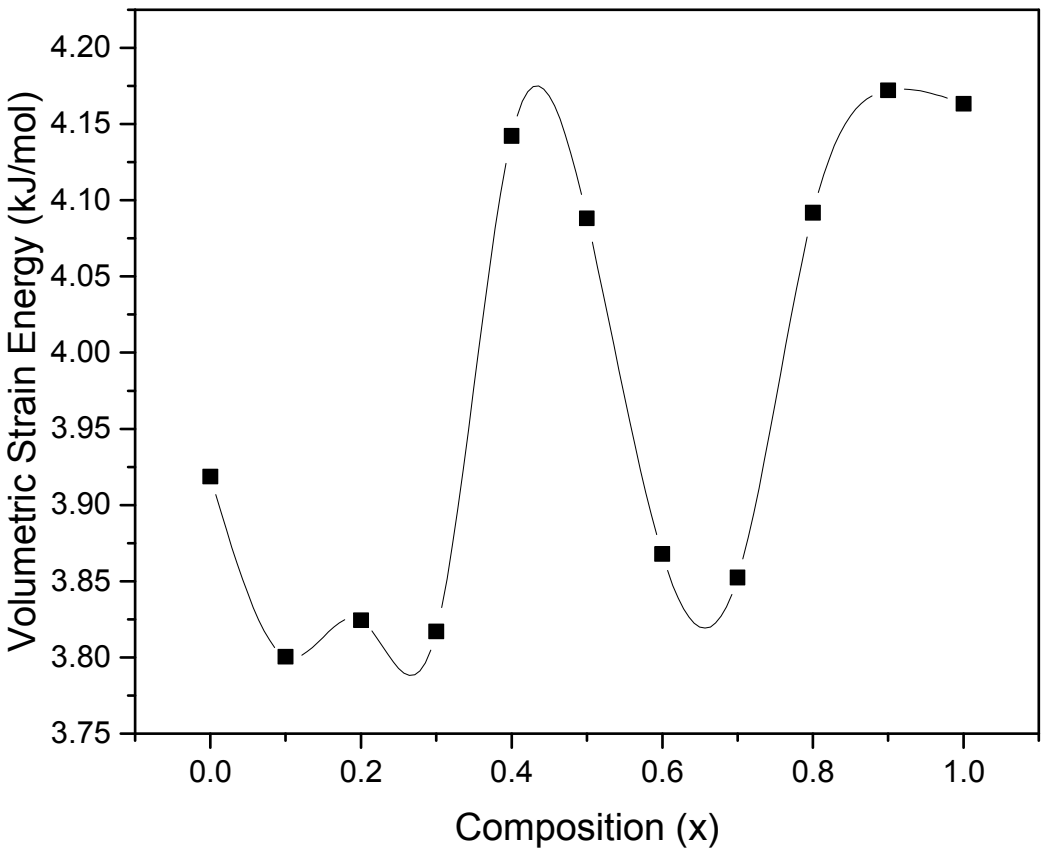

Figure 5.8 Composition Dependence of the calculated volumetric strain Energy

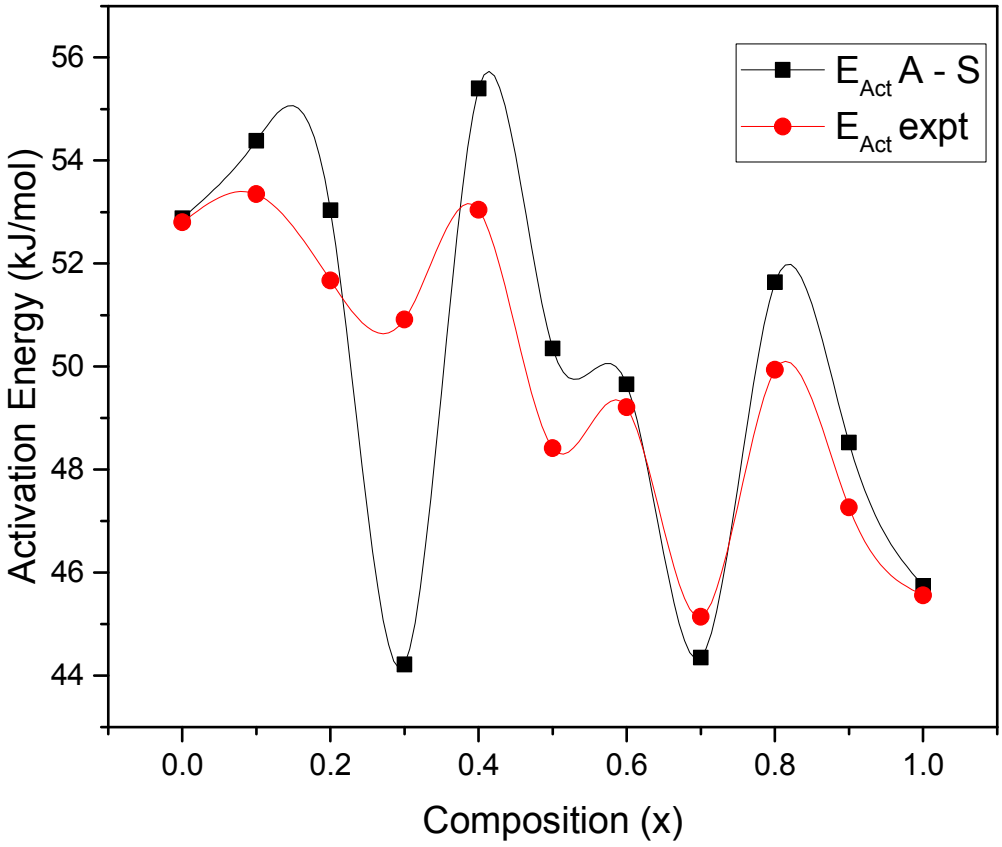

Figure 5.9 Experimental activation energies with the Anderson Stuart model calculated activation energies

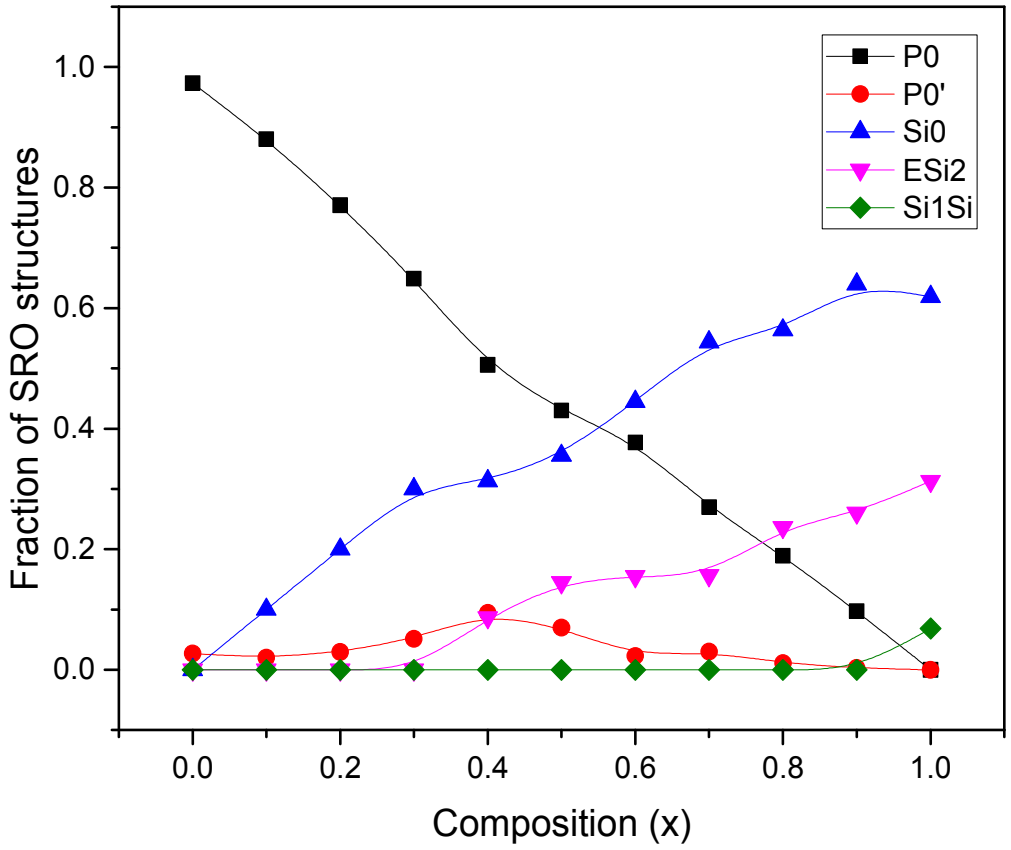

Figure 5.10 Composition Dependence of SRO Structures in the $0.67Na_2S + 0.33[xSiS_2 + (1-x)PS_{5/2}]$

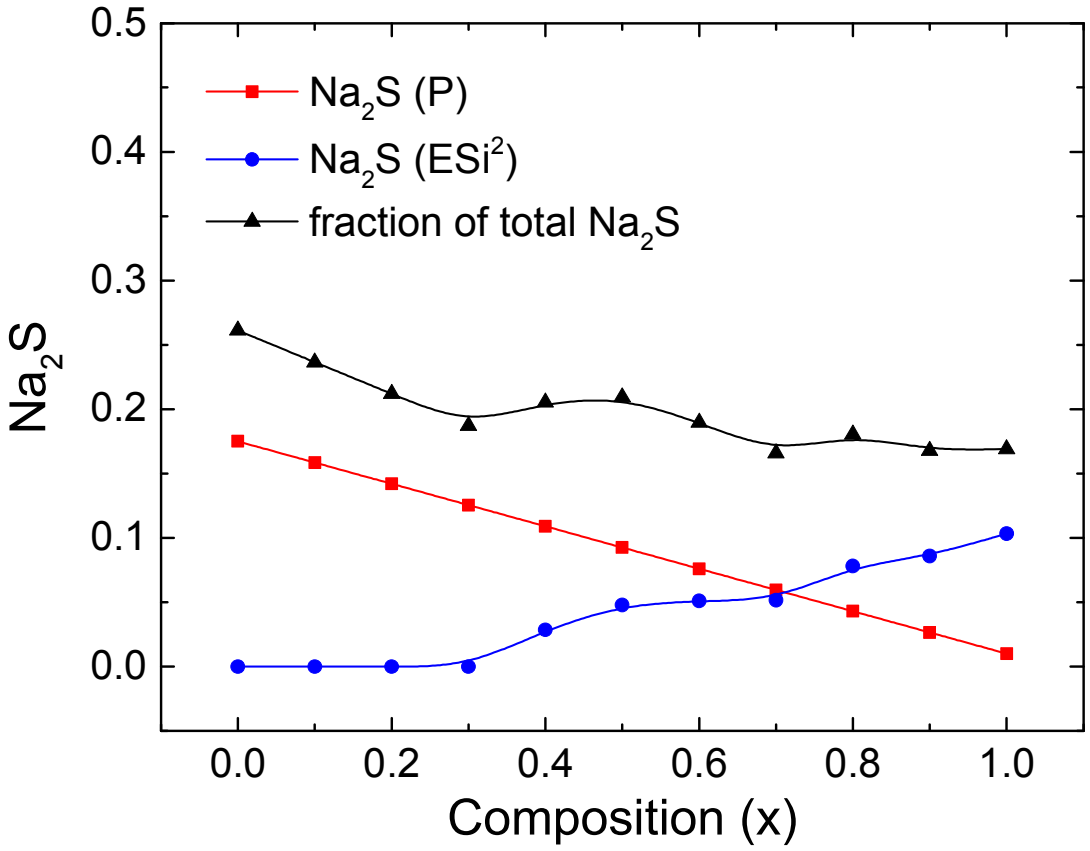

Figure 5.11 Fraction of Free Na_2S in the $0.67Na_2S + 0.33[xSiS_2 + (1\text{-}x)PS_{5/2}]$

5.8 References

1. Vignarooban, K., et al., *Current trends and future challenges of electrolytes for sodium-ion batteries.* International Journal of Hydrogen Energy, 2016. **41**(4): p. 2829-2846.
2. Tang, J., A.D. Dysart, and V.G. Pol, *Advancement in sodium-ion rechargeable batteries.* Current Opinion in Chemical Engineering, 2015. **9**(Supplement C): p. 34-41.
3. Kandagal, V.S., M.D. Bharadwaj, and U.V. Waghmare, *Theoretical prediction of a highly conducting solid electrolyte for sodium batteries:* Journal of Materials Chemistry A, 2015. **3**(24): p. 12992-12999.
4. Hayashi, A., et al., *Characterization of Li_2S–P_2S_5 glass-ceramics as a solid electrolyte for lithium secondary batteries.* Solid State Ionics, 2004. **175**(1–4): p. 683-686.
5. Mizuno, F., et al., *All-solid-state lithium secondary batteries using Li_2S–SiS_2–Li_4SiO_4 glasses and Li_2S–P_2S_5 glass ceramics as solid electrolytes.* Solid State Ionics, 2004. **175**(1–4): p. 699-702.
6. Hayashi, A., et al., *Fast lithium-ion conducting glass-ceramics in the system Li_2S-SiS_2-P_2S_5.* Electrochemical and Solid-State Letters, 2003. **6**(3): p. A47-A49.
7. Hayashi, A., et al., *Formation of superionic crystals from mechanically milled Li_2S–P_2S_5 glasses.* Electrochemistry Communications, 2003. **5**(2): p. 111-114.
8. Hayashi, A., et al., *Characterization of Li_2S–SiS_2–Li_3MO_3 (M=B, Al, Ga and In) oxysulfide glasses and their application to solid state lithium secondary batteries.* Solid State Ionics, 2002. **152–153**: p. 285-290.
9. Hayashi, A., et al., *Characterization of Li_2S–SiS_2–Li_xMO_y (M=Si, P, Ge) amorphous solid electrolytes prepared by melt-quenching and mechanical milling.* Solid State Ionics, 2002. **148**(3–4): p. 381-389.
10. Tatsumisago, M., et al., *Preparation of amorphous solid electrolytes in the system Li_2S–SiS_2–Li_4SiO_4 by mechanical milling.* Solid State Ionics, 2000. **136–137**: p. 483-488.
11. Tatsumisago, M., C.A. Angell, and S.W. Martin, *A New Problem in the Correlation of Nuclear-Spin Relaxation and Ionic Conductivity in Superionic Glasses.* J. Chem. Phys., 1992. **97**: p. 6968.
12. Tatsumisago, M., N. Machida, and T. Minami, *Mixed Anion Effect in Conductivity of Rapidly Quenched Li4SiO4-Li3BO3 Glasses.* J. Ceram. Assoc. Jpn., 1987. **95**: p. 197.
13. Tatsumisago, M., et al., *Ionic Conductivity of Rapidly Quenched Glasses with High Concentration of Lithium Ions.* J. Non-Cryst. Solids, 1987. **95-96**: p. 857.
14. Watson, D.E. and S.W. Martin, *Short range order characterization of the Na_2S + SiS_2 glass system using Raman, infrared and 29 Si magic angle spinning nuclear magnetic resonance spectroscopies.* Journal of Non-Crystalline Solids, 2017. **471**: p. 39-50.
15. Cho, J. and S.W. Martin, *Structures and Ionic Conduction of xNa_2S+ (1-x)SiS_2 Glasses.* Role of Ceramics in Advanced Electrochemical Systems, 1996: p. 85-99.
16. Sills, J.A., S.W. Martin, and D.R. Torgeson, *^{11}B NMR studies of the short range order in wide composition range $xNa_2S + (1 - x)B_2S_3$ glasses.* Journal of Non-Crystalline Solids, 1994. **168**(1): p. 86-96.

17. Sills, J.A., S.W. Martin, and D.R. Torgeson, *^{11}B NMR studies of the short range order in $K_2S + B_2S_3$ glasses.* Journal of Non-Crystalline Solids, 1994. **175**(2): p. 270-277.
18. Martin, S.W. and C.A. Angell, *Dc and ac conductivity in wide composition range $Li_2O \cdot P_2O_5$ glasses.* Journal of Non-Crystalline Solids, 1986. **83**(1): p. 185-207.
19. Bischoff, C., *The Mixed Glass Former Effect in $0.5Na_2S + 0.5[xGeS_2 + (1-x)PS_{5/2}]$ glasses*, in *Materials Science and Engineering*. 2013, Iowa State University. p. 193.
20. Christensen, R., *The mixed glass former effect in $0.35Na_2O + 0.65[xB_2O_3 + (1-x)P_2O_5]$ glasses*, in *Materials Science and Engineering*. 2012, Iowa State University. p. 172.
21. Haynes, M.J., et al., *The mixed glass former effect on the thermal and volume properties of Na_2S-B_2S_3-P_2S_5 glasses.* Physics and Chemistry of Glasses-European Journal of Glass Science and Technology Part B, 2009. **50**(3): p. 144-148.
22. Kim, Y., J. Saienga, and S.W. Martin, *Glass formation in and structural investigation of $Li_2S + GeS_2 + GeO_2$ composition using Raman and IR spectroscopy.* Journal of Non-Crystalline Solids, 2005. **351**(49–51): p. 3716-3724.
23. Larink, D., H. Eckert, and S.W. Martin, *Structure and Ionic Conductivity in the Mixed-Network Former Chalcogenide Glass System $[Na_2S](2/3)[(B_2S_3)(x)(P_2S_5)(1-x)](1/3)$.* Journal of Physical Chemistry C, 2012. **116**(43): p. 22698-22710.

CHAPTER 6. CONCLUSIONS

6.1 General Conclusions

The MGFE in sodium thiosilicophosphates were investigated through characterization of the Tg, density and ionic conductivity. In the $0.50Na_2S + 0.50[xSiS_2 + (1-x)PS_{5/2}]$ glass system the short range order of the network was characterized using Raman, IR and ^{29}Si and ^{31}P MAS NMR spectroscopy and showed the unequal sharing of Na^+ by P, as was observed in the analogous $0.50Na_2S + 0.50[xGeS_2 + (1-x)PS_{5/2}]$ series. The P^1 reacts with Si^2 to form P^0 and Si^3 structures. The system showed a negative MGFE was seen strongly in the T_g but not so in the densities. Due to the challenge in getting bulk disc glass samples throughout this system, the ionic conductivities could not be fully reported for this system. Some planetary milled samples were attempted but could only obtain glasses to a certain point. This may be tied to the difference in the purity of the Na_2S used when this composition was first explored versus what has be used recently. XRD performed on the recent non-glass forming samples showed a predominant tetragonal Na_3PS_4 phase.

The $0.67Na_2S + 0.33[xSiS_2 + (1-x)PS_{5/2}]$ glass system exhibits a negative MGFE in the ionic conductivity, glass transition temperature and densities. The composition creates completely depolymerized units and molecular anions. The expected P^0 and Si^0 was detected in Raman and IR. The Raman also was identified the presences of polysulfide structures in the compositions. Using the ^{29}Si and ^{31}P MAS NMR, $P^{:0}$ and ESi^2 which give rises to the free Na_2S were detected as well. This insight was important in explaining the ionic conductivity and activation energy behavior. The Anderson Stuart model of the activation energies for the y = 0.67 showed that the E_b had a negative MGFE but when Na2S increased suddenly with a change in the ESi^2 concentration, the E_b reached a

maxima at x = 0.4 and 0.8, and then returned to a negative trend. The E_S trended with the overall free sodium Na_2S in the system. Nevertheless, in both components of the activation energy, the addition of SiS_2 led to a decrease in the E_b and E_S.

6.2 Proposed Future work

The y = 0.50 series proved difficult to synthesize with the new high purity sodium sulfide produced in our lab as well as the commercially available sodium sulfide. Part of this may be caused by the fact that the structures generated by this composition, P^0 and Si^3, are non-glass forming compositions. Instead the composition forms a strong Na_3PS_4 phase which corresponds to the y = 0.60 P^0 composition and perhaps a $Na_4Si_4S_{10}$ phase which corresponds to the y = 0.33 Si^3 composition. To get a better glass forming system, going to y = 0.55 may be a viable window for exploration. With the knowledge for the two MGF systems studied here and information from the binary systems, the structure will be well known, making the ability to connect structures and properties fairly straightforward. This also may be a good candidate system for two dimensional phosphorus NMR studies as well.

A thorough investigation of polysulfide structures in the sodium modified glasses is going to be crucial in understanding highly modified sodium compositions for electrolytes. Besides having an apparent effect on the physical properties and glass formability, it is imperative to evaluate the stability of these structures when subjected to an electrochemical environment i.e. inside of a full solid state battery.

6.3 Acknowledgements

I would like to take this opportunity to thank my major professor Dr. Steve W Martin for the opportunity to pursue this PhD degree and guidance throughout this PhD experience. I am grateful for the growth I have experienced and the confidence I have gained as a young scientist. Thank you for the opportunity to travel and research abroad which has led to many great connections and friendships.

Thank you to my GOM research group for their partnership and support. Special thanks to Steven Kmiec for his collaboration, great conversations and inspiration. Thank you to my undergraduate researcher Kah Loong Hoh for his contribution and patience with me as well. Thanks also to Alison Whale for her constant encouragement and affirmation of me, Brittany Curtis for her efforts on the MGFE project and great travel companion, and Josh Roth for conversations and encouragement.

Thank you to Sarah Cady, Shu Xu and Aaron Rossini in the Chemistry department for use of their NMR instruments and guidance in understanding solid state NMR.

I would also like to extend a special thanks to my Cornerstone church family here in Ames. You have made Ames home for me and have been a constant source of strength and joy. Thank you for listening and supporting me throughout my PhD process and also to the PhD community inside Cornerstone for their advice, support and the occasional review of manuscripts!

To my Coe College family in the Physics and Chemistry departments I would also like to extend my thanks. Doc Feller, thank you for your early mentorship and introduction to the glass science field. Thanks for encouraging me to pursue this opportunity. Also to

Maria Dean in the Chemistry department for her mentorship and clear pride and confidence in me. Thank you.

Finally I would like to thank my beloved family. Mom and Dad, thank you for the time, prayer and sacrifices you have made throughout my life to give me a chance to do better than you could. And to my darling sister Diannah, who has lifted me up, especially when I could not do it myself. I love you so much.

This research was supported by the National Science Foundation under DMR grants 1304977 and 0710564